SCUOLA DI DOTTORATO
UNIVERSITÀ DEGLI STUDI DI MILANO-BICOCCA

School of Medicine and Surgery

PhD program in Molecular and Translational Medicine (DIMET)

XXXII Cycle

Curriculum in ***Nanomedicine***

A nanomedicine approach for the treatment of glioblastoma multiforme

Formicola Beatrice

Registration number N 823227

Tutor: Prof. Francesca Re

Coordinator: Prof. Andrea Biondi

ANNO ACCADEMICO / ACADEMIC YEAR
2018/2019

CHAPTER 1

General introduction

1.1 Glioblastoma Multiforme

1.2 Nanomedicine for brain therapy

1.3 Nanomedicine for the treatment of Glioblastoma Multiforme

1.4 *In vitro* and *in vivo* models

Publications outside the thesis topic:

CHAPTER 1

General introduction

1.1 Glioblastoma Multiforme

1.1.1 Overview of the pathology

Glioblastoma multiforme (GBM) represents the most common type of glioma, a group of brain cancers that mainly arise from glial cells of the central nervous system (CNS) [Perrin SL. et al., 2019]. Unlike other cancers, it remains contained in its organ of origin without any systemic spread [Westphal M and Lamszus K, 2011].

Gliomas are classified according to the glial cells that they morphologically most closely resemble, such as astrocytes (astrocytomas) oligodendrocytes (oligodendrogliomas) and ependymal cells (ependymomas). Considering this categorization, GBM is an astrocytoma [Westphal M and Lamszus K, 2011].

GBM is considered a rare disease: there are 10 000 and 100 000 new cases of glioblastoma diagnosed each year in the USA and in the world, respectively. The highest rates of incidence are in the USA, Canada, Australia, and Northern Europe, with a very low 5-year survival rate (about 5%) [Alexander BM and Cloughesy TF, 2017]. Epidemiological studies revealed that the disease affects males 1.6-fold more frequently than females [Hanif F et al., 2017; Xu H et al., 2017; Tamimi AF and Juweid M, 2017; Ostrom QT, et 2015].

The morbidity, mortality, and recurrence of brain tumours are heavily dependent on their location and invasive growth patterns. The 40% of gliomas were located in the frontal lobe; other tumour locations are: the temporal lobe 29%, the parietal lobe 14%, and the occipital lobe 3% [Larjavaara S et al., 2007]. Nowadays, strong evidences suggested that

glioblastoma arises from neural stem cells within the subventricular zone of the brain, rather than mature glia [Perrin SL et al., 2019].

GBMs commonly occur *de novo* and in these cases they are called primary GBMs, but they may also evolve from a pre-existing lower grade tumour, and thus defined assecondary tumours. Primary GBMs represent the 90% of total GBM cases worldwide and they are the ones with the worse prognosis compared to their secondary counterpart.

Moreover, primary GBM affects elderly patients at a much higher occurrence, with a peak incidence beyond 65 years of age, often showing no symptoms before gaining malignancy [Ostrom QT, et al 2015].

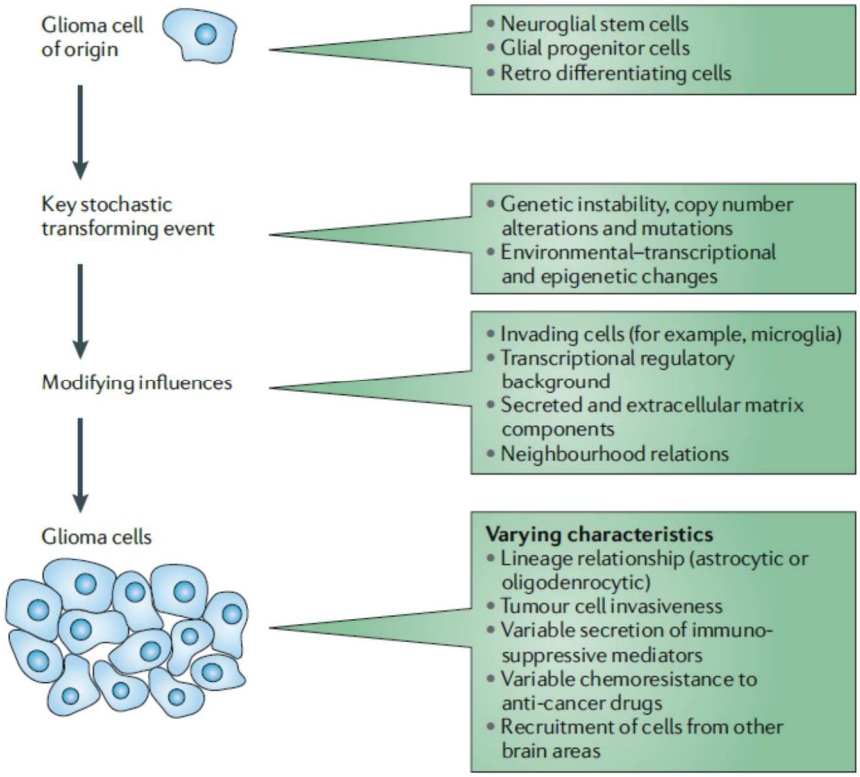

Fig. 1 Sequential events that cause glioma diversity and that are relevant to clinical

tumour characteristics. Depending on the type of cell of origin of a tumour (for example, a neuroglial cell, glial progenitor or retrodifferentiating cell), particular transforming molecular events must occur to initiate that cell along an oncogenic path, the final direction of which is then partly determined by stochastic events such as genomic instability and mutations. There is increasing evidence for additional opportunities for epigenetic regulation of altered cellular gene function, either by regional microenvironmental conditions (secreted or extracellular matrix components) or invading host cells such as microglia, lymphocytes or bone marrow-derived mesenchymal stem cells. Given the diverse mix of genetic and epigenetic factors in determining tumour cell fate, the emerging variety of (gene expression) tumour types with different clinical behaviour is not surprising. From Westphal M 2011.

Common clinical manifestations of GBM include progressive headaches, fatigue, seizures, dizziness, increased intracranial pressure, focal neurological deficits or changes in mental status. However, the symptoms are also related to the tumour-involved area of the brain: tumours in certain areas determine persistent weakness, mood disorders, numbness, loss of vision or language alteration [Alexander BM and Cloughesy TF, 2017].

1.1.2 Histopathological and molecular features

In the last decades, the improvement of high-throughput genetic, genomic, and epigenetic techniques has provided a deeper and comprehensive understanding of histopathological and molecular mechanisms underlying GBM oncogenesis and progression.

Verhaak et al., classified GBM into four different molecular subtypes, namely classical, mesenchymal, proneural and neural, based on gene expression levels [Verhaak RGW et al., 2010].

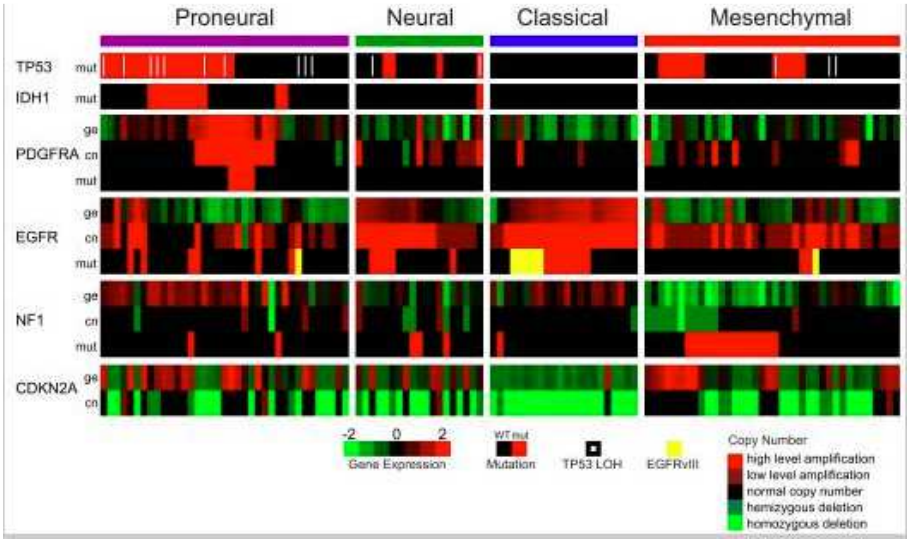

Fig. 2 Integrated view of gene expression and genomic alterations across glioblastoma subtypes. Gene expression data (ge) was standardized (mean equal to zero, standard deviation equal to 1) across the 202 dataset, data are shown for the 116 samples with both mutation and copy number data. Mutations (mut) are indicated by a red cell, a white pipe indicates loss of heterozygosity, and a yellow cell indicates the presence of an EGFRvIII mutation. Copy number events (cn) are illustrated by bright green for homozygous deletions, green for hemizygous deletions, black for copy number neutral, red for low level amplification, and bright red for high level amplifications. A black cell indicates no detected alteration. From Roel G.W. Verhaak et al, 2010.

The classical subtype was characterized by epidermal growth factor receptor (EGFR) amplification, the lack of tumour protein 53 (TP53) mutations and cyclin-dependent kinase Inhibitor 2A (CDKN2A) deletion, while the mesenchymal subtype was enriched for mutation and/or loss of neurofibromin 1 (NF1). On the other hand, the proneural subtype was defined by alterations of platelet-derived growth factor receptor alpha (PDGFRA) and point mutation in isocitrate dehydrogenase 1 (IDH1), and the neural subtype was typified by the expression of neuronal markers such as neurofilament light polypeptide (NEFL), synaptotagmin-1 (SYT1), gamma-aminobutyric acid type A

receptor alpha 1 subunit (GABRA1) and solute carrier SLC12A5 [Verhaak RGW et al., 2010; Burton EC et al., 2002;].

Tumors of the proneural subtype were associated with better survival than other subtypes. However, GBM patients with the proneural subtype rarely benefit from aggressive therapies, which were more effective for patients with the classic and the mesenchymal subtypes [Sasmita AO et al., 2017; Maher EA et al., 2006].

Moreover, from the molecular point of view an additional distinction between primary and secondary GBM have been done. Primary GBM, also defined IDH-wild-type, often shows molecular overexpression and amplification of EGFR, loss of heterozygosity (LOH) 10q and phosphatase and tensin homolog (PTEN) mutations. On the other hand, the most common molecular biomarkers of secondary GBM are represented by TP53 and IDH mutations, which are not frequently observed in primary tumours [Quan AL et al., 2005; Silantyev AS et al., 2019; Rich JN et al., 2005; Maher EA et al., 2006].

The Cancer Genome Atlas (TCGA) Research Network provided a comprehensive catalogue of genomic abnormalities driving GBM tumorigenesis, considering a large cohort containing 206 patient samples. Data showed that the majority of GBM patients present abnormalities in receptor tyrosine kinase, TP53 and RB pathways, suggesting that these alterations are a core requirement for GBM pathogenesis [Verhaak RGW et al., 2010].

A grading system developed by the World Health Organization (WHO) takes into account the histopathology, the cytoarchitecture and the immunohistological marker profile of the cells and distinguishes four

grades (I, II, III and IV) for astrocytomas and two grades (II and III) for oligodendrogliomas and oligoastrocytomas [DeWitt JC et al., 2017].

Grade / Type	WHO grade I	WHO grade II	WHO grade III	WHO grade IV
	Circumscript	Low-grade	Diffuse / High-grade	
Astrocytoma	Pilocytic astrocytoma	Low-grade astrocytoma	Anaplastic astrocytoma	Glioblastoma
Oligodendroglioma		Low-grade oligodendro-glioma	Anaplastic oligodendro-glioma	
Oligo-astrocytoma		Low-grade oligo-astrocytoma	Anaplastic oligo-astrocytoma	

Table 1. The 2016 WHO classification of central nervous system tumors

Lower grade tumours (grade I and II) contain specific genetic alterations, tend to be well differentiated, have increased cell density and some cellular anomalies or atypia, but in general these resemble their non-neoplastic counterparts. Tumours of higher grade (grade III tumours) are anaplastic, show signs of increased vessel density, cellular atypia, elevated mitotic activity and a high cell density. Accordingly, GBM also known as grade IV astrocytoma, is the most aggressive, anaplastic and invading tumour, showing vascular endothelial proliferation, necrosis, a very high cell density and atypia [Cancer Genome Atlas Research, 2008].

Moreover, the WHO classification system divided GBM into three categories according to the key genetic prognostic marker isocitrate dehydrogenase (IDH) in: i) GBM IDH-wildtype, ii) GBM IDH-mutant

and iii) GBM NOS. IDH-wildtype (about 90% of cases) corresponds most frequently to primary or *de novo* GBM and occurs in patients over 55 years of age [Louis DN et al., 2016; Silantyev AS. et al., 2019]. IDH mutations (about 10% of cases) characterize the so-called secondary GBM which preferentially arises in younger patients [Ohgaki H and Kleihues P, 2013]. The NOS definition is reserved to GBM with an inconclusive or not fully investigated IDH expression [Miyai M et al., 2017].

Furthermore, GBM presents a high tumour heterogeneity, both inter-tumoral and intra-tumoral. Recent single cell sequencing analysis of GBM patient's samples suggest that intra-tumoral cellular heterogeneity can be partially due to the tumour cell hierarchy arising from GBM stem cells (GSCs). GSCs as other cancer stem cells, are characterized by self-renewal, multipotency, specific cell marker expression, and the ability to generate tumours *in vivo*. [Ohgaki H and Kleihues P, 2013; Brennan CW et al., 2013]. Usually, when implanted into the cortex of rodents, the tumours produced by these cells presented the molecular profile and signature of the parental GBM-derived cells [Furnari FB et al., 2007]. Importantly, one of the most challenging feature of GSCs is their resistance to radio- and chemotherapy, which led to tumour recurrence.

The recurrence rate after surgery is about 80%, due to the infiltrative nature of cells, and usually a new tumour grows within 2-3 cm of the margins of the original tumour [D'Alessio A et al., 2019; Lara-Velazquez M et al., 2017].

1.1.3 Intercellular communication

The awareness of the presence of different communication modalities in GBM boosted the scientific community to deeply investigate their role in tumorigenesis.

Among communication types, the homotypic communication takes place between same cells (e.g. cancer cells), while heterotypic communication occurs between cancer cells and stroma. This is an useful way to recruit normal cells to promote growth, sustenance and invasion of the tumour into the brain [Lou E et al., 2018].

The GBM recruitment involves multiple communication routes and directive exchanged between tumour cells and surrounding cells in the tumour microenvironment [Lou E, 2017].

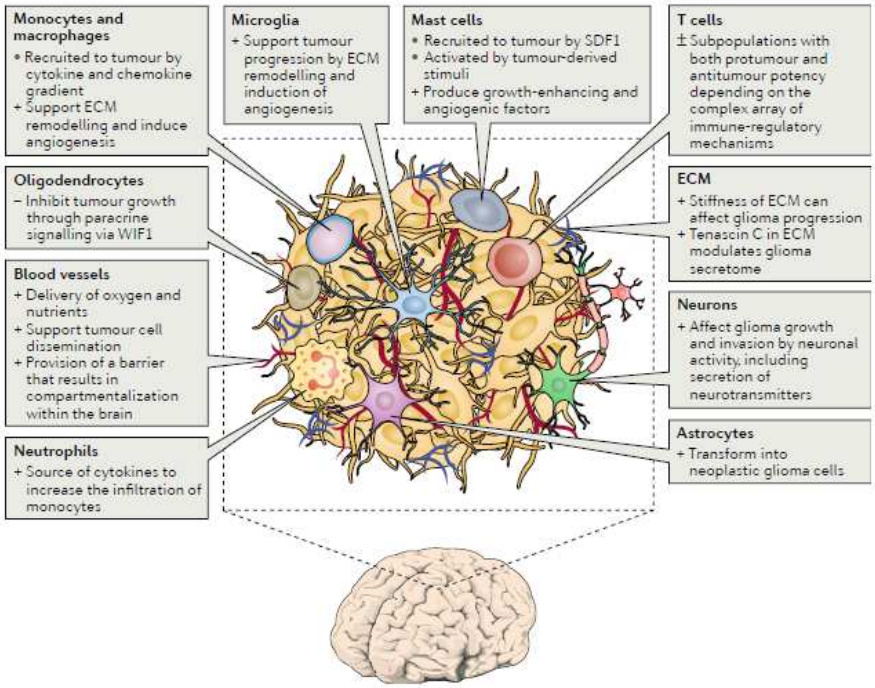

Fig. 3 Glioblastoma microenvironment. The glioblastoma environ consists of tumour cells, extracellular matrix (ECM), blood vessels, innate immune cells (monocytes, macrophages, mast cells, microglia and neutrophils), T cells and non-tumorous

neurons, astrocytes and oligodendrocytes. +, protumour function; –, antitumour function; ±, mixed pro-tumour and anti-tumour functions; SDF1, stromal cell- derived factor 1; WIF1, WNT inhibitory factor 1.

The communication ways include secreted proteins and molecules, gap junctions, extracellular vesicles (EVs), tunnelling nanotubes (TnTs) and microtubes (TmTs) [Broekman ML et al., 2018].

Although cell-secreted soluble factors, including IL-6, transforming growth factor-β (TGFβ), platelet-derived growth factor (PDGF), epidermal growth factor (EGF), vascular endothelial growth factor (VEGF) and stromal cell-derived factor 1 (SDF1) are well known as signalling molecules between cells, recent evidences showed that EVs, TmTs and TnTs play a key role in the inter- and intracellular communication [Rustom A et al., 2004; Broekman ML et al., 2018].

TmTs and TnTs are transient transcellular protrusions with different length, thickness and lifetime that determine a nuclear and cytoplasmic *continuum* with neighbouring cells. In particular, these newly recognized transit routes mediate the exchange of non-secretable molecules, including transcription factors, mithocondria, RNAs and DNA [Ahmad et al., 2014; Thayanithy et al., 2014; Schiller et al., 2013; Onfelt et al., 2006].

In GBM and other tumours, TnTs channels allow the transfer of genetic elements, mitochondria, lysosomes and proteins to normal cells with the aim to change their phenotype, or to other cancer cells in order to rescue them when in trouble, for example as a result of radio- or chemotherapy [Lou E, 2017].

However, non-secretable proteins, transcription factors included, RNA, DNA, lipids and metabolites can be also transferred through EVs released from tumour cells *via* fusion of multivesicular bodies with the

cell membrane. As TnTs, these tumour-derived EVs can change the phenotype of normal cells to promote angiogenesis, tumour cell invasion, immune suppression, and a different metabolic regulation [Fonseca P. et al., 2016; D'Asti E et al., 2016; Redzic et al., 2014].

Gap junctions between adjacent cells are mainly involved in the transfer of small molecules such as Ca^{2+}, ATP, metabolites and microRNAs (miRNAs) [Thuringer D et al., 2016; Hong X et al., 2015].

Connexins, which represents a structural component of these junctions, usually result upregulated in tumour initiating cells and are associated with increased invasiveness of gliomas [Hong X et al., 2015; Balça-Silva J et al., 2017; Sinyuk M et al., 2018].

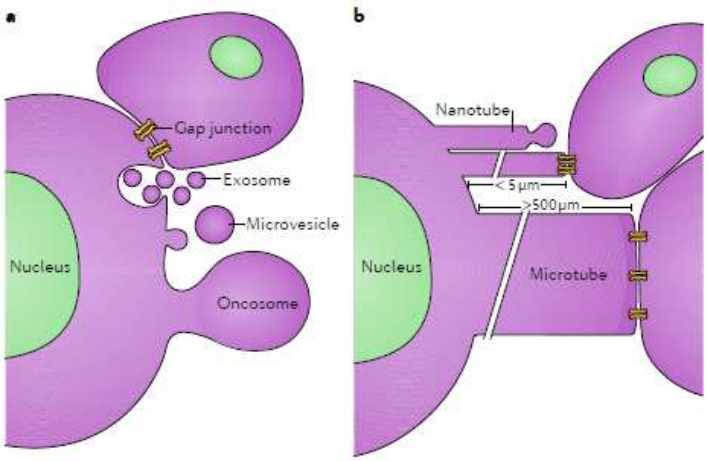

Fig. 4 Routes of communication between tumour cells and cells in their environs. **a**) Gap junctions (24 nm in diameter) form across the adjacent membranes of cells that are in physical contact, enabling the passage of small molecules. Cells also release exosomes (50–100 μm) from multivesicular bodies that fuse with the plasma membrane. In addition, microvesicles (100–200 μm) and even large oncosomes (1–10 μm) bud off from the plasma membrane and can interact with and be taken up by other cells. **b)** Tunnelling nanotubes (50–200 nm in width and up to 5 μm in length) extend out from cells and can either bud off vesicles at their tips or form gap junctions with other cells. Microtubes extend out from tumour cells (1–2 μm in width and >500 μm in length) and can form gap junctions with other cells.

Therefore, a continuously growing body of evidences suggests that the different communication modalities in GBM microenvironments are responsible for the recruitment and activation of various cells of the innate immune system [Broekman ML et al., 2018].

Moreover, damages to the blood–brain barrier (BBB) in the neighbourhood of the the tumour mass, enables bone marrow haematopoietic stem cell- derived monocytes and macrophages to infiltrate the tumour by crossing the BBB [Bowman RL et al., 2016; Muller A et al., 2015].

The tumour environs contain brain-resident microglia and infiltrating monocytes, often grouped together under the term tumour-associated macrophages or myeloid cells (TAMs). The interaction between GBM cells and TAMs is multifactorial and the recruitment of TAMs to GBM is mostly mediated by chemokine and cytokine gradients released by tumour cells and by cell-cell contacts [Hambardzumyan D et al., 2016]. This interplay between GBM cells and TAMs is especially apparent in extracellular matrix (ECM) remodelling and in tumour proliferation and invasiveness. A group of proteins that are main actors in this scenario are matrix metalloproteinases (MMPs) [Kassenbrock K et al., 2010]. In particular, in GBM the MMP2 has a crucial role in ECM degradation, which facilitates GBM cells migration and spreading [Du R. et al., 2008].

In conclusion, a comprehensive understanding of all of the communication routes and these complex interactions between GBM cells and innate immune system cells could improve the therapeutic approach to this disease.

1.1.4 Current GBM diagnosis and treatment

Despite recent advances in diagnostics techniques and cancer biology, treatment outcomes have not changed significantly over the past decades and high-grade gliomas, such as GBM remain fatal, with a median survival timeline of about 15 months after diagnosis [Westphal M and Lamszus K, 2011; Soomro SH et al., 2017; Stupp R et al., 2005]. Moreover, no significant changes in the standard of care of GBM patients have been made in the last 20 years.

Two GBM prognostic biomarkers are mutations in isocitrate dehydrogenase (IDH) and O6-methylguanine-methyltransferase (MGMT) promoter methylation, but the high heterogeneity of this tumour limits their clinical application [Karsy M et al., 2015; Alexander BM and Cloughesy TF, 2017].

Nowadays, no early detection of GBM is available and the magnetic resonance imaging (MRI) represents the most sensitive tool for the detection of GBM. However, once a GBM definable lesion is identified with imaging, the tumour is already at an advanced state.

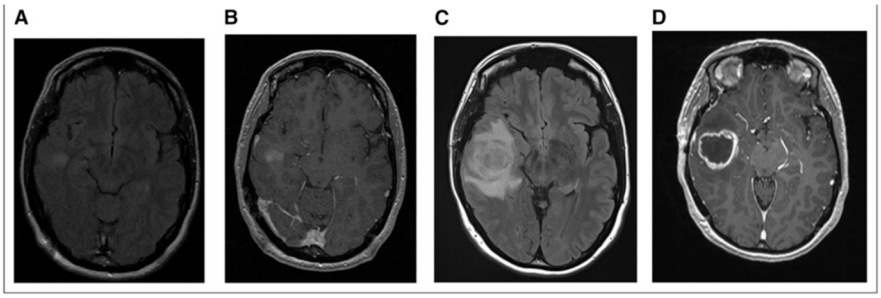

Fig 5 MRI of a GBM during the time. The images show the rapid evolution of the tumour in only 20 days.

The typical imaging of GBM shows ring-shaped lesion with a hypodense center due to necrosis and a surrounding hypodense peritumoral area due to edema [Lima FR et al., 2012; Faria J et al., 2006]. However, some GBM MRI showed the so-called butterfly shape that refers to the symmetric wing-like extensions of the tumour across the midline of the corpus callosum.

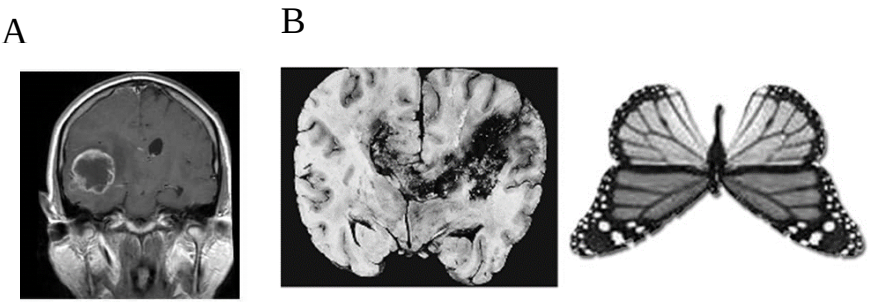

Fig. 6 GBM MRI images. A) ring-shaped GBM with a hypodense center due to necrosis and a surrounding hypodense peritumoral area due to oedema. B) Butterfly shaped GBM due to tumour infiltration across the midline of the corpus callosum.

The diagnosis of GBM is commonly made with formalin fixed, paraffin-embedded tissue from resected or biopsied tumour.

The microscopy observation of immunostained samples typically show an infiltrating glial fibrillary acidic protein immunopositive tumor with marked pleomorphism, brisk mitotic activity, microvascular proliferation, and necrosis [Wood M D et al., 2019; Alexander BM and Cloughesy TF, 2017].

The current standard of care for GBM patients is represented by surgical resection, followed by radiation therapy (RT) and chemotherapy [Alexander BM and Cloughesy TF, 2017].

Temozolomide (TMZ) and Bevacizumab represent the only U.S. Food and Drug Administration (FDA) approved medications for systemically administration for primary and recurrent GBM, respectively [Mooney J et al., 2019; M.H. Cohen, et al., 2012].

Moreover, the therapy for GBM is heterogeneous according to the age of patients. For patients younger than age 70, the current standard of care is surgical resection, followed by RT and concomitant TMZ and then, in the following weeks, adjuvant TMZ. For older patients who cannot receive combined therapy with RT and TMZ, TMZ alone remains the unique reasonable option [Alexander BM and Cloughesy TF, 2017; Okada M et al., 2017].

TMZ is an orally administered cytotoxic alkylating agent with modest efficacy in patients with recurrent high-grade gliomas, GBM included [Ramirez YP et al., 2013; Omar AI and Mason WP, 2009]. It is relatively well-tolerated with low side effects and it has an acceptable safety profile [Groves, MD, et al. 2007; Osoba D, et al., 2000]. Due to its biochemical features, TMZ is rapidly and completely absorbed after oral administration and binds minimally to plasma proteins, resulting in limited interactions with concurrently administered drugs. Moreover, being a small lipophilic molecule, TMZ penetrates the BBB and is therefore one of the few drugs effective on CNS diseases [Karisa CS and Stuart A, 2018].

The action of TMZ is determined by its conversion to the active metabolite 5-(3-methyltriazen-1-yl) imidazole-4-carboxamide (MTIC) in the human body. Among the effects on DNA produced by MTIC, the methylation of guanine at O6 (O6-MeG) is the more critical, generating an altered DNA replication and cell apoptosis [Thomas A et al., 2017].

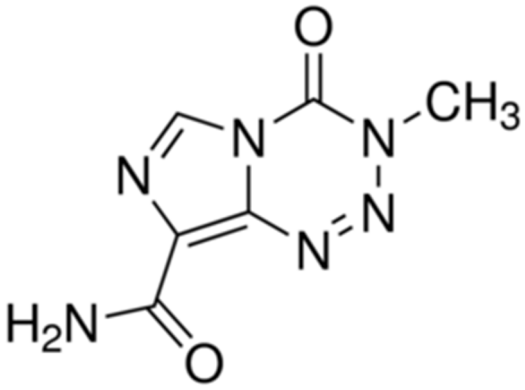

Fig. 7 Chemical structure of TMZ.

Although nowadays TMZ remains the main used drug for GBM treatment, many studies documented cell mechanism of resistance to TMZ mediated by the DNA repair protein MGMT, which removes methyl groups from O6-MeG, thus limiting its use.

Moreover, preliminary studies during clinical trials raised the hypothesis that TMZ induced hypermutation in low-grade gliomas, contributing to their malignant transformation when they recur, worsening the prognosis of patients [Choi S et al., 2018].

The most of GBM tumours are characterized by increased VEGF expression and its over-expression activates the VEGFR pathway, promoting the proliferation, migration, and survival of endothelial cells, resulting in the formation of tumour blood vessels. The first FDA approved human monoclonal antibody Bevacizumab, was developed to act on this pathway, inactivating other processes and determining a decrease in angiogenesis, edema, and tumour burden in GBM patients [Pope WB et al., 2012]. Bevacizumab was initially proposed as a second-line treatment for patients with recurrent GBM and a phase II

study revealed an increased six-month progression-free survival from 9%–15% to 25% when patients were treated with this monoclonal antibody. Unfortunately, a further study showed that GBM tumour cells become resistant to the antibody through the activation of alternative angiogenic pathways that are VEGF independent [Vredenburgh JJ et al., 2007; Friedman HS et al. 2009; Reardon DA et al., 2011].

Moreover, MRIs indicated that the Bevacizumab-resistant tumours were highly infiltrative than the untreated ones. These adverse effects together with no significant improvement in lifetime survival of GBM patients led to the scarce use of this antibody-based drug for GBM treatment.

Randomized clinical trials evaluated the use of 1,3-bis(2-chloroethyl)-l nitrosourea (BCNU) wafers, followed by standard RT. The BCNU wafer is a biodegradable polymer that is implanted after surgical tumour removal and determine a controlled release of the drug. Unfortunately, the median survival for patients treated with BCNU wafers was only 2.1 months higher than the one of patients treated with RT alone [Grossman SA et al., 1992; Kleinberg LR et al., 2004; McGirt MJ et al., 2009].

1.2 Nanomedicine for brain therapy

1.2.1 Nanoparticles for biomedical applications

The term *nanomedicine* indicates the medical application of nanotechnology to healthcare. Nanomedicine can be considered a pillar in personalized medicine because it refers to highly specific medic intervention for curing and/or diagnose diseases or for tissue repairing

and regeneration.

The term nanotechnology refers to a scientific area involved in the manipulation of atoms and molecules leading to the production of materials and tunable devices with the size in the order of billionth of meters and that show peculiar properties (surface area to volume ratio, electrical, chemical, optical properties) [Moghimi M et al., 2005; Holmes D, 2013].

In this context nanostructures such as nanoparticles (NPs), are the main actors.

NPs are colloidal objects ranging from 1 to 100 nm in size as defined by the International Union of Pure and Applied Chemistry (IUPAC), with different shapes, charge and composition. Despite this size restriction, the term nanoparticles commonly refers to structures that are up to several hundred nanometers in size, although key is that design of the nanostructure produces a unique function and property [Shi J et al., 2017].

NPs are very popular and attractive form biomedical purposes due to the possibility to multi-functionalize their surface with one or more targeting ligands like peptides, antibodies and small molecules, to accomplish several functions (i.e. biological barrier crossing, targeting of specific molecules/pathways). To this aim, the large NPs surface-area-to-volume ratio allows the coupling of multiple copies of a ligand, strongly increasing the desired effect [Montet X et al., 2006].

NPs can be divided into organic and inorganic depending on the material they are made of. The most common types of organic NPs are lipid-based NPs (i.e. liposomes, solid lipid nanoparticles (SLNs) and polymer-based NPs, while silica, metallic, iron oxides NPs and

quantum dots are the most used in the inorganic counterpart (see table 2).

Examples of various types of nanoparticles being developed for intracellular applications

Type of nanoparticle	Typical size range/nm	Structure and properties
Inorganic		
Metals (Au, Ag, Cu)	5–250	■ Easy to synthesize over a broad range of sizes and shapes (*e.g.* spheres, rods, core–shells); robust and functionalizable *via* thiol-metal chemistry ■ Surface plasmon resonance; surface enhanced Raman scattering
Iron oxides	5–200	■ Typically magnetite ($M_xFe_{3-x}O_4$, M = Mn, Ni, Co, Fe) or maghemite (Fe_2O_3) ■ Ferromagnetic or superparamagnetic properties
Quantum dots	3–30	■ Typically II–VI or III–V chalcogenides synthesized as core–shell or alloy nanocrystalline colloids (*e.g.* CdSe/ZnS, $CdTe_{1-x}Se_x$) ■ Bright, photostable fluorophores with broad absorption and narrow emission; large two-photon cross section; FRET-donors
Silica	3–100	■ Biodegradable; available also in micro- or mesoporous form for encapsulation of dyes and drugs; easily derivatizable with different surface chemistries using silanes
Layered double hydroxide	50–200	■ $Mg_6Al_2(CO_3)(OH)_{16}{\cdot}4H_2O$ ■ Biocompatible and biodegradable in mildly acidic environments; high drug loading capacity
Calcium phosphate	10–100	■ $Ca_5(PO_4)_3OH$ ■ Biodegradable and biocompatible; can be doped with lanthanides or organic fluorophores
Organic		
Liposomes	Multilayer: 500–5000	■ Spherical self-closed structures composed of one of more concentric phospholipid bi-layers
	Unilayer: 100–500	■ Biocompatible, can entrap both hydrophobic and hydrophilic moieties; protects payload from external environment ■ Size and surface functionality can be tuned by adding new ingredients to the lipid mixture prior to synthesis
Polymer micelles	20–200	■ Self-assembled spherical micelles composed of amphiphilic block co- or tri-polymers containing a hydrophobic core and a hydrophilic corona ■ Hydrophobic payload can be entrapped in the core ■ Geometry and functionality can be modularly controlled *via* the length and composition of the polymer blocks; can be biodegradable
Polymer nanoparticles	50–300	■ Linear polymers with payload conjugated to the sidechain; precipitated into colloidal nanoparticles in solution ■ Controllable size, surface functionality by adjusting polymer length, composition, and synthesis conditions; can be biodegradable
Dendrimers	2–10	■ Radially hyperbranched polymers with regular repeat units ■ High structural and chemical homogeneity; high ligand density and payload capacity per particle; controlled biodegradation ■ Common dendrimers for biological applications: polyether, polyester, PAMAM
Carbon nanotubes	d = 0.5–3 l = 10 nm to several centimetres	■ Single or multi-layered graphene sheets rolled into concentric cylinders ■ NIR-photoluminescence, strong resonance Raman scattering effects; directional conductivity, high tensile strength ■ Water-soluble through covalent chemical modification or non-covalent adsorption; ability to translocate cellular membranes *via* non-endocytosis mechanisms
Viral nanoparticles	25–150	■ Self-assembled protein cages with multivalent surface functionalities ■ Natural ability to internalize and unpack payload within cells

Table 2 The most common types of NPs for biomedical applications.

Moreover, NPs can be loaded with drugs, other NPs and/or contrast agents and usually the entrapment: i) improves the solubility, the pharmacokinetics and pharmacodynamic profiles of these drugs/compounds, ii) enhances their half-life and stability by reducing their degradation in the systemic circulation and iii) increases their concentration at the diseased tissue through active targeting, reducing toxic side effects [Biswas and Torchilin, 2014].

Another feature that makes NPs even more interesting for biomedical

applications is the possibility to be administered by various routes: oral, inhalational, and parenteral included [Petkar KC et al., 2011].

The three physicochemical features that mainly affect NPs applicability in clinics are: size, shape and charge of NPs [Blanco E et al., 2015].

The size of NPs, which with the nanotechnology advancements can be tailored according to the final purpose, plays a key role in the NPs application. This is due to the fact that size drives several biological phenomena with discrete cut-off size ranges that include circulation half-lives, extravasation through leaky vasculature and macrophages uptake. For instance, NPs with <~5 nm diameter rapidly undergo renal clearance, upon intravenous administration, while reticuloendothelial system (RES), liver and spleen determine the clearance of particles >200 nm, due to the size range of inter-endothelial cell slits (about 200–500 nm) [Choi HS et al. 2007; Chen LT and Weiss L, 1973].

Taking into account these and other evidences, NPs with an average size of 100 nm NPs generally have a prolonged circulation time, resulting as the best candidates for these purposes.

The NPs architecture and shape strongly affect their interactions with biological entities. For example, studies showed that discoidal NPs exhibit a better vessel wall interaction than spherical ones, with implications for particle binding and adhesion to endothelium [Gentile F et al., 2008; Dal Magro R et al., 2019]. Moreover, the shape strongly influences the circulation half-life, cellular uptake and barrier crossing of NPs [Geng Y et al., 2007; Champion JA and Mitragotri S 2009; Champion JA and Mitragotri S 2006].

NPs surface charge represents another design feature that can be tailored to prolong circulation lifetimes and selectively enhance and

accumulation at specific sites of interest [Blanco E et al., 2015]. It has been demonstrated that NPs with a neutral or negative surface charge have longer circulation half-lives compared to positively charged ones, because the latter have a higher rate of nonspecific uptake in the majority of cells and a higher affinity for serum proteins, thus promoting the elimination by RES [Alexis F et al., 2008].

Finally, NPs circulation lifetime is strongly affected by the formation of the so-called “protein corona”, consisting in the serum proteins absorption on the NPs surface.

The composition of the protein corona depends on the surface properties of NPs and it is also related to the route of administration [Masserini M, 2013; Blanco E et al., 2015]. The most common way to overcome or at least reduce the NPs protein corona formation is represented by the coating of NPs surface with specific molecules such as polyethylene glycol (PEG), a hydrophilic surfactant that forms a tight association with water molecules, reducing opsonization and the consequent NPs clearance [Saraiva C et al., 2016]. The improvement of NPs blood circulation time is also obtained by alternative strategies to the use of PEG, such as the coating of NPs surface with cellular membranes purified from leukocytes [Parodi A et al., 2013] or with membranes isolated from red blood cells [Hu CM et al., 2011]. However, in some circumstances the protein corona can be exploited as natural target delivery of NPs [Cox A et al., 2018].

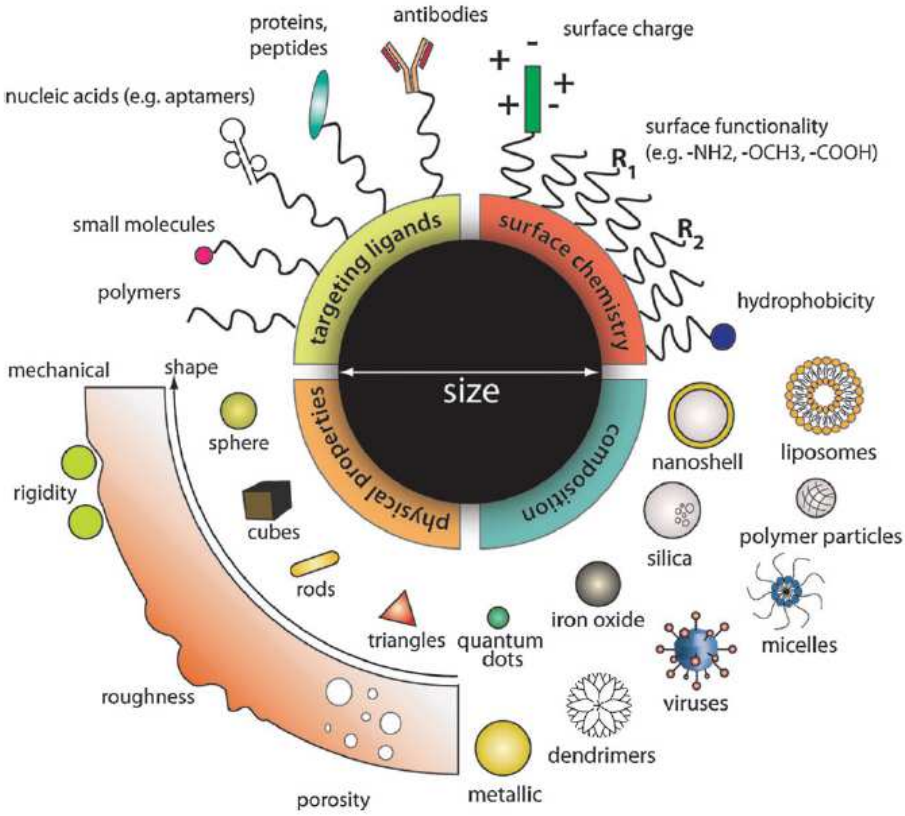

Fig. 8 The variety of NPs types, their features and functionalization ligands. NPs can be modularly assembled from different materials composition with different physical and chemical properties and functionalized with a myriad of ligands for biological targeting. Such flexibility in design freedom enables researchers to tailor nanoparticle for specific applications as contrast agents, drug delivery vehicles and therapeutics. From Chou et al., 2011.

1.2.2 Liposomes

Firstly described by Bangham and colleagues more than 50 years ago [Bangham AD, 1964; Bangham AD, 1974], liposomes are the first generation of nanocarriers used as drug delivery systems. The name

liposome derives from two Greek words: "*lipos*" meaning fat and "*soma*" meaning body.

Liposomes are spherical vesicles, composed by one or more phospholipid bilayers that surround an inner aqueous core. Due to their amphiphilic nature, lipids are arranged with their hydrophobic facing each other fatty acid chains tails buried in the interior, and the hydrophilic phosphate head group oriented to the interior and the exterior aqueous phases [Akbarzadeh A et al., 2013].

Lipids commonly included in liposomes composition are sphingomyelin, phosphatidylcholine, and other glycerophospholipids. Moreover, cholesterol, an important component of cell membranes, is frequently present in liposome formulations because it decreases the bilayer mobility and increases the stability of liposomes *in vivo* [Masserini M, 2013; da Cruz MT et al., 2004]. The choice of bilayer components makes the structure more or less rigid, also influencing the charge of the entire liposome. The saturated phospholipids with long acyl chains (for example, dipalmitoylphosphatidylcholine) determine a more rigidity and a rather impermeable bilayer structure, whereas unsaturated phosphatidylcholine species give much more fluidity and permeability to the structure.

According to the size and the number of layers (also reported as *lamellae*), liposomes can be classified as: i) small unilamellar vesicles (SUV) with one bilayer and a size up to 100 nm, ii) large unilamellar vesicles (LUV) with one bilayer and a size greater than 100 nm, and iii) multilamellar vesicles (MLV) made of concentric phospholipid spheres separated by layers of water, like an onion structure. Usually MLV are

the biggest ones and can reach a size of several μm [Masserini M, 2013].

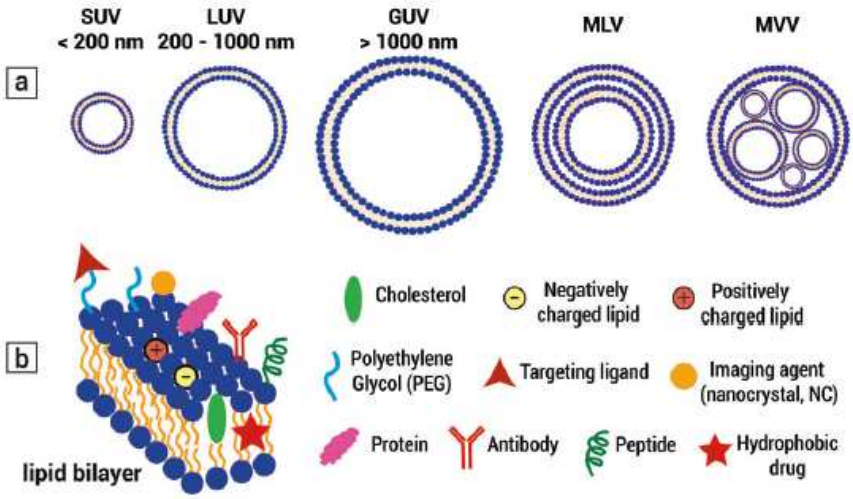

Fig. 9 Schematic representation of lipid-based vesicles. (a) Classification of vesicles regarding their size and lamellarity; (b) structure of the vesicle bilayer (left side) and examples of (bio)-actives to be physically encapsulated or chemically conjugated.

The vesicle size is a crucial characteristic that affect the circulation half-life of liposomes, and both size and number of bilayers influence the amount of drug encapsulation in the NPs.

Different methods have been described to synthesize liposomes. All the methods involve some basic steps consisting in: a) removal of organic solvents from lipids, in order to obtain a dry lipid film, b) lipid film re-hydration in aqueous media.

Liposomes can be prepared using handshaking, re-hydration and reverse-phase evaporation methods, followed by sonication, freeze/thawing cycles or extrusion to downsize the particles produced [Wagner A and Vorauer-Uhl K, 2011].

The choice of the appropriate preparation method depends on several factors, such as: 1) the physicochemical characteristics of the liposome components and those of the drug to be entrapped; 2) the toxicity and the concentration of the loaded substance; 3) additional processes involved in application/delivery of liposomes; 4) optimum size, polydispersity and shelf-life of the liposomes for the intended application and 5) batch-to-batch reproducibility and possibility of large-scale production and good manufacturing issues [Wagner A and Vorauer-Uhl K, 2011].

The lipid bilayer of liposomes is composed of biodegradable and biocompatible lipids, usually present in biological membranes. For this reason, liposomes are also used as plasma membrane models.

Due to their amphiphilic nature, liposomes can enclose both hydrophobic and hydrophilic compounds. Additionally, these nanoparticles are extensively used as carriers for numerous molecules in cosmetic, food and farming industries, and they are approved by FDA.

Liposomes have been widely investigated for systemic delivery of therapeutics. Many studies have been conducted on liposomal drug formulations with the goal of decreasing drug toxicity and improve the drug stability in the bloodstream and/or the targeting of specific cells.

1.2.3 Clinically approved NPs-based pharmaceuticals

To date, about 50 NPs-based pharmaceuticals, comprising lipid-, polymer- and protein-based NPs have been approved by the FDA and are available for use in clinical practice. Moreover, several other

nanoformulations are under clinical trials investigation [Weissig V et al., 2014; Caster JM et al., 2016; Ventola CL, 2017].

However, although the most of nanodrugs approved are directed to tumour treatment, they are also applied to a wide range of pathologies, from infections to autoimmune diseases.

Therapy modality	Generic name and/or proprietary name	Nanotechnology platform	Active pharmaceutical ingredients	Cancer type	Status
Chemotherapy: non-targeted delivery	Liposomal doxorubicin (Doxil)	Pegylated liposome	Doxorubicin	HIV-related Kaposi sarcoma, ovarian cancer, and multiple myeloma	Approved by FDA
	Liposomal daunorubicin (DaunoXome)	Liposome	Daunorubicin	HIV-related Kaposi sarcoma	Approved by FDA
	Liposomal vincristine (Marqibo)	Liposome	Vincristine sulfate	Acute lymphoblastic leukaemia	Approved by FDA
	Liposomal irinotecan (Onivyde or MM-398)	Pegylated liposome	Irinotecan	Post-gemcitabine metastatic pancreatic cancer	Approved by FDA
	Liposomal doxorubicin (Myocet)	Liposome	Doxorubicin	Metastatic breast cancer	Approved in Europe and Canada
	Mifamurtide (Mepact)	Liposome	Muramyl tripeptide phosphatidyl-ethanolamine	Nonmetastatic, resectable osteosarcoma	Approved in Europe
	Nab-paclitaxel (Abraxane)	Albumin NP	Paclitaxel	Breast, lung and pancreatic cancer	Approved by FDA
	SMANCS	Polymer conjugate	Neocarzinostatin	Liver and renal cancer	Approved in Japan
	Polymeric micelle paclitaxel (Genexol-PM)	Polymeric micelle	Paclitaxel	Breast cancer and NSCLC	Approved in Korea
	Liposomal cisplatin (Lipoplatin)	Pegylated liposome	Cisplatin	NSCLC	Phase III
	NK-105	Polymeric micelle	Paclitaxel	Metastatic or recurrent breast cancer	Phase III
	Liposomal paclitaxel (EndoTAG-1)	Liposome	Paclitaxel	Pancreatic cancer, liver metastases and HER2-negative and triple-negative breast cancer	Phase II
	Nab-rapamycin (ABI-009)	Albumin NP	Rapamycin	Advanced malignant PEComa and advanced cancer with mTOR mutations	Phase II
	CRLX-101	Polymeric NP	Camptothecin	NSCLC, metastatic renal cell carcinoma and recurrent ovarian, tubal or peritoneal cancer	Phase II
Chemotherapy: targeted delivery	MM-302	HER2-targeting liposome	Doxorubicin	HER2-positive breast cancer	Phase II/III
	BIND-014	PSMA-targeting polymeric NP	Docetaxel	NSCLC and mCRPC	Phase II
	MBP-426	TfR-targeting liposome	Oxaliplatin	Gastric, oesophageal and gastro-oesophageal adenocarcinoma	Phase I/II
	Anti-EGFR immunoliposomes loaded with doxorubicin	EGFR-targeting liposome	Doxorubicin	Solid tumours	Phase I
Chemotherapy: stimuli-responsive delivery	ThermoDox	Liposome	Doxorubicin	Hepatocellular carcinoma	Phase III
Chemotherapy: combinatorial delivery	Liposomal cytarabine–daunorubicin (CPX-351 or Vyxeos)	Liposome	Cytarabine and daunorubicin (5:1)	High-risk acute myeloid leukaemia	Phase III
	CPX-1	Liposome	Irinotecan and floxuridine (1:1)	Advanced colorectal cancer	Phase II

Table 3 List of some clinical-stage nanomedicines for cancer therapy from Shi et al., 2017.

The clinical approval of pharmaceuticals is a very long and expensive process: it takes about 10 years for a product, NPs-based ones included, to pass from its discovery to its approval and commercialization.

Furthermore, for NPs-based drugs this process sometimes is longer for some of the intrinsic features of NPs formulations.

Among others, their production on large scale can be a very limiting step, especially for multifunctionalized NPs, the multiple synthesis phases require continuous optimization, taking a lot of time.

Then many accurate *in vitro* and *in vivo* preclinical studies are needed to exclude the toxicity of the nanoformulation and to investigate its interaction with organs and tissues [Bozzuto G and Molinari A, 2015; Sercombe L et al., 2015].

Due to their biocompatibility and biodegradability, liposomes, in the form of Doxil®, a PEGylated liposomal doxorubicin formulation, were the first NPs-based drug approved by FDA in 1995, for the treatment of Kaposi's sarcoma in AIDS patients [James ND et al., 1994; Udhrain As et al., 2007].

Later, Myocet, a non-PEGylated liposomal formulation of doxorubicin, in combination with cyclophosphamide was approved for the treatment of metastatic breast cancer in Europe in 2000.

The driving force in the approval by FDA of drugs liposomal formulation is the reduction of side effects to normal tissues and the improvement of therapeutics bioavailability and stability.

1.2.4 Smart NPs for BBB crossing

The efficacy of therapies for CNS disorders is mainly limited by the presence of the BBB, but also by the dynamic force of cerebrospinal fluid (CSF) flow in the brain *interstitium* and by the complex cerebral cellular organization. These obstacles strongly contribute to the failure of targeted treatments for brain disorders.

The BBB is one of the most specialized biological barrier in the human body and represents a semipermeable structure that separates the circulating blood from the brain, guaranteeing its homeostasis [Daneman R et al., 2015].

The main components of this structure are: specialized microvascular endothelial cells, astrocytes end-feet, basement membrane, neurons, and pericytes. Some authors define the structure constituted by the set of these elements and microglia as "*neurovascular unit*" (NVU) [Keaney J et al, 2015].

The BBB endothelial cells (BECs), that maintain a very delicate equilibrium in the brain, differ from endothelial cells in the rest of the body by the absence of fenestrations, more extensive tight junctions (TJs), high expression of efflux transporters and sparse pinocytic vesicular transport [Ballabh P et al., 2004]. In order to ensure the integrity and tightness of the BBB, the brain capillary endothelial cells express specific proteins that form tight Junctions (TJs) and adherens junctions (AJs). The presence of TJs and AJs in the interconnected endothelial cells also prevent the passage of undesired molecules, neurotoxins and circulating cells [Luissint, AC et al., 2012]. TJs are complex units formed by different types of proteins such as claudins (1, 3, 5 and 12), occludin, zonula occludens proteins such as ZO1, ZO2 and

ZO3, and accessory proteins. AJs are constituted by cadherins, platelet endothelial cell adhesion molecule (PECAM1), and three junctional adhesion molecules JAMA, JAMB, JAMC [Masserini M., 2013; Saraiva, C. et al., 2016]. Many studies demonstrate that alterations in the structure and/or in the function of any of these proteins compromise the integrity and the functionality of the BBB, for example by facilitating paracellular diffusion through endothelial cells [Sweeney, MD et al., 2018; Zhou et al., 2018].

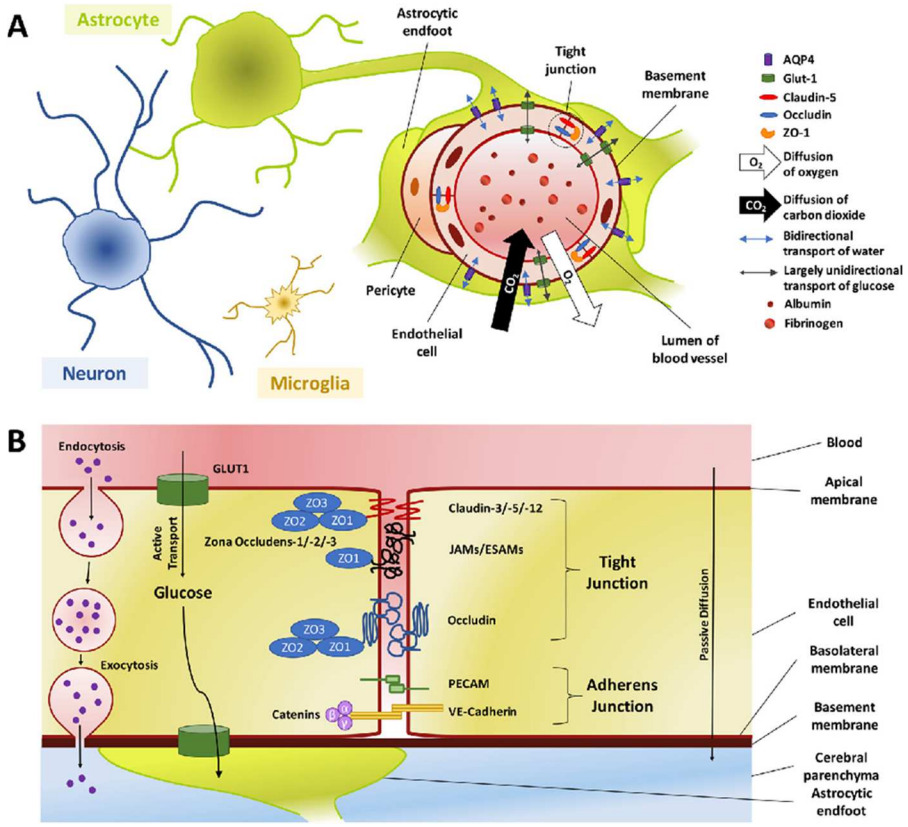

Fig. 10 (**A**) The neurovascular unit (NVU) is made up of numerous cell types including neurons, astrocytes, microglia, pericytes, and endothelial cells with the cells being arranged around cerebral blood vessels. The BBB is a complex involving endothelial cells, pericytes, endfoot processes from astrocytes, and the basement membrane. It allows for essential nutrients to pass into the cerebral parenchyma (e.g.

oxygen and glucose), removal of unwanted material (e.g. carbon dioxide), and limits access to the brain of potentially damaging molecules in the bloodstream (e.g. albumin, fibrinogen, and 98 % of drugs). **(B)** Transport across the BBB is limited by a number of mechanisms; active transcellular transport is controlled by specific transporter proteins in the endothelial cell membrane (e.g. glucose transporter-1, GLUT1) or endocytotic processes, but passive diffusion of lipophilic molecules is also possible, particularly at low molecular weights. Paracellular transport is limited by the protein complexes composing the tight and adherens junctions found between the endothelial cells. AQP4=Aquaporin- 4; ESAMs=endothelial cell-selective adhesion molecules; GLUT1=Glucose transporter-1; JAMs=Junctional Adhesion Molecules; PECAM=Platelet Endothelial Cell Adhesion Molecule; VE-Cadherin=Vascular Endothelial Cadherin; ZO=Zonula Occludens. From Kealy J., 2018.

In spite of this well organized fenced structure, to some selected molecules is given the chance of crossing by paracellular or transcellular mechanisms. The latter is finer regulated and includes: i) simple diffusion, ii) carrier-mediated transport (CMT), iii) adsorptive-mediated transcytosis (AMT), iv) active efflux and v) receptor-mediated transcytosis (RMT) as shown in figure 10.

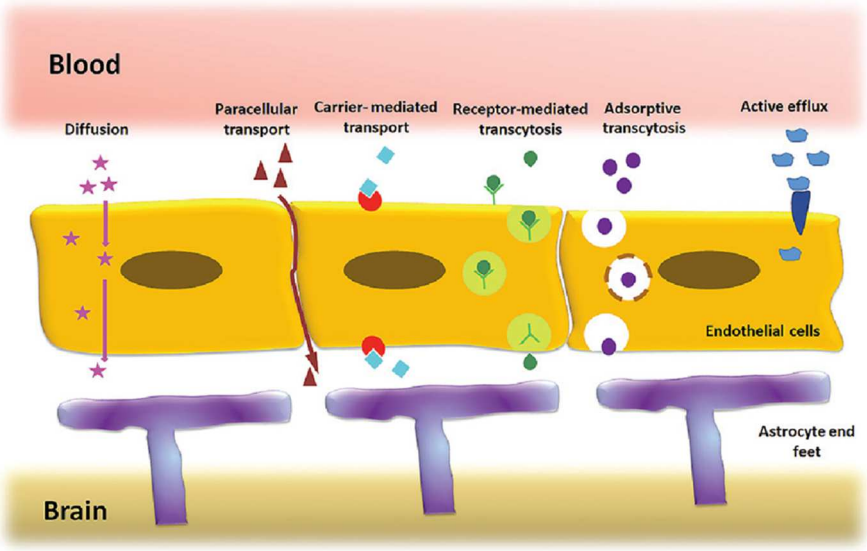

Fig. 11 Transport pathways of endothelial cells in the BBB. From N. Poovaiah et al., 2018

It is well known that hydrophobic compounds with a molecular weight around 400–600 Da and with at most 8–10 hydrogen bonds can passively diffuse across the BECs membrane lipid bilayer. This dimension limit is lower for hydrophilic molecules, which can only cross the BBB if they are <150 Da [Pardridge WM., 2015]. On the other hand, most anticancer drugs, proteins, antibodies and antibiotics are normally excluded unless their transport is mediated by channels, transporters or membrane receptors.

The CMT is the route for vitamins, hormones, carbohydrates, fatty acids, organic anions/cations, and nucleotides to cross the BBB. CMT also facilitates CNS-to blood clearance of excitatory aminoacids as aspartate and glutamate [Ceña V and Játiva P, 2018].

AMT is one of the strategies used for brain drug delivery, which is triggered by electrostatic interaction between cationic molecules and anionic microdomains on the membrane of the BECs. In this context, a lot of research was focused on the use of basic oligopeptides and cationic proteins, such as cell-penetrating agents [Foged C and Nielsen HM, 2008].

At the BBB level, the delivery of several drugs is reduced by efflux pumps like glycoprotein-P (PgP), ATP-binding cassette transporters (ABC), and multidrug resistance proteins. When these efflux pumps are physiologically impaired, due to either aging or a pathological condition, brain influx of certain drugs can increase, potentially leading to CNS toxicity.

Noteworthy, also selected large MW molecules can cross the BBB by RMT or caveolar-based internalization. Proteins such as apolipoproteins, insulin, transferrin and α2-macroglobulin cross the

BBB by RMT in both directions, while some viruses use *caveolae* to enter cells.

It should be pointed out that RMT and caveolar trafficking are able to carry large entities across the BBB, differently from the other mechanisms above described. This feature makes them particularly interesting for pharmacology and nanomedicine, thus they have received much attention in the last years [Broadwell RD, 1989; Muro S et al., 2004].

As a consequence, an arsenal of nanostructures differing for chemical composition, size, shape and physicochemical features has been generated to cross the BBB and to target different molecular mechanisms.

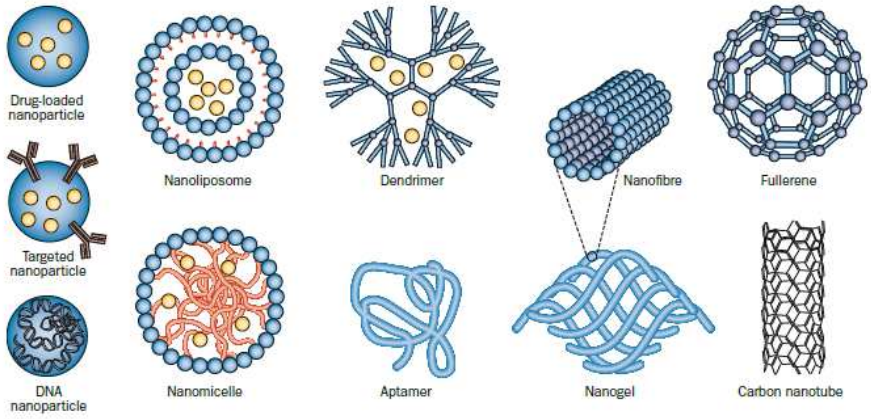

Fig. 12 Types of nanostructures commonly used for BBB crossing. From Srikanth, M. & Kessler, 2012.

Among others, polymer based NPs (poly (lactide-co-glycolides) PLGA NPs, dendrimers), lipid-based NPs (solid lipid NPs, liposomes, niosomes) and naturally circulating NPs (extracellular vesicles, exosomes) are the most intriguing tools, potentially able to solve the

unmet problem of enhancing drug transport across the BBB [Masserini M, 2013].

Polymeric NPs, solid carrier vehicles made from natural or synthetic polymers that form a core in which pharmaceuticals can be incorporated, have been widely investigated and used for drugs BBB crossing and CNS pathologies treatment, for their biodegradability and their extended half-life in the bloodstream [Crucho C.I.C. et al., 2017]. To this purpose, Falanga et al. produced a PLGA-polyethylene glycol (PEG) co-polymer (PELGA) nanosystem functionalized with a cell penetrating peptide gH625 and a cyclic iron-mimicking peptide CRTIGPSVC (CRT) used as RMT-targeting ligand. *In vitro* experiments demonstrated that these bi-functionalized NPs are potentially able to cross the BBB, escaping endo-lysosomal entrapment [Falanga AP et al., 2018].

In another work from Sánchez-López et al., memantine, a drug approved for moderate to severe AD has been incorporated into PLGA NPs surface-coated with PEG. These NPs were able to cross the BBB *in vitro* and *in vivo* without exerting toxicity on BBB cells [Sánchez-López et al., 2018].

One of the most recent study directed by investigates the role of novel mixed surface dendrimers in *in vivo* BBB crossing of C57BL/6J mice when injected through the carotid artery, suggesting their potential use to deliver drugs and/or biomolecules and to selectively target neurons [Srinageshwar B et al., 2017].

Moreover, Łukasiewicz S. and co-workers investigate the interaction of 100 nm clozapine-loaded polymeric nano capsules (CLO-NCs) with the BBB *in vitro* model hCMEC/D3. Results indicate that these pegylated

clozapine-loaded NCs were the most efficient in the transcytosis experiments and the less toxic to hCMEC/D3 cells [Łukasiewicz S. et al., 2017].

In a work of Song H. and colleagues, borneol-modified solid lipid nanoparticle (SLNs) to target brain have been proposed. *In vitro* and *in vivo* studies demonstrated that the chemical modification of SLNs with borneaol improved the BBB permeability while maintaining a lower cytotoxicity, a higher cell uptake and a good targeting ability [Song H. et al., 2018].
Similar findings have been obtained by Dal Magro R. e al. In their work, SLNs modified with a fragment of the human apolipoprotein E (namely SLN-mApoE) were able to cross intact a BBB *in vitro* model, exploiting different administration routes to reach the brain. [Dal Magro R et al., 2017]

Liposomes have been extensively proposed for the treatment of neurodegenerative disorders like AD and different types of cancers.
In an *in vivo* study performed by Papadia K. et al. 2017, multifunctional liposomes, decorated for BBB and Aβ targeting, resulted very effective on APP/PS1 mice. Moreover, the incorporation of a near IR fluorescent probe, gave the possibility to conduct *in vivo* live imaging, highlighting the BBB crossing and the theranostic potential of these nanoparticles.
Moreover, in a previous work, Mancini S. et al., showed the ability of liposomes bi-functionalized with phosphatidic acid and with an ApoE-derived peptide to withdraw amyloid peptides from the brain, after BBB crossing both *in vitro* and *in vivo* [Mancini S. et al., 2016].

Regarding extracellular vesicles and exosomes, virtually all brain cells are able to secrete them, including neurons, astrocytes, microglia and oligodendrocytes. They contribute to intercellular communication into the brain through their basal release and uptake by surrounding cells, or release into the CSF and blood, both in physiological and in pathological conditions. Moreover, several studies showed that exosomes are endowed of a good capability to cross the BBB [Rufino-Ramos D et al., 2017]. For instance, the group of Yang T. proved that exosomes released from BECs are able to deliver doxorubicin and paclitaxel into the brain after BBB crossing in a zebrafish model [Yang T et al., 2015].

However, further investigations are needed to better understand the exosome targets and exchange mechanisms between NVU cells.

1.3 Nanomedicine for the treatment of Glioblastoma Multiforme

1.3.1 Drug delivery strategies for GBM

In order to obtain a more efficient delivery of drugs for GBM treatment, many strategies have been proposed over the years:

One of these involved the TJs opening, by using chemicals or physical modalities such as mannitol, sodium dodecyl sulphate and polysorbate 80, or electromagnetic waves and ultrasounds respectively. Although the temporarily and reversibly disruption of the BBB by opening the TJs resulted a promising method to increase drug delivery to GBM and other brain disorders, many drawbacks associated to this technique have been reported. Some of them involve the possibility of tumour

spreading to the periphery and/or the exposure of the brain to neurotoxins present in bloodstream. For these and other reasons, this technique remain poorly exploited [Reatul Karimet et al., 2016].

Another strategy to improve drug delivery to GBM take into account the inhibition of efflux transporters such as P-gp and ABC family members [Kabanov AV et al., 2003**;** Kuntner C et al., 2010]. Since they are directly involved in avoiding drug entrance into the brain, some studies focused their attention on their inhibition, in order to improve the drugs concentration into the brain, without affecting the BBB integrity. However, this strategy is very challenging and further investigations are needed to obtain clinical tranferable results.

On the other hand, the chemical modification of the drug to produce a more lipophilic prodrug can be used to increase the BBB crossing and the tumour delivery [Gabathuler R, 2010]. Despite some evidences, it is important to consider that increase the lipidic nature of the drug may also enhance the nonspecific uptake of the pharmaceutical molecule by other tissues, thus reducing its specificity and therefore increase its toxic effects.

A brain drug delivery strategy that allows the local distribution of a significant amount of highly concentrated therapeutic molecules with very low systemic effects is the convection-enhanced delivery technique. In this delivery modality, a catheter, connected to a syringe pump, is placed in the tumour tissue and the drugs are administered continuously under positive pressure through it. Despite the advantages of this technique, its use is limited for the risk of drug release in healthy brain tissue and the consequent reduction of the therapy effectiveness [Allard E et al., 2009].

The drug delivery strategy that has gained huge research attention for the treatment of GBM, over the last few decades, requires the use of nanocarriers.

1.3.2 NPs for GBM treatment

Despite the efforts to develop innovative therapeutics for GBM, the complexity and heterogeneity of this pathology strongly contribute to the failure of the desired outcomes.
The raising search of new strategies for enhancing the treatment efficiency and the prognosis of the disease includes nanomedicine and the use of NPs and various nanocarriers.
Moreover, the advancements in nanotechnology of the last decades may contribute to the development of new treatments or to the improvement of existing therapies [Ortiz R et al., 2019].
In the case of GBM, it is also necessary to search for target molecules to cross the BBB and the blood–brain tumor barrier (BBTB) for the selectively reaching of the tumour mass and GSCs.

Among all the NPs, lipid based, polymer-based, dendrimers, albumin, chitosan and silica NPs have been the most widely studied as therapeutic agents carriers for GBM. Herein below some examples of recent applications of these types of nanoparticles.
Considering the lipid-based NPs, liposomes have been widely used to achieve targeted drug delivery to GMB cell lines, tumour-bearing mice and human tumour-derived neurospheres. On the other hand, lipid nano

capsules have been used to interfere with GBM signalling pathways [Játiva P and Ceña V, 2017].

In this context, the most common approach consists in decorating the liposomes surface with targeting peptides in order to increase selective uptake and to enhance their targeted delivery ability.

Functionalized liposomes have been also used: i) to target compounds of the extracellular tumor environment [Zhao Y et al., 2016], ii) to target overexpressed proteins and receptors [Shein SA et al., 2016], iii) as siRNA vectors [Yang ZZ et al., 2014].

For example, in the study proposed by Ying M. and co-workers, a more sophisticated drug delivery system to target BBB, blood-brain tumour barrier (BBTB), and glioma cells has been described. In this work PEGylated liposomes were modified on the surface with two D-peptides (DCDX and DA7R-LS) and the efficacy of DCDX- and DA7R-LS-liposomes in crossing the BBB/BBTB and targeting glioma cells, were assessed both *in vitro* and *in vivo*. Furthermore, when loaded with DOX, a high anti-tumour effect of these D-peptides modified liposomes was observed in nude mice bearing intracranial U87 glioma cells, indicating these NPs as a promising strategy to advance chemotherapy [Ying M et al., 2016].

Moreover, some groups investigate the simultaneously use of different strategies. To this purpose Yang F.Y. et al., combined focused ultrasounds and interleukin-4 receptor-targeted DOX loaded liposomes for the treatment of GBM8401 cell-derived tumour-bearing mice, and the results showed an increased survival rate of the treated mice. [Yang FY et al., 2012].

The other type of lipid-based NPs, developed and extensively used to deliver both antitumor drugs and nucleic acids to GBM cells, with quite promising results, is represented by SLNs [Battaglia L et al., 2014**;** Battaglia L et al., 2015**;** Kuo YC et al., 2016].

In this context the work of Jin J. et al., presented the high therapeutic potential of c-Met siRNA loaded SLNs to target and affect the tumour *in vivo* [Jin J et al., 2011].

Another promising approach has been proposed by Wu M. et al., for the dual delivery of two chemotherapeutic drugs, vincristine and TMZ, with SLNs [Wu M et al., 2016].

PLGA NPs are another type of synthetic NPs that have been widely used in the fields of tissue engineering, medical imaging, diagnosis and drug delivery, as carriers for both hydrophobic and lipophilic pharmaceuticals.

Due to their biocompatibility and biodegradability a high number of studies have outlined the usefulness of PLGA NPs for GBM treatment. In this context monomethoxy-PEG (mPEG)-PLGA NPs have been used for co-delivery of paclitaxel and TMZ to U87 and C6 glioma cells, achieving better results in inhibiting growth and inducing apoptosis, both *in vitro* and *in vivo*, when compared to the use of the free drugs [Xu Y et al., 2016].

Moreover, DTX-loaded PLGA NPs have shown an increased penetration ability into C6 GBM cell spheroids and improved survival rates in C6 glioma-bearing nude mice, as compared with free DTX [Kang T et al., 2015].

In another work Tamborini et al., proposed a nanovehicle composed of silver NPs entrapped in PLGA NPs conjugated to chlorotoxin, a peptide

reported to selectively target glioma cells. Combining these functionalized PLGA NPs with X-ray irradiation, they obtained an efficient antitumor synergistic effect able to inhibit *in vivo* tumor growth [Tamborini M et al., 2016].

Albumin NPs have been considered useful drug carriers for their high biocompatibility and the lack of toxicity and immunogenicity.
Recently, Ruan et al. developed effective albumin-based NPs loaded with paclitaxel and functionalized with a ligand for neurokinin-1, which is overexpressed in tumours like GBM. The *in vivo* results showed that these NPs display a greater accumulation at the tumour site, associated with a higher antitumor effect and a low systemic toxicity [Ruan C et al., 2018].
Moreover, Byeon HJ et al., have been reported that mannose-modified albumin NPs markedly reduce (more than 15 fold) the IC50 for DOX in U87-MG cells [Byeon HJ et al. 2016].

Several studies on GBM focused their attention on dendrimers-based NPs. Although some of them showed a lower tumour growth in treated animals as compared with non-treated ones, several issues on their cytotoxicity are still open [Tomalia DA et al., 2012; Kannan RM, et al., 2014; Mukherjee SP et al., 2010].

In an attempt to achieve an improvement of drugs lifetime and a successful targeted delivery, the use of NPs composed of biopolymers such as chitosan has been investigated. For example, CTX coated chitosan NPs have been used to deliver TMZ to GBM cells, significantly increasing its half-life at a physiological pH, as compared

with the free drug, and achieving at least a twofold reduction in the IC50 as compared with the NPs not containing CTX [Fang C et al2015].

Another type of NPs used to deliver antitumor drugs to GBM cells both *in vitro* and in xenograft models, are silica-based NPs.
In this context the work of Li ZY et al., demonstrated an almost 80% decrease in cell viability in U87-MG treated with camptothecin-loaded and DOX-conjugated mesoporous silica NPs (MSNs) [Li ZY et al. 2013].
In another paper Goel et al., used an anti-VEGFR ligand loaded into PEGylated MSNs to effectively treat U87-MG GBM-bearing mice. [Goel S et al., 2014].
However, more research is needed in this area, to better understand the behaviour and the toxic effect of silica NPs with regard to tumour and healthy CNS cells.

1.4.1 In vitro model of the BBB

In the early 1970s the isolation of endothelial cells from brain capillaries started [Joó F and Karnushina I, 1973]. These intact and almost pure brain capillaries endothelial cells (BCECs) were firstly obtained through a combination of mechanical homogenization of brain tissue and sucrose gradient centrifugations. Then the isolation techniques were modified including filtration steps, which guaranteed improvements in the final product.
BCECs were widely used to study the BBB properties such as tight junction integrity, transport mechanisms and molecular pathways [Czupalla CJ et al., 2014].

Different BBB *in vitro* models are available from decades and are based both on animals (mouse, pig, bovine, rat) and on human endothelial cells [Dehouck MP, et al., 1990; Patabendige A et al., 2013; Burek M et al., 2012; Cecchelli R,ì et al., 1999; Helms HC et al., 2016; Cecchelli R et al., 2014].

BCECs from non-human origin have provided many information on the physiology and pathophysiology of the BBB and have allowed very valuable cross-validation between models.

Instead, the human brain tissue is difficult to obtain, thus limiting the development of primary cultures of human brain endothelial cells However, some different groups established and characterized immortalized human brain capillary endothelial cells [Weksler BB et al., 2005; Stins MF et al., 2001] allowing a deeper understanding of the cellular and molecular mechanisms underlying BBB establishment and functions.

The Risau group published the first work using mouse brain endothelial cell lines, generated by immortalization with Polyoma middle T antigen. bEND.5 and bEND.3 are commercially available cell lines based on this immortalization strategy [Wagner EF and Risau W, 1994]. Forster et al. produced alternative cell lines, namely cEND and cerebEND, from mouse cerebral and cerebellar capillaries, respectively. Both cell lines form monolayers and show spindle-shaped morphology [Burek M et al., 2012; Forster C et al., 2005; Silwedel C and Forster C, 2006].

Considering monolayer integrity parameters, bEND.5 and bEND.3 generally display low TEER (around $50\,\Omega\,cm^2$), while cEND and cerebEND cell lines showed TEER varying from 300 to $800\,\Omega\,cm^2$ and

strong occludin and claudin-5 expression at the tight junctions [Omidi Y et al., 2003; Steiner O et al., 2011].

Since rat brains were the first source of BCECs for development of BBB models [Joó F and Karnushina I, 1973] many studies were conducted on these cells, but their use were abandoned soon due to the impossibility to remove contaminating pericytes [Abbott NJ et al 1992; Szabo CA et al., 1997]. Rat models generally display low to medium TEER (around 100–300 $\Omega\,cm^2$) depending on the culture method. Moreover, the rat models have been shown to express the most common tight junction proteins such as claudin-5, occludin and ZO-1 [Calabria AR, et al., 2006; Cardoso FL et al., 2012].

During the years, efforts have been made to create alternative models based on human immortalized brain endothelial cells or human-derived stem cells [Weksler BB et al., 2005; Lippmann ES et al., 2012; Boyer-Di Ponio J et al., 2014].

The most widespread and well characterized of the published human immortalized brain endothelial cell lines is the human Cerebral Microvascular Endothelial (hCMEC/D3) cell line [Weksler B, et al., 2013].

More than 150 publications have applied and further characterized the hCMEC/D3 cell line: in the first passage, these cells were sequentially immortalized by lentiviral vector transduction with the catalytic subunit of human telomerase (hTERT) and SV40 large T antigen.

The hTERT/SV40-immortalized hCMEC/D3 clonal cell line is derived from human temporal lobe microvessels isolated from tissue resected during surgery for epilepsy [Helms HC et al., 2016].

This cell line shows a spindle-shaped, elongated morphology similar to primary cultures of brain endothelial cells, and forms contact-inhibited monolayer of elongated cells on collagen type I or type IV.

Moreover, hCMEC/D3 expresses junction-associated IgG-like proteins such as PECAM-1 and JAM-A, adherens and tight junction structural proteins such as VE-cadherin, claudin-3, claudin-5 and occludin, scaffolding proteins such as β-catenin, ZO-1 and ZO-2 as well as the cell polarity complex Par-3/Par-6/PKCz, which further contributes to the control of tight junction integrity and apical-basal polarity [Kroll S et al., 2009; Wedel-Parlow MV and Galla H. 2010; Artus C, et al., 2014].

Since the expression level of claudin-5, which is important for junctional tightness, has been reported to be lower in hCMEC/D3 than in intact microvessels, the TEER of this cell line is in the range of 30–50 $\Omega\,cm^2$ [Urich E et al., 2012].

For its characteristics, the hCMEC/D3 cell line represents an easy to use, thoroughly characterized model of human origin, which appears particularly well suited for drug uptake studies [Bernard SC et al., 2014]. However, an optimization in culture condition to improve the tightness of the monolayers formed by the hCMEC/D3 cells to perform mechanistic studies, represents a still open challenge in this field.

Recently, human brain endothelial cells have been also obtained from stem cell sources, including human pluripotent stem cells (hPSCs) [Lippmann ES et al., 2012]. These renewable sources for human BBB models offer the opportunity to study the signalling pathways involved in the interacting cells of the neurovascular unit (NVU) and the dynamic

changes that may occur during the BBB development. [Boyer-Di Ponio J et al., 2014; Cecchelli R et al., 2014; Lippmann ES et al., 2014]
Moreover, with the hPSC system it would also be possible to recreate a more realistic model of a diseased NVU, using endothelial and neural cells derived from patients.

1.4.2 In vitro models of GBM

Considering the already widely explained GBM inter- and intra-tumoral heterogeneity, the seek for a model that reflects the main characteristics of the disease is a still open need [Da Hora CC, et al., 2019; Robertson FL, et al., 2019].
In the last 30 years, the high demand for readily available and relevant cell models of GBM generated several GC lines, including U87-MG, which is the most popular one with about 2000 citations in PubMed, but also U251, T98G, LN18 and A172, among others.
These cell lines have been employed extensively in both *in vitro* and *in vivo* research on GBM, providing valuable knowledge about this type of tumour [Le Mercier M et al., 2009].
The invasive potential of U87-MG cells is higher as compared to other GBM cell lines such as U-118, and for this and other reasons researchers focused their attention on it.
The U87-MG cell line is a morphologically heterogeneous line, which contains two different cell types: adherent cells and small spherical cells forming aggregates [Urbanska K and Mandal CC, 2014]. This cell line

was originally derived from a Caucasian man tumour, resected and characterized by Ponten et al in 1975.

The U87-MG is a hypodiploid cell line, with the modal chromosome number of 44 occurring in 48% of cells and genome analysis have identified different classes of genetic mutations including insertions/deletions, translocations and single-nucleotide variations [http://www.lgcstandards-atcc.org].

Moreover, U87-MG cells express a wild-type TP53 and synthesize the mutant form of the tumour suppressor PTEN protein, which play a key role in proliferation, angiogenesis and resistance to apoptosis [Cerrato JA et al., 2001; Jacobs VL et al., 2011].

Glioma cell lines derived from human counterparts, such as U87-MG cells, are widely used as pre-clinical model in *in vitro* studies, to test the cytotoxic activity of antitumor agents, nanoparticles and plant extracts included. On the other hand, many studies focused on proliferation, migration, invasion, chemoresistance or radioresistance of this cell line [Agrawala PK et al., 2009; Xin H et al., 2012; Ye L et al., 2014].

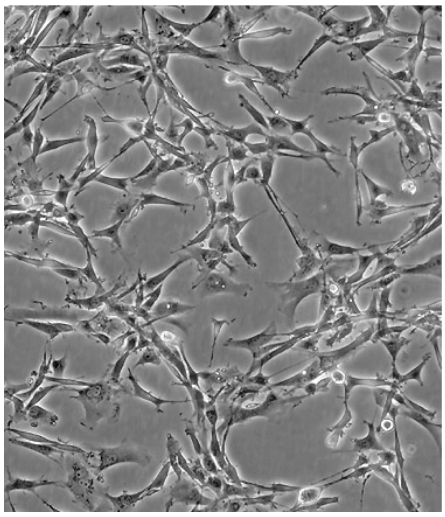

Fig 13 U87MG cells

An in vivo mature GBM tumour has a very complex structure, generally consisting of regions of regularly dividing cells, hypoxic cells, and necrosis, at increasing distances from blood vessels [Zhang X et al 2005; Becher OJ et al., 2006].

Since the high complexity of GBM, models reflecting its structural, morphological and physiological heterogeneity are needed. In this context, many efforts have been done to create three dimensional models such as spheroids to better mimic the tumour microenvironment, the 3D cells architecture and the complex interactions that exist between the tumour and its host [Dufau I et al., 2012].

U87-MG cells usually generate tight spheroids, with excellent reproducibility and a quite long lifetime (up to 14-days) [Urbanska K and Mandal CC, 2014].

However, a halo of mystery surround the U87-MG cell line.

The authors, whose laboratory developed the cell line almost 50 years ago, compared the genetics of this cell line (obtained from ATCC) with those of the original tumour, and the DNA profile of the current cell line worldwide used for research on gliomas is different from that of the original cells. Therefore, the genomic analysis confirmed that the U87-MG is likely to be a human glioblastoma cell line but with unknown origins [Allen M et al., 2016].

There are several non-human GBM cell lines available, which are derived from animals such as rats and mice. The most common ones are the CNS-1 and C6 from rat and GL261 from mice, but these are chemical induced glial tumours, not spontaneous.

However, all the human-derived and the non-human-derived GBM models are imperfect for several reasons and present some drawbacks. The first drawback is due to the fact that the serum-containing medium in which these cell lines are grown alters both their transcriptomes and genomes and determines a depletion of stem-like tumour cells [Lee J et al., 2006]. Secondly, intracranial injections of these cell lines into the brains of mice rarely develop tumours with the GBM morphological features [Lee et al., 2006; Mahesparan R et al., 2003]. The third issue is the lack of a clinical characterization of the tumours derived from these cell lines, that makes impossible a correlation between these models and patients-derived tumours [Yuan Xie et al., 2015].

In this context, glioblastoma stem-like cells (GSCs) may represent a solution to overcome all the issues presented by GBM cell models.

GSCs have been recognized as tumor-initiating cells, and are the main actors in the mechanisms of tumour invasion/migration, recurrence, and therapeutic resistance [Balvers RK et al., 2017].

During the years, different GSCs have been characterized. For example, some patient-derived GSCs, such as GBM8 and GBM6, showed a butterfly-like growth pattern, a well-known characteristic of GBM, spreading from one brain hemisphere to the opposite one *via* the corpus callosum. Moreover, the GBM8-based model also tend to expand alongside the subventricular areas, leading to a compression of the lateral ventricles.

All GSCs lines were able to show histological hallmarks of the original tumours, including necrosis, invasiveness, and increased angiogenesis, thus representing the most suitable models to investigate the effect of novel therapies [Bao S et al., 2006; Wakimoto H et al., 2009].

1.4.3 Animal models of GBM

Preclinical mouse models are essential for many reasons such as analysing the biology of GBM, identifying new molecular targets, and evaluating the effectiveness of new therapeutic strategies. Nowadays the preclinical GBM models are classified into three categories: xenografts, genetically engineered mouse (GEM) models, and syngenic murine models.

Moreover, GBM xenografts are also divided into two categories: glioblastoma cell line-derived xenografts (CDX) and patient-derived xenografts (PDX). [Kijima N and Kanemura Y, 2017]

GBM CDX were usually obtained after intracranial injection of commercially available human GBM cell lines (such as U87-MG, U251, T98G, among others) into immunodeficient mice like

NOD/SCID mice and NOD/SCID gamma mice, or with rat C6 glioma cells in Wistar rats or in C57BL/6 mice (allograft models) [Babu PP, and Deshpande RP, 2018].

Many studies revealed high engraftment rate, good reproducibility, and reliable disease growth and progression of GBM CDX [Huszthy PC et al., 2012]. On the other hand, some evidences suggested that GBM CDX do not properly reflect the clinical characteristics of the original patient tumour [Martens T et al., 2008]. In particular, these tumours are usually circumscribed and do not show single-cell invasion. Moreover, some differences were observed in the major histocompatibility complex (MHC) expression and in the immune response, suggesting that the xenografted tumours were not phenotypically identic to the original patient tumour [Anderson RC et al., 2002].

These disadvantages raise the doubt on the use of GBM CDX in preclinical trials.

For these reasons GBM research recently focused on PDX, a model with the advantage of retain both the genetic and histological features of the primary tumour from which it was derived [Jin K et al., 2010; Hidalgo M et al., 2014]. Moreover, the cells of these models did not show stresses signs than normally arise in CDX models [Daniel VC et al., 2009; Fichtner I et al., 2008].

PDX models are generally obtained by ortothopic injection of glioblastoma tumour spheres, produced under serum-free culture conditions, into immunodeficient mice brain. This technique allow the maintenance of the patient's original tumour features, molecular profile and tumorigenicity included [Chen R et al., 2010]. Other studies also revealed the preservation of single-cell invasion ability and tumour

angiogenesis in PDX models [Günther HS et al., 2008; Wakimoto H et al., 2012]. For its wide range suitability, PDX models are expected to be a pillar in the future of translational GBM research, from studies on signalling pathways to innovative therapies tests.

GEM models are usually obtained by gene expression manipulation using Tet-regulation or Cre-inducible gene alleles to overexpress or inactivate specific genes in defined cells. Moreover, GEM models can be established by somatic-cell gene transfection, using retroviral or adenoviral vectors, as in the RCAS/Tva system [Federspiel MJ et al., 1994].
GBM GEM models play a pivotal role in the study of genetic alterations involved in tumour initiation and progression and for this reason are also useful for targeted pharmaceuticals testing.

Syngenic GBM mouse models have long been used as indispensable tools for research on this disease.
GL261 models among others are the most extensively used syngenic GBM mouse model. These models are reported to recapitulate the main GBM histologic and biological features. Furthermore, since these models require the use of immunocompetent mice, they turned out to be very suitable for analysing GBM tumour immunology and for immunotherapeutic research [Kijima N and Kanemura Y, 2017].
Despite the benefits coming from the use of all the animal models above mentioned, it is important to highlight that the heterogeneity of GBM and the intrinsic differences between humans and animals could sometimes limits their use.

In table 4 a summary of the characteristics of currently available mouse models of glioblastoma, underlying their advantages and disadvantages.

Characteristics of Each Glioblastoma Mouse Model

Model	Advantage	Disadvantage
Cell-line xenograft	High engraftment and growth rates Good reproducibility Reliable disease growth and progression	Does not recapitulate genetic and phenotypical feature of original tumor Need to use immunodeficient mice
Patient-derived xenograft	Recapitulate genetic and phenotypical feature of original tumor	Relatively low engraftment and growth rates Need to use immunodeficient mice
Genetically engineered mouse model	Identify the molecular events responsible for tumor initiation and progression Analyze the role of the microenvironment	Does not completely reflect the intratumoral genomic and phenotypic heterogeneity Tumor initiation cannot be controlled
Syngenic mouse model	Suitable for tumor immunity and immunotherapeutic research	Might be different from human glioblastoma

Table 4 Different types of GBM mouse models.

1.5 Premises for the thesis

1.5.1 mApoE modified liposomes for BBB crossing

In the context of GBM treatment, the main hurdles to overcome are represented by the presence of the BBB that is intact in the brain region where GSCs are infiltrating and by all the driving forces of tumour formation and progression, like the high invasiveness and proliferation rates and resistance to radiation and chemotherapy.

To potentially answer these issues, liposomes (LIP) composed of sphingomyelin (Sm) and cholesterol (Chol), embedding the

chemotherapeutic drug doxorubicin (DOX) and functionalized with a modified peptide derived from the receptor-binding domain of Apolipoprotein E (mApoE) were proposed.

Liposomes composed of a matrix of Sm and Chol in equimolar ratio have been widely used both *in vitro* and *in vivo* for therapeutic purposes, displaying good circulation times in blood, biocompatibility, resistance to hydrolysis, low ion permeability [Webb MS et al., 1995; Thomas DA et al., 2006; Re F et al., 2011].

In the searching for a strategy to cross the BBB, the attention was focused on the low-density lipoprotein receptor (LDLr)-mediated pathway (Cerletti et al., 2000; Markoutsa et al., 2011). LDLr is present on capillary endothelial cells of several species and its expression is upregulated in the BBB with respect to other endothelia [Dehouck et al., 1994; Malcor JD et al., 2012]. Moreover, the presence of LDLr was also reported on GBM cells indicating the potential of this receptor to be exploited for both BBB crossing and tumour targeting [Joo KM et al., 2013; Villa GR et al., 2016; Guo D; et al., 2011].

In particular, NPs interacting with the LDLr via a specific apolipoprotein E (ApoE) amino acid sequence (corresponding to the binding domain of the ApoE, aa. 141-150) were shown to be transported across the BBB by transcytosis, bypassing the lysosomal degradation [Dehouck et al., 1997].

In order to exploit the LDL-r pathway, the sequence corresponding to residues 141-150 of human ApoE, modified with the attachment of the three aminoacid residues (CWG sequence), CWG-LRKLRKRLLR, was attached at high density (2.5 mol%) as a monomer to Sm/Chol liposomes. The mApoE binding on LIP surface was obtained by using

the thiol-maleimide covalent coupling by exploiting the cys of the peptide and a maleimide-modified lipid (DSPE-PEG2000-MAL) as already reported [Salvati E et al., 2013].

The functionalization of LIP with mApoE increased the uptake of non-functionalized NPs by endothelial cells and enhanced the transport of a drug payload through the BBB *in vitro* as already demonstrated [Re F. et al., 2011].

Taken together, the results obtained by other researchers of the group I belong to, laid the foundations for the use of mApoE- LIP for the *in vivo* BBB crossing and pave the way to test them for GBM treatment.

1.6 Scope of the thesis

GBM is one of the most challenging malignancies to treat in the entire oncology field.

Despite advances in cancer therapies, nanomedicine approaches included, the treatment of GBM remains inefficient. These failures are likely attributable to a) the complex, and not yet completely know, biology of this tumour, which is responsible for its strong invasiveness, high proliferation rates and resistance to radiation and chemotherapy, and b) the presence of the BBB that limit the drugs entrance into the brain.

Moreover, the intimate connection through which the cells communicate between them plays an important role in these biological processes. In this scenario, tunneling nanotubes (TnTs) are recently gaining importance as a key features in tumor progression and in particular in the re-growth of GBM after surgery.

GBM Stem-like Cells (GSCs) represent a subpopulation of cells characterized by increased resistance to chemo- and radiotherapy (RT). Due to their intrinsic tumor-initiating potential and invasiveness, residual resistant GSCs lead to GBM recurrence and progression and represent a crucial target for effective therapies. However targeting GSCs is hardly difficult and complex, due to the presence of the BBB and for GSCs infiltrative nature arousing their dispersion within the brain parenchyma.

In this context, we design and prepared doxorubicin-loaded liposomes (LIPs) functionalized to cross the BBB, to target GSCs targeting and to promote anti-tumor immune response activation.

In Chapter 2, the efficacy of mApoE-DOX LIP in an *in vivo* GBM model has been proved. The encapsulation of DOX into mApoE-LIPs prevents its toxicity on BBB cells and enhances its accumulation within the mouse brain *in vivo*. The presence of mApoE confers to LIP a specific activity on GSCs through the engagement of the LDL receptor. When administered to GSC patient-derived xenografted NOD/SCID mouse, mApoE-DOX-LIPs triggered GSC apoptosis resulting in a remarkable reduction of tumour growth and invasion to the contralateral hemisphere. Importantly, the concomitant administration of radiation enhanced the anti-tumour effects of mApoE-DOX-LIP by altering BBB permeability and promoting the expression of LDLr on both BBB and GSCs. RT and adjuvant administration of drug-loaded targeted LIPs represent an effective strategy to deliver cytotoxic

molecules, circumventing BBB hurdles and targeting GSCs at the tumour burden, the forefront of GBM recurrence.
In order to improve the tumor selectivity of mApoE-DOX-LIP, LIPs were further functionalized with chlorotoxin (ClTx), a peptide derived from the venom of the giant Israeli yellow scorpion, recently studied for its intriguing anti-cancer activity [Cohen-Inbar O et al., 2016].

In chapter 3, the synergistic activity of ClTx-mApoE in boosting DOX-loaded liposomes across the BBB, keeping the anti-tumour activity of the drug loaded have been demonstrated: mApoE acts promoting cellular uptake, while ClTx promotes exocytosis of liposomes from the basolateral side of brain endothelial cells.

The paper reported in Chapter 4 investigate the potential of TnTs as drug-delivery channels for cancer therapy, facilitating the intercellular redistribution of the drug in close and far away cells, thus reaching isolated tumour niches that are hardly targeted by simple drug diffusion in the brain parenchyma. In this work, the differences identified in TnTs formed by GBM cells and normal human astrocytes have been exploited to increase treatments precision and specificity.

1.7 References

- Abbott NJ, Hughes CC, Revest PA, Greenwood J. *Development and characterisation of a rat brain capillary endothelial culture: towards an in vitro blood-brain barrier*. J Cell Sci. **1992** Sep;103 (Pt 1):23-37. PubMed PMID: 1429907.
- Agrawala PK, Adhikari JS. *Modulation of radiation-induced cytotoxicity in U 87 cells by RH-3 (a preparation of Hippophae rhamnoides).* Indian J Med Res. **2009** Nov;130(5):542-9. PubMed PMID: 20090102.
- Ahmad T, Mukherjee S, Pattnaik B, Kumar M, Singh S, Kumar M, Rehman R, Tiwari BK, Jha KA, Barhanpurkar AP, et al. *Miro1 regulates intercellular mitochondrial transport & enhances mesenchymal stem cell rescue efficacy.* EMBO J. **2014** May 2;33(9):994-1010. doi: 10.1002/embj.201386030. PubMed PMID: 24431222.
- Akbarzadeh A, Rezaei-Sadabady R, Davaran S, Joo SW, Zarghami N, Hanifehpour Y, Samiei M, Kouhi M, Nejati-Koshki K. *Liposome: classification, preparation, and applications.* Nanoscale Res Lett. **2013** Feb 22;8(1):102. doi: 10.1186/1556-276X-8-102. PubMed PMID: 23432972.
- Alexander BM, Cloughesy TF. *Adult Glioblastoma*. J Clin Oncol. **2017** Jul20;35(21):2402-2409. doi: 10.1200/JCO.2017.73.0119. Review. PubMed PMID: 28640706.
- Alexis F, Pridgen E, Molnar LK, Farokhzad OC. *Factors affecting the clearance and biodistribution of polymeric nanoparticles*. Mol Pharm. **2008** Jul-Aug;5(4):505-15. doi: 10.1021/mp800051m. Review. PubMed PMID: 18672949.
- Allard E, Passirani C, Benoit JP. *Convection-enhanced delivery of nanocarriers for the treatment of brain tumors*. Biomaterials. **2009** Apr;30(12):2302-18. doi: 10.1016/j.biomaterials.2009.01.003. Review. PubMed PMID:19168213.
- Allen M, Bjerke M, Edlund H, Nelander S, Westermark B. *Origin of the U87MG glioma cell line: Good news and bad news.* Sci Transl Med. **2016** Aug 31;8(354):354re3. doi: 10.1126/scitranslmed.aaf6853. PubMed PMID: 27582061.

- Anderson RC, Elder JB, Brown MD, Mandigo CE, Parsa AT, Kim PD, Senatus P, Anderson DE, Bruce JN. *Changes in the immunologic phenotype of human malignant glioma cells after passaging in vitro.* Clin Immunol. **2002** Jan;102(1):84-95. PubMed PMID: 11781071.
- Artus C, Glacial F, Ganeshamoorthy K, Ziegler N, Godet M, Guilbert T, Liebner S, Couraud PO. *The Wnt/planar cell polarity signaling pathway contributes to the integrity of tight junctions in brain endothelial cells.* J Cereb Blood Flow Metab. **2014** Mar;34(3):433-40. doi: 10.1038/jcbfm.2013.213. PubMed PMID: 24346691.
- Babu PP, Deshpande RP. *Animal Model for Glioma: A Brief Overview*. Arch Med Biotechnol. **2018** 1:1.
- Balça-Silva J, Matias D, Dubois LG, Carneiro B, do Carmo A, Girão H, Ferreira F, Ferrer VP, Chimelli L, Filho PN, Tão H, Rebelo O, Barbosa M, Sarmento-Ribeiro AB, Lopes MC, Moura-Neto V. *The Expression of Connexins and SOX2 Reflects the Plasticity of Glioma Stem-Like Cells*. Transl Oncol. **2017** Aug;10(4):555-569. doi: 10.1016/j.tranon.2017.04.005. PubMed PMID: 28654819.
- Ballabh P, Braun A, Nedergaard M. *The blood-brain barrier: an overview: structure, regulation, and clinical implications*. Neurobiol Dis. **2004** Jun;16(1):1-13. Review. PubMed PMID: 15207256.
- Balvers RK, Dirven CM, Leenstra S, Lamfers ML. *Malignant Glioma In Vitro Models: On the Utilization of Stem-like Cells*. Curr Cancer Drug Targets. **2017**;17(3):255-266. doi: 10.2174/1568009616666160813191809. Review. PubMed PMID: 27528360.
- Bangham AD, Hill MW, Miller NG. *Preparation and use of liposomes as models of biological membranes*. In: Korn ED, editor. Methods in Membrane Biology. Vol. 1. New York: Plenum; **1974**. pp. 1–68.
- Bangham AD, Horne RW. *Negative staining of phospholipids and their structural modification by surface-active agents as observed in the electron microscope.* J Mol Biol. **1964**;8:660–668. PubMed PMID: 14187392.

- Bao S, Wu Q, McLendon RE, Hao Y, Shi Q, Hjelmeland AB, Dewhirst MW, Bigner DD, Rich JN. *Glioma stem cells promote radioresistance by preferential activation of the DNA damage response.* Nature. **2006** Dec 7;444(7120):756-60. PubMed PMID: 17051156.
- Battaglia L, Gallarate M, Peira E, Chirio D, Muntoni E, Biasibetti E, Capucchio MT, Valazza A, Panciani PP, Lanotte M, et al. *Solid lipid nanoparticles for potential doxorubicin delivery in glioblastoma treatment: preliminary in vitro studies.* J Pharm Sci. **2014** Jul;103(7):2157-2165. doi: 10.1002/jps.24002. PubMed PMID: 24824141.
- Battaglia L, Gallarate M, Peira E, Chirio D, Solazzi I, Giordano SM, Gigliotti CL, Riganti C, Dianzani C. *Bevacizumab loaded solid lipid nanoparticles prepared by the coacervation technique: preliminary in vitro studies*. Nanotechnology. **2015** Jan 26;26(25):255102. doi: 10.1088/0957-4484/26/25/255102. PubMed PMID: 26043866.
- Becher OJ, Holland EC. *Genetically engineered models have advantages over xenografts for preclinical studies*. Cancer Res. **2006** Apr 1;66(7):3355-8, discussion 3358-9. PubMed PMID: 16585152.
- Bernard SC, Simpson N, Join-Lambert O, Federici C, Laran-Chich MP, Maïssa N, Bouzinba-Ségard H, Morand PC, Chretien F, Taouji S et al. *Pathogenic Neisseria meningitidis utilizes CD147 for vascular colonization*. Nat Med. **2014** Jul;20(7):725-31. doi: 10.1038/nm.3563. Epub 2014 Jun 1. PubMed PMID: 24880614.
- Biswas S, Torchilin VP. Nanopreparations for organelle-specific delivery in cancer. Adv Drug Deliv Rev. 2014 Feb;66:26-41. doi: 10.1016/j.addr.2013.11.004. Review. PubMed PMID: 24270008.
- Blanco E, Shen H, Ferrari M. *Principles of nanoparticle design for overcoming biological barriers to drug delivery*. Nat Biotechnol. **2015** Sep;33(9):941-51. doi: 10.1038/nbt.3330. PubMed PMID: 26348965.
- Bowman RL, Klemm F, Akkari L, Pyonteck SM, Sevenich L, Quail DF, Dhara S, Simpson K, Gardner EE, Iacobuzio-Donahue CA, Brennan CW, Tabar V, Gutin PH, Joyce JA. *Macrophage Ontogeny*

Underlies Differences in Tumor-Specific Education in Brain Malignancies. Cell Rep. **2016** Nov 22;17(9):2445-2459. doi: 10.1016/j.celrep.2016.10.052. PubMed PMID: 27840052.

- Boyer-Di Ponio J, El-Ayoubi F, Glacial F, Ganeshamoorthy K, Driancourt C, Godet M, Perrière N, Guillevic O, Couraud PO, Uzan G. *Instruction of circulating endothelial progenitors in vitro towards specialized blood-brain barrier and arterial phenotypes.* PLoS One. **2014** Jan 2;9(1):e84179. doi: 10.1371/journal.pone.0084179. eCollection 2014. PubMed PMID: 24392113.
- Bozzuto G, Molinari A. *Liposomes as nanomedical devices.* Int J Nanomedicine. **2015** Feb 2;10:975-99. doi: 10.2147/IJN.S68861. eCollection 2015. Review. PubMed PMID: 25678787.
- Brennan CW, Verhaak RG, McKenna A, Campos B, Noushmehr H, Salama SR, Zheng S, Chakravarty D, Sanborn JZ, Berman SH, Beroukhim R, et al. TCGA Research Network. *The somatic genomic landscape of glioblastoma.* Cell. **2013** Oct 10;155(2):462-77. doi: 10.1016/j.cell.2013.09.034. PubMed PMID: 24120142.
- Broadwell RD. *Transcytosis of macromolecules through the blood-brain barrier: a cell biological perspective and critical appraisal.* Acta Neuropathol. **1989**;79(2):117-28. Review. PubMed PMID: 2688350.
- Broekman ML, Maas SLN, Abels ER, Mempel TR, Krichevsky AM, Breakefield XO. *Multidimensional communication in the microenvirons of glioblastoma*. Nat Rev Neurol. **2018** Aug;14(8):482-495. doi: 10.1038/s41582-018-0025-8. Review. PubMed PMID: 29985475.
- Burek M, Salvador E, Förster CY. *Generation of an immortalized murine brain microvascular endothelial cell line as an in vitro blood brain barrier model.* J Vis Exp. **2012** Aug 29;(66):e4022. doi: 10.3791/4022. PubMed PMID: 22951995.
- Burek M, Salvador E, Förster CY. *Generation of an immortalized murine brain microvascular endothelial cell line as an in vitro blood brain barrier model.* J Vis Exp. **2012** Aug 29;(66):e4022. doi: 10.3791/4022. PubMed PMID: 22951995

- Burton EC, Lamborn KR, Feuerstein BG, Prados M, Scott J, Forsyth P, Passe S, Jenkins RB, Aldape KD. *Genetic aberrations defined by comparative genomic hybridization distinguish long-term from typical survivors of glioblastoma.* Cancer Res. **2002** Nov 1;62(21):6205-10. PubMed PMID: 12414648.
- Byeon HJ, Thao le Q, Lee S, Min SY, Lee ES, Shin BS, Choi HG, Youn YS. *Doxorubicin-loaded nanoparticles consisted of cationic- and mannose-modified-albumins for dual-targeting in brain tumors.* J Control Release. **2016** Mar 10;225:301-13. doi: 10.1016/j.jconrel.2016.01.046. PubMed PMID: 26826308.
- Calabria AR, Weidenfeller C, Jones AR, de Vries HE, Shusta EV. *Puromycin-purified rat brain microvascular endothelial cell cultures exhibit improved barrier properties in response to glucocorticoid induction*. J Neurochem. **2006** May;97(4):922-33. PubMed PMID: 16573646.
- Cancer Genome Atlas Research Network. *Comprehensive genomic characterization defines human glioblastoma genes and core pathways*. Nature. **2008** Oct 23;455(7216):1061-8. doi: 10.1038/nature07385Erratum in: Nature. 2013 Feb 28;494(7438):506. PubMed PMID: 18772890.
- Cardoso FL, Kittel A, Veszelka S, Palmela I, Tóth A, Brites D, Deli MA, Brito MA. *Exposure to lipopolysaccharide and/or unconjugated bilirubin impair the integrity and function of brain microvascular endothelial cells*. PLoS One. **2012**;7(5):e35919. doi: 10.1371/journal.pone.0035919. PubMed PMID: 22586454.
- Caster JM, Patel AN, Zhang T, Wang A. *Investigational nanomedicines in 2016: a review of nanotherapeutics currently undergoing clinical trials.* Wiley Interdiscip Rev Nanomed Nanobiotechnol. **2017** Jan;9(1). doi: 10.1002/wnan.1416. Review. PubMed PMID: 27312983.
- Cecchelli R, Aday S, Sevin E, Almeida C, Culot M, Dehouck L, Coisne C, Engelhardt B, Dehouck MP, Ferreira L. *A stable and reproducible human blood-brain barrier model derived from hematopoietic stem cells.* PLoS One. **2014** Jun 17;9(6):e99733. doi:

10.1371/journal.pone.0099733. eCollection 2014. PubMed PMID: 24936790.

- Cecchelli R, Dehouck B, Descamps L, Fenart L, Buée-Scherrer V V, Duhem C, Lundquist S, Rentfel M, Torpier G, Dehouck MP. *In vitro model for evaluating drug transport across the blood-brain barrier.* Adv Drug Deliv Rev. **1999** Apr 5;36(2-3):165-178. PubMed PMID: 10837714.
- Ceña V, Játiva P. *Nanoparticle crossing of blood-brain barrier: a road to new therapeutic approaches to central nervous system diseases*. Nanomedicine (Lond). **2018** Jul;13(13):1513-1516. doi: 10.2217/nnm-2018-0139. PubMed PMID: 29998779.
- Cerrato JA, Yung WK, Liu TJ. *Introduction of mutant p53 into a wild-type p53-expressing glioma cell line confers sensitivity to Ad-p53-induced apoptosis.* Neuro Oncol. **2001** Apr;3(2):113-22. doi: 10.1093/neuonc/3.2.113. PubMed PMID:11296482.
- Champion JA, Mitragotri S. *Role of target geometry in phagocytosis.* Proc Natl Acad Sci U S A. **2006** Mar 28;103(13):4930-4 PubMed PMID: 16549762.
- Champion JA, Mitragotri S. *Shape induced inhibition of phagocytosis of polymer particles.* Pharm Res. **2009** Jan;26(1):244-9. doi: 10.1007/s11095-008-9626-z. PubMed PMID: 18548338.
- Chen LT, Weiss L. *The role of the sinus wall in the passage of erythrocytes through the spleen*. Blood. **1973** Apr;41(4):529-37. PubMed PMID: 4688868.
- Chen R, Nishimura MC, Bumbaca SM, Kharbanda S, Forrest WF, Kasman IM, Greve JM, Soriano RH, Gilmour LL, Rivers CS, et al. *A hierarchy of self-renewing tumor-initiating cell types in glioblastoma*. Cancer Cell. **2010** Apr 13;17(4):362-75. doi: 10.1016/j.ccr.2009.12.049. PubMed PMID: 20385361.
- Choi HS, Liu W, Misra P, Tanaka E, Zimmer JP, Itty Ipe B, Bawendi MG, Frangioni JV. *Renal clearance of quantum dots.* Nat Biotechnol. **2007** Oct;25(10):1165-70. PubMed PMID: 17891134.
- Choi S, Yu Y, Grimmer MR, Wahl M, Chang SM, Costello JF. *Temozolomide-associated hypermutation in gliomas*. Neuro Oncol.

2018 Sep 3;20(10):1300-1309. doi: 10.1093/neuonc/noy016. Review. PubMed PMID: 29452419.

- Cohen-Inbar O, Zaaroor M. *Glioblastoma multiforme targeted therapy: The Chlorotoxin story*. J Clin Neurosci. **2016**; 33: 52-58.
- Cohen MH, Johnson JR, Justice R, Pazdur R. *Approval summary: imatinib mesylate for one or three years in the adjuvant treatment of gastrointestinal stromal tumors*. Oncologist. **2012**;17(7):992-7. doi: 10.1634/theoncologist.2012-0109. PubMed PMID: 22643537.
- Cox A, Andreozzi P, Dal Magro R, Fiordaliso F, Corbelli A, Talamini L, Chinello C, Raimondo F, Magni F, Tringali M, Krol S, Jacob Silva P, Stellacci F, Masserini M, Re F. *Evolution of Nanoparticle Protein Corona across the Blood-Brain Barrier*. ACS Nano. **2018** Jul 24;12(7):7292-7300. doi:10.1021/acsnano.8b03500. PubMed PMID: 29953205.
- Crucho CIC, Barros MT. *Polymeric nanoparticles: A study on the preparation variables and characterization methods*. Mater Sci Eng C Mater Biol Appl. **2017** Nov 1;80:771-784. doi: 10.1016/j.msec.2017.06.004. PubMed PMID: 28866227.
- Czupalla CJ, Liebner S, Devraj K. *In vitro models of the blood-brain barrier*. Methods Mol Biol. **2014**;1135:415-37. doi: 10.1007/978-1-4939-0320-7_34. PubMed PMID: 24510883.
- da Cruz MT, Simões S, de Lima MC. *Improving lipoplex-mediated gene transfer into C6 glioma cells and primary neurons*. Exp Neurol. **2004** May;187(1):65-75. PubMed PMID: 15081589.
- da Hora CC, Schweiger MW, Wurdinger T, Tannous BA. *Patient-Derived Glioma Models: From Patients to Dish to Animals*. Cells. **2019** Sep 30;8(10). pii: E1177. doi: 10.3390/cells8101177. Review. PubMed PMID: 31574953.
- Dal Magro R, Ornaghi F, Cambianica I, Beretta S, Re F, Musicanti C, Rigolio R, Donzelli E, Canta A, Ballarini E, Cavaletti G, Gasco P, Sancini G. *ApoE-modified solid lipid nanoparticles: A feasible strategy to cross the blood-brain barrier*. J Control Release. **2017** Mar 10;249:103-110. doi: 10.1016/j.jconrel.2017.01.039. PubMed PMID: 28153761.

- Dal Magro R, Simonelli S, Cox A, Formicola B, Corti R, Cassina V, Nardo L, Mantegazza F, Salerno D, Grasso G, et al. *The Extent of Human Apolipoprotein A-I Lipidation Strongly Affects the β-Amyloid Efflux Across the Blood-Brain Barrier in vitro*. Front Neurosci. **2019** May16;13:419. doi: 10.3389/fnins.2019.00419. eCollection 2019. PubMed PMID: 31156358.
- D'Alessio A, Proietti G, Sica G, Scicchitano BM. *Pathological and Molecular Features of Glioblastoma and Its Peritumoral Tissue.* Cancers (Basel). **2019** Apr 3;11(4). pii: E469. doi: 10.3390/cancers11040469. Review. PubMed PMID: 30987226.
- Daneman R, Prat A. *The blood-brain barrier.* Cold Spring Harb Perspect Biol. **2015** Jan 5;7(1):a020412. doi: 10.1101/cshperspect.a020412. Review. PubMed PMID: 25561720.
- Daniel VC, Marchionni L, Hierman JS, Rhodes JT, Devereux WL, Rudin CM, Yung R, Parmigiani G, Dorsch M, Peacock CD, Watkins DN. *A primary xenograft model of small-cell lung cancer reveals irreversible changes in gene expression imposed by culture in vitro*. Cancer Res. **2009** Apr 15;69(8):3364-73. doi: 10.1158/0008-5472.CAN-08-4210. PubMed PMID: 19351829.
- D'Asti E, Chennakrishnaiah S, Lee TH, Rak J. *Extracellular Vesicles in Brain Tumor Progression.* Cell Mol Neurobiol. **2016** Apr;36(3):383-407. doi: 10.1007/s10571-015-0296-1. Review. PubMed PMID: 26993504.
- Dehouck B, Dehouck MP, Fruchart JC, Cecchelli R. *Upregulation of the low density lipoprotein receptor at the blood-brain barrier: intercommunications between brain capillary endothelial cells and astrocytes.* J Cell Biol. **1994** Jul;126(2):465-73. PubMed PMID: 8034745.
- Dehouck B, Fenart L, Dehouck MP, Pierce A, Torpier G, Cecchelli R. *A new function for the LDL receptor: transcytosis of LDL across the blood-brain barrier*. J Cell Biol. **1997** Aug 25;138(4):877-89. PubMed PMID: 9265653.
- Dehouck MP, Méresse S, Delorme P, Fruchart JC, Cecchelli R. *An easier, reproducible, and mass-production method to study the*

blood-brain barrier in vitro. J Neurochem. **1990** May;54(5):1798-801. PubMed PMID: 2182777.

- DeWitt JC, Mock A, Louis DN. *The 2016 WHO classification of central nervous system tumors: what neurologists need to know*. Curr Opin Neurol. **2017** Dec;30(6):643-649. doi: 10.1097/WCO.0000000000000490. Review. PubMed PMID: 28901970.
- Du R, Petritsch C, Lu K, Liu P, Haller A, Ganss R, Song H, Vandenberg S, Bergers G. *Matrix metalloproteinase-2 regulates vascular patterning and growth affecting tumor cell survival and invasion in GBM*. Neuro Oncol. **2008** Jun;10(3):254-64. doi: 10.1215/15228517-2008-001. Epub 2008 Mar 21. PubMed PMID: 18359864
- Dufau I, Frongia C, Sicard F, Dedieu L, Cordelier P, Ausseil F, Ducommun B, Valette A. *Multicellular tumor spheroid model to evaluate spatio-temporal dynamics effect of chemotherapeutics: application to the gemcitabine/CHK1 inhibitor combination in pancreatic cancer*. BMC Cancer. **2012** Jan 13;12:15. doi:10.1186/1471-2407-12-15. PubMed PMID: 22244109.
- Falanga AP, Melone P, Cagliani R, Borbone N, D'Errico S, Piccialli G, Netti PA, Guarnieri D. *Design, Synthesis and Characterization of Novel Co-Polymers Decorated with Peptides for the Selective Nanoparticle Transport across the Cerebral Endothelium.* Molecules. **2018** Jul 6;23(7). pii: E1655. doi: 10.3390/molecules23071655. PubMed PMID: 29986452.
- Fang C, Wang K, Stephen ZR, Mu Q, Kievit FM, Chiu DT, Press OW, Zhang M. *Temozolomide nanoparticles for targeted glioblastoma therapy*. ACS Appl Mater Interfaces. **2015** Apr 1;7(12):6674-82. doi: 10.1021/am5092165. PubMed PMID: 25751368.
- Faria J, Romão L, Martins S, Alves T, Mendes FA, de Faria GP, Hollanda R, Takiya C, Chimelli L, Morandi V, de Souza JM, Abreu JG, Moura Neto V. *Interactive properties of human glioblastoma cells with brain neurons in culture and neuronal modulation of glial*

laminin organization. Differentiation. **2006** Dec;74(9-10):562-72. PubMed PMID: 17177853.

- Federspiel MJ, Bates P, Young JA, Varmus HE, Hughes SH. *A system for tissue-specific gene targeting: transgenic mice susceptible to subgroup A avian leukosis virus-based retroviral vectors*. Proc Natl Acad Sci U S A. **1994** Nov 8;91(23):11241-5. PubMed PMID: 7972042.
- Fichtner I, Rolff J, Soong R, Hoffmann J, Hammer S, Sommer A, Becker M, Merk J. *Establishment of patient-derived non-small cell lung cancer xenografts as models for the identification of predictive biomarkers*. Clin Cancer Res. **2008** Oct15;14(20):6456-68. doi: 10.1158/1078-0432.CCR-08-0138. PubMed PMID: 18927285.
- Foged C, Nielsen HM. *Cell-penetrating peptides for drug delivery across membrane barriers*. Expert Opin Drug Deliv. **2008** Jan;5(1):105-17. Review. PubMed PMID: 18095931.
- Fonseca P, Vardaki I, Occhionero A, Panaretakis T. *Metabolic and Signaling Functions of Cancer Cell-Derived Extracellular Vesicles.* Int Rev Cell Mol Biol. **2016**; 326:175-99. doi: 10.1016/bs.ircmb.2016.04.004. PubMed PMID: 27572129.
- Förster C, Silwedel C, Golenhofen N, Burek M, Kietz S, Mankertz J, Drenckhahn D. *Occludin as direct target for glucocorticoid-induced improvement of blood-brain barrier properties in a murine in vitro system*. J Physiol. **2005** Jun 1;565(Pt 2):475-86. Epub 2005 Mar 24. PubMed PMID: 15790664.
- Friedman HS, Prados MD, Wen PY, Mikkelsen T, Schiff D, Abrey LE, Yung WK, Paleologos N, Nicholas MK, Jensen R, Vredenburgh J, Huang J, Zheng M, Cloughesy T. *Bevacizumab alone and in combination with irinotecan in recurrent glioblastoma*. J Clin Oncol. **2009** Oct 1;27(28):4733-40. doi: 10.1200/JCO.2008.19.8721. PubMed PMID: 19720927.
- Furnari FB, Fenton T, Bachoo RM, Mukasa A, Stommel JM, Stegh A, Hahn WC, Ligon KL, Louis DN, Brennan C, Chin L, DePinho RA, Cavenee WK. *Malignant astrocytic glioma: genetics, biology, and paths to treatment.* Genes Dev. **2007** Nov 1;21(21):2683-710. Review. PubMed PMID: 17974913.

- Gabathuler R. *Approaches to transport therapeutic drugs across the blood-brain barrier to treat brain diseases.* Neurobiol Dis. **2010** Jan;37(1):48-57. doi: 10.1016/j.nbd.2009.07.028. Review. PubMed PMID: 19664710.
- Geng Y, Dalhaimer P, Cai S, Tsai R, Tewari M, Minko T, Discher DE. *Shape effects of filaments versus spherical particles in flow and drug delivery*. Nat Nanotechnol. **2007** Apr;2(4):249-55. doi: 10.1038/nnano.2007.70. PubMed PMID: 18654271.
- Gentile F, Chiappini C, Fine D, Bhavane RC, Peluccio MS, Cheng MM, Liu X, Ferrari M, Decuzzi P. *The effect of shape on the margination dynamics of non-neutrally buoyant particles in two-dimensional shear flows.* J Biomech. **2008** Jul 19;41(10):2312-8. doi: 10.1016/j.jbiomech.2008.03.021. PubMed PMID: 18571181.
- Goel S, Chen F, Hong H, Valdovinos HF, Hernandez R, Shi S, Barnhart TE, Cai W. *$VEGF_{121}$-conjugated mesoporous silica nanoparticle: a tumor targeted drug delivery system*. ACS Appl Mater Interfaces. **2014** Dec 10;6(23):21677-85. doi: 10.1021/am506849p. PubMed PMID: 25353068.
- Grossman SA, Reinhard C, Colvin OM, Chasin M, Brundrett R, Tamargo RJ, Brem H. *The intracerebral distribution of BCNU delivered by surgically implanted biodegradable polymers*. J Neurosurg. **1992** Apr;76(4):640-7. PubMed PMID: 1545259.
- Groves MD, Puduvalli VK, Chang SM, Conrad CA, Gilbert MR, Tremont-Lukats IW, Liu TJ, Peterson P, Schiff D, Cloughesy TF, Wen PY, Greenberg H, Abrey LE, DeAngelis LM, Hess KR, Lamborn KR, Prados MD, Yung WK. *A North American brain tumor consortium (NABTC 99-04) phase II trial of temozolomide plus thalidomide for recurrent glioblastoma multiforme.* J Neurooncol. **2007** Feb;81(3):271-7. PubMed PMID: 17031561.
- Günther HS, Schmidt NO, Phillips HS, Kemming D, Kharbanda S, Soriano R, Modrusan Z, Meissner H, Westphal M, Lamszus K. *Glioblastoma-derived stem cell-enriched cultures form distinct subgroups according to molecular and phenotypic criteria.* Oncogene. **2008** May 1;27(20):2897-909. PubMed PMID: 18037961.

- Guo D, Reinitz F, Youssef M, Hong C, Nathanson D, Akhavan D, Kuga D, Amzajerdi AN, Soto H, Zhu S, Babic I, et al. *An LXR agonist promotes glioblastoma cell death through inhibition of an EGFR/AKT/SREBP-1/LDLR-dependent pathway.* Cancer Discov. **2011** Oct;1(5):442-56. doi: 10.1158/2159-8290.CD-11-0102. PubMed PMID: 22059152.
- Hambardzumyan D, Gutmann DH, Kettenmann H. *The role of microglia and macrophages in glioma maintenance and progression.* Nat Neurosci. **2016** Jan;19(1):20-7. doi: 10.1038/nn.4185. Review. PubMed PMID: 26713745.
- Hanif F, Muzaffar K, Perveen K, Malhi SM, Simjee ShU. Glioblastoma Multiforme: *A Review of its Epidemiology and Pathogenesis through Clinical Presentation and Treatment.* Asian Pac J Cancer Prev. **2017** Jan 1;18(1):3-9. PubMed PMID: 28239999.
- Helms HC, Abbott NJ, Burek M, Cecchelli R, Couraud PO, Deli MA, Förster C, Galla HJ, Romero IA, Shusta EV, et al. *In vitro models of the blood-brain barrier: An overview of commonly used brain endothelial cell culture models and guidelines for their use.* J Cereb Blood Flow Metab. **2016** May;36(5):862-90. doi: 10.1177/0271678X16630991. PubMed PMID: 26868179.
- Helms HC, Abbott NJ, Burek M, Cecchelli R, Couraud PO, Deli MA, Förster C, Galla HJ, Romero IA, et al. *In vitro models of the blood-brain barrier: An overview of commonly used brain endothelial cell culture models and guidelines for their use.* J Cereb Blood Flow Metab. **2016** May;36(5):862-90. doi: 10.1177/0271678X16630991. Review. PubMed PMID: 26868179.
- Hidalgo M, Amant F, Biankin AV, Budinská E, Byrne AT, Caldas C, Clarke RB, de Jong S, Jonkers J, Mælandsmo GM, et al. *Patient-derived xenograft models: an emerging platform for translational cancer research.* Cancer Discov. **2014** Sep;4(9):998-1013. doi: 10.1158/2159-8290.CD-14-0001. Review. PubMed PMID: 25185190.
- Holmes D. *The next big things are tiny*. Lancet Neurol. **2013** Jan;12(1):31-2. doi: 10.1016/S1474-4422(12)70313-7. Review. PubMed PMID: 23237899.

- Hong X, Sin WC, Harris AL, Naus CC. *Gap junctions modulate glioma invasion by direct transfer of microRNA*. Oncotarget. **2015** Jun 20;6(17):15566-77. PubMed PMID: 25978028
- http://www.lgcstandards-atcc.org
- Hu CM, Zhang L, Aryal S, Cheung C, Fang RH, Zhang L. *Erythrocyte membrane-camouflaged polymeric nanoparticles as a biomimetic delivery platform*. Proc Natl Acad Sci U S A. **2011** Jul 5;108(27):10980-5. doi: 10.1073/pnas.1106634108. PubMed PMID: 21690347.
- Huszthy PC, Daphu I, Niclou SP, Stieber D, Nigro JM, Sakariassen PØ, Miletic H, Thorsen F, Bjerkvig R. *In vivo models of primary brain tumors: pitfalls and perspectives*. Neuro Oncol. **2012** Aug;14(8):979-93. doi: 10.1093/neuonc/nos135. Review. PubMed PMID: 22679124.
- Jacobs VL, Valdes PA, Hickey WF, De Leo JA. *Current review of in vivo GBM rodent models: emphasis on the CNS-1 tumour model*. ASN Neuro. **2011** Aug 3;3(3):e00063. doi: 10.1042/AN20110014. Review. PubMed PMID: 21740400.
- James ND, Coker RJ, Tomlinson D, Harris JR, Gompels M, Pinching AJ, Stewart JS. *Liposomal doxorubicin (Doxil): an effective new treatment for Kaposi's sarcoma in AIDS*. Clin Oncol (R Coll Radiol). **1994**;6(5):294-6. PubMed PMID:7530036.
- Játiva P, Ceña V. *Use of nanoparticles for glioblastoma treatment: a new approach*. Nanomedicine (Lond). **2017** Oct;12(20):2533-2554. doi: 10.2217/nnm-2017-0223. Review. PubMed PMID: 28952878.
- Jin J, Bae KH, Yang H, Lee SJ, Kim H, Kim Y, Joo KM, Seo SW, Park TG, Nam DH. *In vivo specific delivery of c-Met siRNA to glioblastoma using cationic solid lipid nanoparticles*. Bioconjug Chem. **2011** Dec 21;22(12):2568-72. doi: 10.1021/bc200406n. PubMed PMID: 22070554.
- Jin K, Teng L, Shen Y, He K, Xu Z, Li G. *Patient-derived human tumour tissue xenografts in immunodeficient mice: a systematic review.* Clin Transl Oncol. **2010** Jul;12(7):473-80. doi: 10.1007/s12094-010-0540-6. Review. PubMed PMID: 20615824.

- Joó F, Karnushina I. *A procedure for the isolation of capillaries from rat brain*. Cytobios. **1973** Sep-Oct;8(29):41-8. PubMed PMID: 4774116.
- Joo KM, Kim J, Jin J, Kim M, Seol HJ, Muradov J, Yang H, Choi YL, Park WY, Kong DS, et al. *Patient-specific orthotopic glioblastoma xenograft models recapitulate the histopathology and biology of human glioblastomas in situ*. Cell Rep. **2013** Jan 31;3(1):260-73. doi: 10.1016/j.celrep.2012.12.013. PubMed PMID: 23333277.
- Kabanov AV, Batrakova EV, Miller DW. *Pluronic block copolymers as modulators of drug efflux transporter activity in the blood-brain barrier.* Adv Drug Deliv Rev. **2003** Jan 21;55(1):151-64. Review. PubMed PMID: 12535579.
- Kang T, Jiang M, Jiang D, Feng X, Yao J, Song Q, Chen H, Gao X, Chen J. *Enhancing Glioblastoma-Specific Penetration by Functionalization of Nanoparticles with an Iron-Mimic Peptide Targeting Transferrin/Transferrin Receptor Complex*. Mol Pharm. **2015** Aug 3;12(8):2947-61. doi: 0.1021/acs.molpharmaceut.5b00222. PubMed PMID: 26149889.
- Kannan RM, Nance E, Kannan S, Tomalia DA. *Emerging concepts in dendrimer-based nanomedicine: from design principles to clinical applications.* J Intern Med. **2014** Dec;276(6):579-617. doi: 10.1111/joim.12280. Review. PubMed PMID: 24995512.
- Karim R, Palazzo C, Evrard B, Piel G. *Nanocarriers for the treatment of glioblastoma multiforme: Current state-of-the-art*. J Control Release. **2016** Apr 10;227:23-37. doi: 10.1016/j.jconrel.2016.02.026. Review. PubMed PMID: 26892752.
- Karsy M, Neil JA, Guan J, Mahan MA, Colman H, Jensen RL. *A practical review of prognostic correlations of molecular biomarkers in glioblastoma.* Neurosurg Focus **2015** Mar;38(3):E4. doi: 10.3171/2015.1.FOCUS14755. Review. PubMed PMID: 25727226.
- Kealy J, Greene C, Campbell M. *Blood-brain barrier regulation in psychiatric disorders.* Neurosci Lett. **2018** Jun 30:133664. doi: 10.1016/j.neulet.2018.06.033. Review. PubMed PMID: 29966749.

- Keaney J, Campbell M. *The dynamic blood-brain barrier.* FEBS J. **2015** Nov;282(21):4067-79. doi: 10.1111/febs.13412. PubMed PMID: 26277326.
- Kessenbrock K, Plaks V, Werb Z. *Matrix metalloproteinases: regulators of the tumor microenvironment.* Cell. **2010** Apr 2;141(1):52-67. doi: 10.1016/j.cell.2010.03.015. Review. PubMed PMID: 20371345.
- Kijima N, Kanemura Y. *Mouse Models of Glioblastoma*. In: De Vleeschouwer S, editor. Glioblastoma [Internet]. Brisbane (AU): Codon Publications; **2017** Sep 27. Chapter 7. Available from http://www.ncbi.nlm.nih.gov/books/NBK469985/PubMed PMID: 29251866.
- Kleinberg LR, Weingart J, Burger P, Carson K, Grossman SA, Li K, Olivi A, Wharam MD, Brem H. *Clinical course and pathologic findings after Gliadel and radiotherapy for newly diagnosed malignant glioma: implications for patient management*. Cancer Invest. **2004**;22(1):1-9. PubMed PMID: 15069758.
- Kröll S, El-Gindi J, Thanabalasundaram G, Panpumthong P, Schrot S, Hartmann C, Galla HJ. *Control of the blood-brain barrier by glucocorticoids and the cells of the neurovascular unit.* Ann N Y Acad Sci. **2009** May;1165:228-39. doi:10.1111/j.1749-6632.2009.04040.x. PubMed PMID: 19538311.
- Kuntner C, Bankstahl JP, Bankstahl M, Stanek J, Wanek T, Stundner G, Karch R, Brauner R, Meier M, Ding X, Müller M, Löscher W, Langer O. *Dose-response assessment of tariquidar and elacridar and regional quantification of P-glycoprotein inhibition at the rat blood-brain barrier using (R)-[(11)C]verapamil PET*. Eur J Nucl Med Mol Imaging. **2010** May;37(5):942-53. doi: 10.1007/s00259-009-1332-5. PubMed PMID: 20016890.
- Kuo YC, Cheng SJ. *Brain targeted delivery of carmustine using solid lipid nanoparticles modified with tamoxifen and lactoferrin for antitumor proliferation*. Int J Pharm. **2016** Feb 29;499(1-2):10-19. doi: 10.1016/j.ijpharm.2015.12.054. PubMed PMID: 26721730.
- Lara-Velazquez M, Al-Kharboosh R, Jeanneret S, Vazquez-Ramos C, Mahato D, Tavanaiepour D, Rahmathulla G, Quinones-Hinojosa

A. *Advances in Brain Tumor Surgery for Glioblastoma in Adults*. Brain Sci. **2017** Dec 20;7(12). pii: E166. doi: 10.3390/brainsci7120166. Review. PubMed PMID: 29261148.

- Larjavaara S, Mäntylä R, Salminen T, Haapasalo H, Raitanen J, Jääskeläinen J, Auvinen A. *Incidence of gliomas by anatomic location.* Neuro Oncol. **2007** Jul;9(3):319-25. PubMed PMID: 17522333.
- Le Mercier M, Fortin S, Mathieu V, Roland I, Spiegl-Kreinecker S, Haibe-Kains B, Bontempi G, Decaestecker C, Berger W, et al. *Galectin 1 proangiogenic and promigratory effects in the Hs683 oligodendroglioma model are partly mediated through the control of BEX2 expression*. Neoplasia. **2009** May;11(5):485-96. PubMed PMID: 19412433.
- Lee J, Kotliarova S, Kotliarov Y, Li A, Su Q, Donin NM, Pastorino S, Purow BW, Christopher N, Zhang W, Park JK, Fine HA. *Tumor stem cells derived from glioblastomas cultured in bFGF and EGF more closely mirror the phenotype and genotype of primary tumors than do serum-cultured cell lines*. Cancer Cell. **2006** May;9(5):391-403. PubMed PMID: 16697959.
- Li ZY, Liu Y, Wang XQ, Liu LH, Hu JJ, Luo GF, Chen WH, Rong L, Zhang XZ. *One-pot construction of functional mesoporous silica nanoparticles for the tumor-acidity-activated synergistic chemotherapy of glioblastoma*. ACS Appl Mater Interfaces. **2013** Aug 28;5(16):7995-8001. doi: 10.1021/am402082d. PubMed PMID: 23869943.
- Lima FR, Kahn SA, Soletti RC, Biasoli D, Alves T, da Fonseca AC, Garcia C, Romão L, Brito J, Holanda-Afonso R, Faria J, Borges H, Moura-Neto V. *Glioblastoma: therapeutic challenges, what lies ahead*. Biochim Biophys Acta. **2012** Dec;1826(2):338-49. doi: 10.1016/j.bbcan.2012.05.004. Review. PubMed PMID: 22677165.
- Lippmann ES, Al-Ahmad A, Azarin SM, Palecek SP, Shusta EV. *A retinoic acid-enhanced, multicellular human blood-brain barrier model derived from stem cell sources*. Sci Rep. **2014** Feb 24;4:4160. doi: 10.1038/srep04160. PubMed PMID:24561821.

- Lippmann ES, Azarin SM, Kay JE, Nessler RA, Wilson HK, Al-Ahmad A, Palecek SP, Shusta EV. *Derivation of blood-brain barrier endothelial cells from human pluripotent stem cells*. Nat Biotechnol. **2012** Aug;30(8):783-91. PubMed PMID:22729031.
- Lou E, Zhai E, Sarkari A, Desir S, Wong P, Iizuka Y, Yang J, Subramanian S, McCarthy J, Bazzaro M, Steer CJ. *Cellular and Molecular Networking Within the Ecosystem of Cancer Cell Communication via Tunneling Nanotubes*. Front Cell Dev Biol. **2018** Oct 2;6:95. doi: 10.3389/fcell.2018.00095. eCollection 2018. PubMed PMID: 30333973.
- Lou E. *Can you hear them now? Tumor microtubes form cellular communication networks that protect gliomas from surgical lesions and chemotherapy treatments*. Neuro Oncol. **2017** Oct 1;19(10):1289-1291. doi: 10.1093/neuonc/nox103. PubMed PMID: 28922861
- Louis DN, Perry A, Reifenberger G, von Deimling A, Figarella-Branger D, Cavenee WK, Ohgaki H, Wiestler OD, Kleihues P, Ellison DW. *The 2016 World Health Organization Classification of Tumors of the Central Nervous System: a summary.* Acta Neuropathol. **2016** Jun;131(6):803-20. doi: 10.1007/s00401-016-1545-1. Review. PubMed PMID: 27157931.
- Luissint AC, Artus C, Glacial F, Ganeshamoorthy K, Couraud PO. *Tight junctions at the blood brain barrier: physiological architecture and disease-associated dysregulation*. Fluids Barriers CNS. **2012** Nov 9;9(1):23. doi: 10.1186/2045-8118-9-23. PubMed PMID: 23140302.
- Łukasiewicz S, Błasiak E, Szczepanowicz K, Guzik K, Bzowska M, Warszyński P, Dziedzicka-Wasylewska M. *The interaction of clozapine loaded nanocapsules with the hCMEC/D3 cells - In vitro model of blood brain barrier.* Colloids Surf B Biointerfaces. **2017** Nov 1;159:200-210. doi: 10.1016/j.colsurfb.2017.07.053. PubMed PMID: 28797970.
- Maher EA, Brennan C, Wen PY, Durso L, Ligon KL, Richardson A, Khatry D, Feng B, Sinha R, Louis DN, Quackenbush J, Black PM, Chin L, DePinho RA. *Marked genomic differences characterize*

primary and secondary glioblastoma subtypes and identify two distinct molecular and clinical secondary glioblastoma entities. Cancer Res. **2006** Dec 1;66(23):11502-13. PubMed PMID: 17114236.

- Mahesparan R, Read TA, Lund-Johansen M, Skaftnesmo KO, Bjerkvig R, Engebraaten O. *Expression of extracellular matrix components in a highly infiltrative in vivo glioma model*. Acta Neuropathol. **2003** Jan;105(1):49-57. PubMed PMID: 12471461.
- Malcor JD, Payrot N, David M, Faucon A, Abouzid K, Jacquot G, Floquet N, Debarbieux F, Rougon G, Martinez J, et al. *Chemical optimization of new ligands of the low-density lipoprotein receptor as potential vectors for central nervous system targeting*. J Med Chem. **2012** Mar 8;55(5):2227-41. doi: 10.1021/jm2014919. PubMed PMID: 22257077.
- Mancini S, Minniti S, Gregori M, Sancini G, Cagnotto A, Couraud PO, Ordóñez-Gutiérrez L, Wandosell F, Salmona M, Re F. *The hunt for brain Aβ oligomers by peripherally circulating multi-functional nanoparticles: Potential therapeutic approach for Alzheimer disease.* Nanomedicine. **2016** Jan;12(1):43-52. doi: 10.1016/j.nano.2015.09.003. PubMed PMID: 26410276.
- Martens T, Laabs Y, Günther HS, Kemming D, Zhu Z, Witte L, Hagel C, Westphal M, Lamszus K. *Inhibition of glioblastoma growth in a highly invasive nude mouse model can be achieved by targeting epidermal growth factor receptor but not vascular endothelial growth factor receptor-2*. Clin Cancer Res. **2008** Sep 1;14(17):5447-58. doi: 10.1158/1078-0432.CCR-08-0147. PubMed PMID: 18765536.
- Masserini M. *Nanoparticles for brain drug delivery*. ISRN Biochem. **2013** May 21;2013:238428. doi: 10.1155/2013/238428. eCollection 2013. Review. PubMed PMID: 25937958.
- McGirt MJ, Than KD, Weingart JD, Chaichana KL, Attenello FJ, Olivi A, Laterra J, Kleinberg LR, Grossman SA, Brem H, Quiñones-Hinojosa A. *Gliadel (BCNU) wafer plus concomitant temozolomide therapy after primary resection of glioblastoma multiforme*. J

Neurosurg. **2009** Mar;110(3):583-8. doi: 10.3171/2008.5.17557. PubMed PMID: 19046047.

- Miyai M, Tomita H, Soeda A, Yano H, Iwama T, Hara A. *Current trends in mouse models of glioblastoma.* J Neurooncol. **2017** Dec;135(3):423-432. doi: 10.1007/s11060-017-2626-2. PubMed PMID: 29052807.
- Moghimi SM, Hunter AC, Murray JC. *Nanomedicine: current status and future prospects.* FASEB J. **2005** Mar;19(3):311-30. Review. PubMed PMID: 15746175.
- Montet X, Funovics M, Montet-Abou K, Weissleder R, Josephson L. *Multivalent effects of RGD peptides obtained by nanoparticle display*. J Med Chem. **2006** Oct 5;49(20):6087-93. PubMed PMID: 17004722.
- Mooney J, Bernstock JD, Ilyas A, Ibrahim A, Yamashita D, Markert JM, Nakano I. *Current Approaches and Challenges in the Molecular Therapeutic Targeting of Glioblastoma*. World Neurosurg. **2019** Sep;129:90-100. doi: 10.1016/j.wneu.2019.05.205. Review. PubMed PMID: 31152883.
- Mukherjee SP, Davoren M, Byrne HJ. *In vitro mammalian cytotoxicological study of PAMAM dendrimers - towards quantitative structure activity relationships.* Toxicol In Vitro. **2010** Feb;24(1):169-77. doi: 10.1016/j.tiv.2009.09.014. PubMed PMID: 19778601.
- Müller A, Brandenburg S, Turkowski K, Müller S, Vajkoczy P. *Resident microglia, and not peripheral macrophages, are the main source of brain tumor mononuclear cells.* Int J Cancer. **2015** Jul 15;137(2):278-88. doi: 10.1002/ijc.29379. PubMed PMID: 25477239.
- Muro S, Muzykantov VR, Murciano JC. *Characterization of endothelial internalization and targeting of antibody-enzyme conjugates in cell cultures and in laboratory animals*. Methods Mol Biol. **2004**;283:21-36. PubMed PMID: 15197300.
- Ohgaki H, Kleihues P. *The definition of primary and secondary glioblastoma*. Clin Cancer Res. **2013** Feb 15;19(4):764-72. doi:

10.1158/1078-0432.CCR-12-3002. Review. PubMed PMID: 23209033.

- Okada M, Miyake K, Tamiya T. *Glioblastoma Treatment in the Elderly*. Neurol Med Chir (Tokyo). **2017** Dec 15;57(12):667-676. doi: 10.2176/nmc.ra.2017-0009. Review. PubMed PMID: 29081442.
- Omar AI, Mason WP. *Temozolomide: The evidence for its therapeutic efficacy in malignant astrocytomas*. Core Evid. **2010** Jun 15;4:93-111. PubMed PMID: 20694068
- Omidi Y, Campbell L, Barar J, Connell D, Akhtar S, Gumbleton M. *Evaluation of the immortalised mouse brain capillary endothelial cell line, b.End3, as an in vitro blood-brain barrier model for drug uptake and transport studies.* Brain Res. **2003** Nov 14;990(1-2):95-112. PubMed PMID: 14568334.
- Onfelt B, Nedvetzki S, Benninger RK, Purbhoo MA, Sowinski S, Hume AN, Seabra MC, Neil MA, French PM, Davis DM. *Structurally distinct membrane nanotubes between human macrophages support long-distance vesicular traffic or surfing of bacteria.* J Immunol. **2006** Dec 15;177(12):8476-83. PubMed PMID: 17142745.
- Ortiz R, Cabeza L, Perazzoli G, Jimenez-Lopez J, García-Pinel B, Melguizo C, Prados J. *Nanoformulations for glioblastoma multiforme: a new hope for treatment.* Future Med Chem. **2019** Sep;11(18):2459-2480. doi: 10.4155/fmc-2018-0521. PubMed PMID: 31544490.
- Osoba D, Brada M, Yung WK, Prados M. *Health-related quality of life in patients treated with temozolomide versus procarbazine for recurrent glioblastoma multiforme.* J Clin Oncol. **2000** Apr;18(7):1481-91. PubMed PMID: 10735896.
- Ostrom QT, Gittleman H, Fulop J, Liu M, Blanda R, Kromer C, Wolinsky Y, Kruchko C, Barnholtz-Sloan JS. *CBTRUS Statistical Report: Primary Brain and Central Nervous System Tumors Diagnosed in the United States in 2008-2012*. Neuro Oncol. **2015** Oct;17 Suppl 4:iv1-iv62. doi: 10.1093/neuonc/nov189. PubMed PMID: 26511214.

- Papadia K, Giannou AD, Markoutsa E, Bigot C, Vanhoute G, Mourtas S, Van der Linded A, Stathopoulos GT, Antimisiaris SG. *Multifunctional LUV liposomes decorated for BBB and amyloid targeting - B. In vivo brain targeting potential in wild-type and APP/PS1 mice*. Eur J Pharm Sci. **2017** May 1;102:180-187. doi: 10.1016/j.ejps.2017.03.010. PubMed PMID: 28285172.
- Pardridge WM. *Blood-brain barrier endogenous transporters as therapeutic targets: a new model for small molecule CNS drug discovery.* Expert Opin Ther Targets. **2015**;19(8):1059-72. doi: 10.1517/14728222.2015.1042364. Review. PubMed PMID: 25936389.
- Parodi A, Quattrocchi N, van de Ven AL, Chiappini C, Evangelopoulos M, Martinez JO, Brown BS, Khaled SZ, Yazdi IK, Enzo MV, Isenhart L, Ferrari M, Tasciotti E. *Synthetic nanoparticles functionalized with biomimetic leukocyte membranes possess cell-like functions.* Nat Nanotechnol. **2013** Jan;8(1):61-8. doi: 10.1038/nnano.2012.212. PubMed PMID: 23241654
- Patabendige A, Skinner RA, Morgan L, Abbott NJ. *A detailed method for preparation of a functional and flexible blood-brain barrier model using porcine brain endothelial cells.* Brain Res. **2013** Jul 12;1521:16-30. doi:10.1016/j.brainres.2013.04.006. PubMed PMID: 23603406.
- Perrin SL, Samuel MS, Koszyca B, Brown MP, Ebert LM, Oksdath M, Gomez GA. *Glioblastoma heterogeneity and the tumour microenvironment: implications for preclinical research and development of new treatments*. Biochem Soc Trans. **2019** Apr 30;47(2):625-638. doi: 10.1042/BST20180444. PubMed PMID: 30902924.
- Petkar KC, Chavhan SS, Agatonovik-Kustrin S, Sawant KK. *Nanostructured materials in drug and gene delivery: a review of the state of the art.* Crit Rev Ther Drug Carrier Syst. **2011**;28(2):101-64. Review. PubMed PMID: 21663574.
- Poovaiah N, Davoudi Z, Peng H, Schlichtmann B, Mallapragada S, Narasimhan B, Wang Q. *Treatment of neurodegenerative disorders through the blood-brain barrier using nanocarriers*. Nanoscale.

2018 Sep 20;10(36):16962-16983. doi: 10.1039/c8nr04073g. Review. PubMed PMID: 30182106.

- Pope WB, Qiao XJ, Kim HJ, Lai A, Nghiemphu P, Xue X, Ellingson BM, Schiff D, Aregawi D, Cha S, Puduvalli VK, et al. *Apparent diffusion coefficient histogram analysis stratifies progression-free and overall survival in patients with recurrent GBM treated with bevacizumab: a multi-center study*. J Neurooncol. **2012** Jul;108(3):491-8. doi: 10.1007/s11060-012-0847-y. Epub 2012 Mar 18. PubMed PMID: 22426926.
- Quan AL, Barnett GH, Lee SY, Vogelbaum MA, Toms SA, Staugaitis SM, Prayson RA, Peereboom DM, Stevens GH, Cohen BH, Suh JH. *Epidermal growth factor receptor amplification does not have prognostic significance in patients with glioblastoma multiforme.* Int J Radiat Oncol Biol Phys. **2005** Nov 1;63(3):695-703. PubMed PMID: 15936158.
- Ramirez YP, Weatherbee JL, Wheelhouse RT, Ross AH. *Glioblastoma multiforme therapy and mechanisms of resistance*. Pharmaceuticals (Basel). **2013** Nov 25;6(12):1475-506. doi: 10.3390/ph6121475. PubMed PMID: 24287492.
- Re F, Cambianica I, Zona C, Sesana S, Gregori M, Rigolio R, La Ferla B, Nicotra F, Forloni G, Cagnotto A, et al. *Functionalization of liposomes with ApoE-derived peptides at different density affects cellular uptake and drug transport across a blood-brain barrier model*. Nanomedicine. **2011** Oct;7(5):551-9. doi: 10.1016/j.nano.2011.05.004. PubMed PMID: 21658472.
- Reardon DA, Galanis E, DeGroot JF, Cloughesy TF, Wefel JS, Lamborn KR, Lassman AB, Gilbert MR, Sampson JH, Wick W, Chamberlain MC, Macdonald DR, Mehta MP, Vogelbaum MA, Chang SM, Van den Bent MJ, Wen PY. *Clinical trial end points for high-grade glioma: the evolving landscape*. Neuro Oncol. **2011** Mar;13(3):353-61. doi: 10.1093/neuonc/noq203. Review. PubMed PMID: 21310734.
- Redzic JS, Balaj L, van der Vos KE, Breakefield XO. *Extracellular RNA mediates and marks cancer progression*. Semin Cancer Biol.

2014 Oct;28:14-23. doi: 10.1016/j.semcancer.2014.04.010. Review. PubMed PMID: 24783980.

- Rich JN, Hans C, Jones B, Iversen ES, McLendon RE, Rasheed BK, Dobra A, Dressman HK, Bigner DD, Nevins JR, West M. *Gene expression profiling and genetic markers in glioblastoma survival.* Cancer Res. **2005** May 15;65(10):4051-8. PubMed PMID: 15899794.
- Robertson FL, Marqués-Torrejón MA, Morrison GM, Pollard SM. *Experimental models and tools to tackle glioblastoma*. Dis Model Mech. **2019** Sep 6;12(9). pii: dmm040386. doi: 10.1242/dmm.040386. Review. PubMed PMID: 31519690.
- Ruan C, Liu L, Lu Y, Zhang Y, He X, Chen X, Zhang Y, Chen Q, Guo Q, Sun T, Jiang C. *Substance P-modified human serum albumin nanoparticles loaded with paclitaxel for targeted therapy of glioma*. Acta Pharm Sin B. **2018** Jan;8(1):85-96. doi: 10.1016/j.apsb.2017.09.008. PubMed PMID: 29872625.
- Rufino-Ramos D, Albuquerque PR, Carmona V, Perfeito R, Nobre RJ, Pereira de Almeida L. *Extracellular vesicles: Novel promising delivery systems for therapy of brain diseases.* J Control Release. **2017** Sep 28;262:247-258. doi: 10.1016/j.jconrel.2017.07.001. Review. PubMed PMID: 28687495.
- Rustom A, Saffrich R, Markovic I, Walther P, Gerdes HH. *Nanotubular highways for intercellular organelle transport*. Science. **2004** Feb 13;303(5660):1007-10. PubMed PMID: 14963329.
- Salvati E, Re F, Sesana S, Cambianica I, Sancini G, Masserini M, Gregori M. *Liposomes functionalized to overcome the blood-brain barrier and to target amyloid-β peptide: the chemical design affects the permeability across an in vitro model.* Int J Nanomedicine. **2013**;8:1749-58. doi: 10.2147/IJN.S42783. PubMed PMID: 23674890.
- Sánchez-López E, Ettcheto M, Egea MA, Espina M, Cano A, Calpena AC, Camins A, Carmona N, Silva AM, Souto EB, García ML. *Memantine loaded PLGA PEGylated nanoparticles for Alzheimer's disease: in vitro and in vivo characterization.* J

Nanobiotechnology. **2018** Mar 27;16(1):32. doi: 10.1186/s12951-018-0356-z. PubMed PMID: 29587747.

- Saraiva C, Praça C, Ferreira R, Santos T, Ferreira L, Bernardino L. *Nanoparticle-mediated brain drug delivery: Overcoming blood-brain barrier to treat neurodegenerative diseases*. J Control Release. **2016** Aug 10;235:34-47. doi: 10.1016/j.jconrel.2016.05.044. Review. PubMed PMID: 27208862.
- Sasmita AO, Wong YP, Ling APK. *Biomarkers and therapeutic advances in glioblastoma multiforme.* Asia Pac J Clin Oncol. **2018** Feb;14(1):40-51. doi: 10.1111/ajco.12756. Review. PubMed PMID: 28840962.
- Schiller C, Huber JE, Diakopoulos KN, Weiss EH. *Tunneling nanotubes enable intercellular transfer of MHC class I molecules.* Hum Immunol. **2013** Apr;74(4):412-6. doi: 10.1016/j.humimm.2012.11.026. PubMed PMID: 23228397.
- Schreck KC, Grossman SA. *Role of Temozolomide in the Treatment of Cancers Involving the Central Nervous System*. Oncology (Williston Park). **2018** Nov 15;32(11):555-60, 569. Review. PubMed PMID: 30474103.
- Sercombe L, Veerati T, Moheimani F, Wu SY, Sood AK, Hua S. *Advances and Challenges of Liposome Assisted Drug Delivery*. Front Pharmacol. **2015** Dec 1;6:286. doi: 10.3389/fphar.2015.00286. eCollection 2015. Review. PubMed PMID: 26648870.
- Shein SA, Kuznetsov II, Abakumova TO, Chelushkin PS, Melnikov PA, Korchagina AA, Bychkov DA, Seregina IF, Bolshov MA, Kabanov AV, Chekhonin VP, Nukolova NV. *VEGF- and VEGFR2-Targeted Liposomes for Cisplatin Delivery to Glioma Cells*. Mol Pharm. **2016** Nov 7;13(11):3712-3723. PubMed PMID: 27654150.
- Shi J, Kantoff PW, Wooster R, Farokhzad OC. *Cancer nanomedicine: progress, challenges and opportunities.* Nat Rev Cancer. **2017** Jan;17(1):20-37. doi: 10.1038/nrc.2016.108. Review. PubMed PMID: 27834398.
- Silantyev AS, Falzone L, Libra M, Gurina OI, Kardashova KS, Nikolouzakis TK, Nosyrev AE, Sutton CW, Mitsias PD, Tsatsakis

A. *Current and Future Trends on Diagnosis and Prognosis of Glioblastoma: From Molecular Biology to Proteomics.* Cells. **2019** Aug 9;8(8). pii: E863. doi: 10.3390/cells8080863. Review. PubMed PMID: 31405017.

- Silwedel C, Förster C. *Differential susceptibility of cerebral and cerebellar murine brain microvascular endothelial cells to loss of barrier properties in response to inflammatory stimuli.* J Neuroimmunol. **2006** Oct;179(1-2):37-45. PubMed PMID: 16884785.
- Sinyuk M, Mulkearns-Hubert EE, Reizes O, Lathia J. *Cancer Connectors: Connexins, Gap Junctions, and Communication.* Front Oncol. **2018** Dec 21;8:646. doi: 10.3389/fonc.2018.00646. PubMed PMID: 30622930.
- Song H, Wei M, Zhang N, Li H, Tan X, Zhang Y, Zheng W. *Enhanced permeability of blood-brain barrier and targeting function of brain via borneol-modified chemically solid lipid nanoparticle*. Int J Nanomedicine. **2018** Mar 28;13:1869-1879. doi: 10.2147/IJN.S161237. eCollection 2018. PubMed PMID: 29636606.
- Soomro SH, Ting LR, Qing YY, Ren M. *Molecular biology of glioblastoma: Classification and mutational locations.* J Pak Med Assoc. **2017** Sep;67(9):1410-1414. Review. PubMed PMID: 28924284.
- Srikanth M, Kessler JA. *Nanotechnology-novel therapeutics for CNS disorders.* Nat Rev Neurol. **2012** Apr 24;8(6):307-18. doi: 10.1038/nrneurol.2012.76. Review. PubMed PMID: 22526003
- Srinageshwar B, Peruzzaro S, Andrews M, Johnson K, Hietpas A, Clark B, McGuire C, Petersen E, Kippe J, Stewart A, Lossia O, et al. J. *PAMAM Dendrimers Cross the Blood-Brain Barrier When Administered through the Carotid Artery in C57BL/6J Mice.* Int J Mol Sci. **2017** Mar 14;18(3). pii: E628. doi: 10.3390/ijms18030628. PubMed PMID: 28335421.
- Steiner O, Coisne C, Engelhardt B, Lyck R. *Comparison of immortalized bEnd5 and primary mouse brain microvascular endothelial cells as in vitro blood-brain barrier models for the study*

of T cell extravasation. J Cereb Blood Flow Metab. **2011** Jan;31(1):315-27. doi: 10.1038/jcbfm.2010.96. PubMed PMID: 20606687.

- Stins MF, Badger J, Sik Kim K. *Bacterial invasion and transcytosis in transfected human brain microvascular endothelial cells*. Microb Pathog. **2001** Jan;30(1):19-28. PubMed PMID: 11162182.
- Stupp R, Mason WP, van den Bent MJ, Weller M, Fisher B, Taphoorn MJ, Belanger K, Brandes AA, Marosi C, Bogdahn U, Curschmann J, et al. European Organisation for Research and Treatment of Cancer Brain Tumor and Radiotherapy Groups; National Cancer Institute of Canada Clinical Trials Group. *Radiotherapy plus concomitant and adjuvant temozolomide for glioblastoma*. N Engl J Med. **2005** Mar 10;352(10):987-96. PubMed PMID: 15758009.
- Sweeney MD, Sagare AP, Zlokovic BV. *Blood-brain barrier breakdown in Alzheimer disease and other neurodegenerative disorders.* Nat Rev Neurol. **2018** Mar;14(3):133-150. doi: 10.1038/nrneurol.2017.188. Review. PubMed PMID: 29377008.
- Szabó CA, Deli MA, Ngo TK, Joó F. *Production of pure primary rat cerebral endothelial cell culture: a comparison of different methods*. Neurobiology (Bp). **1997**;5(1):1-16. PubMed PMID: 9302692.
- Tamborini M, Locatelli E, Rasile M, Monaco I, Rodighiero S, Corradini I, Franchini MC, Passoni L, Matteoli M. *A Combined Approach Employing Chlorotoxin-Nanovectors and Low Dose Radiation To Reach Infiltrating Tumor Niches in Glioblastoma.* ACS Nano. **2016** Feb 23;10(2):2509-20. doi: 10.1021/acsnano.5b07375. PubMed PMID: 26745323.
- Tamimi AF, Juweid M. *Epidemiology and Outcome of Glioblastoma.* In: De Vleeschouwer S, editor. Glioblastoma [Internet]. Brisbane (AU): Codon Publications; **2017** Sep 27. Chapter 8. PubMed PMID: 29251870.
- Thayanithy V, Dickson EL, Steer C, Subramanian S, Lou E. *Tumor-stromal cross talk: direct cell-to-cell transfer of oncogenic microRNAs via tunnelling nanotubes.* Transl Res. **2014**

Nov;164(5):359-65. doi: 10.1016/j.trsl.2014.05.011. PubMed PMID: 24929208.

- Thomas A, Tanaka M, Trepel J, Reinhold WC, Rajapakse VN, Pommier Y. *Temozolomide in the Era of Precision Medicine*. Cancer Res**. 2017** Feb 15;77(4):823-826. doi: 10.1158/0008-5472.CAN-16-2983. Review. PubMed PMID: 28159862.
- Thomas DA, Sarris AH, Cortes J, Faderl S, O'Brien S, Giles FJ, Garcia-Manero G, Rodriguez MA, Cabanillas F, Kantarjian H. *Phase II study of sphingosomal vincristine in patients with recurrent or refractory adult acute lymphocytic leukemia.* Cancer. **2006** Jan 1;106(1):120-7. PubMed PMID: 16331634.
- Thuringer D, Boucher J, Jego G, Pernet N, Cronier L, Hammann A, Solary E, Garrido C. *Transfer of functional microRNAs between glioblastoma and microvascular endothelial cells through gap junctions.* Oncotarget. **2016** Nov 8;7(45):73925-73934. doi: 10.18632/oncotarget.12136. PubMed PMID: 27661112.
- Tomalia DA, Christensen JB, Boas U. *Dendrimers, Dendrons, and Dendritic Polymers. Discovery, Applications and the Future.* Cambridge University Press, Cambridge, UK. **2012** Book 978-0-521-51580-1.
- Udhrain A, Skubitz KM, Northfelt DW. *Pegylated liposomal doxorubicin in the treatment of AIDS-related Kaposi's sarcoma*. Int J Nanomedicine. **2007**;2(3):345-52. Review. PubMed PMID: 18019833.
- Urbanska K, Mandal CC. *Advanced Views of Glioblastoma Multiforme U-87 Cells for Therapy of Brain Tumor*. IJCBR. 2014 1(1):59-66.
- Urich E, Lazic SE, Molnos J, Wells I, Freskgård PO. *Transcriptional profiling of human brain endothelial cells reveals key properties crucial for predictive in vitro blood-brain barrier models*. PLoS One. **2012**;7(5):e38149. doi:10.1371/journal.pone.0038149. PubMed PMID: 22675443.
- Ventola CL. *Progress in Nanomedicine: Approved and Investigational Nanodrugs*. P T. **2017** Dec;42(12):742-755. PubMed PMID: 29234213.

- Verhaak RG, Hoadley KA, Purdom E, Wang V, Qi Y, Wilkerson MD, Miller CR, Ding L, Golub T, Mesirov JP, Alexe G, Lawrence M, O'Kelly M, Tamayo P, Weir BA, Gabriel S, Winckler W, Gupta S, Jakkula L, Feiler HS, Hodgson JG, James CD, Sarkaria JN, Brennan C, Kahn A, Spellman PT, Wilson RK, Speed TP, Gray JW, Meyerson M, Getz G, Perou CM, Hayes DN; Cancer Genome Atlas Research Network. *Integrated genomic analysis identifies clinically relevant subtypes of glioblastoma characterized by abnormalities in PDGFRA, IDH1, EGFR, and NF1*. Cancer Cell. **2010** Jan 19;17(1):98-110. doi: 10.1016/j.ccr.2009.12.020. PubMed PMID: 20129251.
- Villa GR, Hulce JJ, Zanca C, Bi J, Ikegami S, Cahill GL, Gu Y, Lum KM, Masui K, Yang H, et al. *An LXR-Cholesterol Axis Creates a Metabolic Co-Dependency for Brain Cancers*. Cancer Cell. **2016** Nov 14;30(5):683-693. doi: 10.1016/j.ccell.2016.09.008. PubMed PMID: 27746144.
- Vredenburgh JJ, Desjardins A, Herndon JE 2nd, Dowell JM, Reardon DA, Quinn JA, Rich JN, Sathornsumetee S, Gururangan S, Wagner M, Bigner DD, et al. *Phase II trial of bevacizumab and irinotecan in recurrent malignant glioma*. Clin Cancer Res. **2007** Feb 15;13(4):1253-9. PubMed PMID: 17317837.
- Wagner A, Vorauer-Uhl K. *Liposome technology for industrial purposes.* J Drug Deliv. **2011**;2011:591325. doi: 10.1155/2011/591325. PubMed PMID: 21490754.
- Wagner EF, Risau W. *Oncogenes in the study of endothelial cell growth and differentiation*. Semin Cancer Biol. **1994** Apr;5(2):137-45. Review. PubMed PMID: 7520302.
- Wakimoto H, Kesari S, Farrell CJ, Curry WT Jr, Zaupa C, Aghi M, Kuroda T, Stemmer-Rachamimov A, Shah K, Liu TC, et al. *Human glioblastoma-derived cancer stem cells: establishment of invasive glioma models and treatment with oncolytic herpes simplex virus vectors*. Cancer Res. **2009** Apr 15;69(8):3472-81. doi: 10.1158/0008-5472.CAN-08-3886. PubMed PMID: 19351838.
- Wakimoto H, Mohapatra G, Kanai R, Curry WT Jr, Yip S, Nitta M, Patel AP, Barnard ZR, Stemmer-Rachamimov AO, Louis DN,

Martuza RL, Rabkin SD. *Maintenance of primary tumor phenotype and genotype in glioblastoma stem cells*. Neuro Oncol. 2012 Feb;14(2):132-44. doi: 10.1093/neuonc/nor195. PubMed PMID: 22067563.

- Webb MS, Harasym TO, Masin D, Bally MB, Mayer LD. *Sphingomyelin-cholesterol liposomes significantly enhance the pharmacokinetic and therapeutic properties of vincristine in murine and human tumour models*. Br J Cancer. **1995** Oct;72(4):896-904. PubMed PMID: 7547237.
- Wedel-Parlow Mv, Galla H. *A microscopic in vitro study of neutrophil diapedesis across the blood- brain barrier, in Microscopy: Science, Technology, Applications and Education.* In: Mendez-Vilas A, Díaz J, editors. (eds). Microscopy: Science, Technology, Applications and Education, The Badajoz, Spain: Formatex, **2010**, 1161–1167.
- Weissig V, Pettinger TK, Murdock N. *Nanopharmaceuticals (part 1): products on the market.* Int J Nanomedicine. **2014** Sep 15;9:4357-73. doi: 10.2147/IJN.S46900. eCollection 2014. Review. PubMed PMID: 25258527.
- Weksler B, Romero IA, Couraud PO. *The hCMEC/D3 cell line as a model of the human blood brain barrier*. Fluids Barriers CNS. **2013** Mar 26;10(1):16. doi:10.1186/2045-8118-10-16. PubMed PMID: 23531482.
- Weksler BB, Subileau EA, Perrière N, Charneau P, Holloway K, Leveque M, Tricoire-Leignel H, Nicotra A, Bourdoulous S, Turowski P, et al. *Blood-brain barrier-specific properties of a human adult brain endothelial cell line*. FASEB J. **2005** Nov;19(13):1872-4. PubMed PMID: 16141364.
- Westphal M, Lamszus K. *The neurobiology of gliomas: from cell biology to the development of therapeutic approaches*. Nat Rev Neurosci. **2011** Aug 3;12(9):495-508. doi: 10.1038/nrn3060. Review. PubMed PMID: 21811295.
- Wood MD, Halfpenny AM, Moore SR. *Applications of molecular neuro-oncology - a review of diffuse glioma integrated diagnosis and emerging molecular entities.* Diagn Pathol. **2019** Apr

9;14(1):29. doi: 10.1186/s13000-019-0802-8. Review. PubMed PMID: 30967140.

- Wu M, Fan Y, Lv S, Xiao B, Ye M, Zhu X. *Vincristine and temozolomide combined chemotherapy for the treatment of glioma: a comparison of solid lipid nanoparticles and nanostructured lipid carriers for dual drugs delivery.* Drug Deliv. **2016** Oct;23(8):2720-2725. PubMed PMID: 26203691.
- Xie Y, Bergström T, Jiang Y, Johansson P, Marinescu VD, Lindberg N, Segerman A, Wicher G, Niklasson M, Baskaran S, Sreedharan S, et al. *The Human Glioblastoma Cell Culture Resource: Validated Cell Models Representing All Molecular Subtypes.* EBioMedicine. **2015** Aug 15;2(10):1351-63. doi: 10.1016/j.ebiom.2015.08.026. eCollection 2015 Oct. PubMed PMID: 26629530.
- Xin H, Sha X, Jiang X, Zhang W, Chen L, Fang X. *Anti-glioblastoma efficacy and safety of paclitaxel-loading Angiopep-conjugated dual targeting PEG-PCL nanoparticles.* Biomaterials. **2012** Nov;33(32):8167-76. doi: 10.1016/j.biomaterials.2012.07.046. PubMed PMID: 22889488.
- Xu H, Chen J, Xu H, Qin Z. *Geographic Variations in the Incidence of Glioblastoma and Prognostic Factors Predictive of Overall Survival in US Adults from 2004-2013*. Front Aging Neurosci**. 2017** Nov 7;9:352. doi: 10.3389/fnagi.2017.00352. PubMed PMID: 29163134.
- Xu Y, Shen M, Li Y, Sun Y, Teng Y, Wang Y, Duan Y. *The synergic antitumor effects of paclitaxel and temozolomide co-loaded in mPEG-PLGA nanoparticles on glioblastoma cells.* Oncotarget. **2016** Apr 12;7(15):20890-901. doi: 10.18632/oncotarget.7896. PubMed PMID: 26956046.
- Yang FY, Wong TT, Teng MC, Liu RS, Lu M, Liang HF, Wei MC. *Focused ultrasound and interleukin-4 receptor-targeted liposomal doxorubicin for enhanced targeted drug delivery and antitumor effect in glioblastoma multiforme*. J Control Release. **2012** Jun 28;160(3):652-8. doi: 10.1016/j.jconrel.2012.02.023. PubMed PMID: 22405901.

- Yang T, Martin P, Fogarty B, Brown A, Schurman K, Phipps R, Yin VP, Lockman P, Bai S. *Exosome delivered anticancer drugs across the blood-brain barrier for brain cancer therapy in Danio rerio*. Pharm Res. **2015** Jun;32(6):2003-14. doi: 10.1007/s11095-014-1593-y. PubMed PMID: 25609010.
- Yang ZZ, Li JQ, Wang ZZ, Dong DW, Qi XR. *Tumor-targeting dual peptides-modified cationic liposomes for delivery of siRNA and docetaxel to gliomas*. Biomaterials. **2014** Jun;35(19):5226-39. doi: 10.1016/j.biomaterials.2014.03.017. PubMed PMID: 24695093.
- Ye L, Wang C, Yu G, Jiang Y, Sun D, Zhang Z, Yu X, Li X, Wei W, et al. *Bmi-1 induces radioresistance by suppressing senescence in human U87 glioma cells*. Oncol Lett. **2014** Dec;8(6):2601-2606. PubMedPMID: 25364434.
- Ying M, Zhan C, Wang S, Yao B, Hu X, Song X, Zhang M, Wei X, Xiong Y, Lu W. *Liposome-Based Systemic Glioma-Targeted Drug Delivery Enabled by All-d Peptides.* ACS Appl Mater Interfaces. **2016** Nov 9;8(44):29977-29985. PubMed PMID: 27797175.
- Zhang X, Wang W, Yu W, Xie Y, Zhang X, Zhang Y, Ma X. *Development of an in vitro multicellular tumor spheroid model using microencapsulation and its application in anticancer drug screening and testing.* Biotechnol Prog. **2005** Jul-Aug;21(4):1289-96. PubMed PMID: 16080713.
- Zhang X, Zhang W, Cao WD, Cheng G, Zhang YQ. *Glioblastoma multiforme: Molecular characterization and current treatment strategy (Review*). Exp Ther Med. **2012** Jan;3(1):9-14. PubMed PMID: 22969836.
- Zhao Y, Ren W, Zhong T, Zhang S, Huang D, Guo Y, Yao X, Wang C, Zhang WQ, Zhang X, Zhang Q. *Tumor-specific pH-responsive peptide-modified pH-sensitive liposomes containing doxorubicin for enhancing glioma targeting and anti-tumor activity.* J Control Release. **2016** Jan 28;222:56-66. doi: 10.1016/j.jconrel.2015.12.006. PubMed PMID: 26682502.
- Zhou Y, Peng Z, Seven ES, Leblanc RM. *Crossing the blood-brain barrier with nanoparticles.* J Control Release. **2018** Jan 28;270:290-

303. doi:10.1016/j.jconrel.2017.12.015. Review. PubMed PMID: 29269142.

CHAPTER 2

Radiotherapy and Adjuvant Drug-Loaded Liposomes target Glioblastoma Stem Cells and Trigger Immune Response

Marco Pizzocri*, Beatrice Formicola*, Matteo Tamborini, Elisabetta Stanzani, Eliana Lauranzano, Federica Ungaro, Simona Rodighiero, Maura Francolini, Maria Gregori, Alessandro Perin, Francesco DiMeco, Massimo Masserini, Francesca Re, Michela Matteoli, Lorena Passoni

* Equally contributed

Accepted by Theranostics, 24th October 2019.

ABSTRACT

Main prognostic factor for GBM survival is the extent of surgical resection. However, due to the infiltrative capacity of GBM cells complete eradication is most of the time impossible to achieve. Therefore, to control tumor growth, and ultimately cure patients, it is essential to develop treatment strategies to kill therapy refractory cells and to mount robust immunosurveillance to prevent disease recurrence. The radio- and chemo- resistance of GSCs together with their innate tumor-initiating aptitude, make this cell population a crucial target for effective therapies. However targeting GSCs is hardly difficult and complex, due to the presence of the BBB and for GSCs infiltrative nature arousing their dispersion within the brain parenchyma.

Methods: To enable BBB crossing, selective GSCs targeting and anti-tumor immune response activation, doxorubicin as paradigm of cytotoxic drug triggering ICD, was encapsulated into LIPs surface-functionalized with an ApoE-derived peptide (mApoE).

Results: Our results indicate that encapsulation into mApoE-LIPs prevents DOXO toxicity on BBB cells and enhances its accumulation within mouse brain *in vivo*. mApoE confers GSC specificity through the engagement of the Low-Density Lipoprotein Receptor. When administered to patient-derived GSC NOD/SCID mouse xenograft mApoE-DOXO-LIPs, but not DOXO-LIPs, triggered GSC apoptosis resulting in a remarkable reduction of tumor growth and invasion of the contralateral hemisphere through commissural fibers. Apoptotic GSCs prompted microglia/macrophage phagocytic activity coupled to the activation of the antigen-presenting machinery propaedeutic to T cell priming. Importantly, the concomitant administration of radiation

(2Gy) enhanced the anti-tumor effects by altering BBB permeability and promoting the expression of LDLR on both BBB and GSCs.

Conclusion: Our results advocate for RT and adjuvant administration of drug-loaded targeted nanovector as an effective strategy to deliver cytotoxic molecules, immune cell death inducers particularly, circumventing BBB hurdles and targeting GSCs at the tumor burden, the forefront of GBM recurrence. The proposed combined approach responds to the need of selective targeting of the GBM stem cells remaining after surgery within the irradiated field while preserving healthy brain by harmful side effects.

1. INTRODUCTION

Glioblastoma (GBM) is the most common and aggressive primary human brain tumor, associated with very poor prognosis and survival (5-year survival rate less than 5%) [1]. Genetic heterogeneity, angiogenesis, high invasive potential and stemness properties are crucial factors concurring to GBM recurrence and high mortality rates. Additionally, the presence of the BBB, which controls the passage of substances from the blood to the brain, contributes to the therapeutic failure. Indeed, while the core of large and advanced brain tumors are associated with disrupted BBB integrity, the peripheral area hosting the invading cells contains regions with intact BBB [2] which favors the creation of microenvironmental niches suitable for cancer cell growth and spreading.

Glioma Stem-like Cells (GSCs) represent a subpopulation of cells characterized by increased resistance to chemo- and radiotherapy. Due to their intrinsic tumor-initiating potential and invasiveness, residual resistant GSCs lead GBM recurrence and progression. Therefore, GSCs are a relevant target for anti-GBM therapeutic strategies, and GSC-xenografts represent the GBM experimental model closest to the clinical scenario [3].

Thanks to an extensively reprogrammed cellular metabolism, tumor cells survive and proliferate under nutrient and oxygen deprivation. In this context, GBM cells are highly dependent on cholesterol supply for survival [4]. Recently Villa and colleagues [5] showed that GBM relies on the uptake of exogenous cholesterol mediated by Low-Density Lipoprotein Receptor (LDLR). Indeed, LDLR is highly expressed in GBM patient, tumor xenografts and cell

lines and its upregulation correlates with tumor progression and drug resistance [4,6,7]. LDLR is also expressed at the BBB level [8] and has been already exploited to improve delivery of therapeutics by transcytosis [9] across the BBB into the brain [10]. Thus, LDLR can be profited to develop new drug delivery systems, with dual-targeting capability for both the BBB and the glioma cells.

A strategy either to target cancer cells and to deliver otherwise impermeant drugs across the BBB is represented by the exploitation of nano-based drug delivery systems [11]. Several drug delivery nanosystems, in particular nanoparticles, are currently undergoing advanced clinical trials or, as in the case of LIPs, have been approved for clinical applications in oncology [12,13].

Here we utilized LIPs functionalized with the ApoE-derived peptide (amino acid residues 141-150; mApoE), previously shown to cross the BBB both *in vitro* and *in vivo* in the Alzheimer Disease experimental model [14,15], as carriers of DOXO to the brain (mApoE-DOXO-LIPs).

Cancer cells exposed to certain chemotherapeutic including DOXO and radiotherapy (RT) undergo to immunogenic cell death (ICD). ICD refers to a functionally unique form of cell death that occurs when apoptotic cells trigger an antigen-specific immune response able to reactivate an antitumour immune response [16]. A critical step for ICD is the engulfment of dying cancer cells by professional macrophages and the activation of a variety of cells of the innate immunity leading to the priming of the adaptive immune response involving T cells [17,18].

Using Patient-Derived Xenografts (PDXs), obtained by intracranial injection of patient-derived GSCs in NOD/SCID mice, we provide evidence for mApoE-DOXO-LIP therapeutic potential by causing GSC apoptosis and ICD triggering. DOXO-LIP administration elicits no effects. Importantly, concomitant mApoE-DOXO-LIP/radiation administration achieves an improved outcome thanks to increased mApoE-DOXO-LIP diffusion and GSC cellular uptake within the irradiated field.

2. METHODS

In vitro transwell BBB model

Human brain endothelial hCMEC/D3 cells (7×10^4 cells/cm^2, passages 25-35) were seeded on 12-well transwell inserts (PET 12-well, pore size 0.4 μm, translucent membrane insert 1.12 cm^2; Euroclone) coated with type I collagen and cultured with 0.5 ml or 1 ml of culture medium in the upper and in the lower chamber. Monolayer formation (approximately 14 days after seeding) was monitored by measuring EP of [^{14}C]-sucrose and [^{3}H]-propranolol and TEER measured by EVOMX meter, STX2 electrode (World Precision Instruments). For permeability experiments, after 3 h of incubation with 2.5 or 25 μg/ml of DOXO, free or embedded into LIPs, the amount of DOXO in the basolateral compartment was measured by fluorescence and the EP to DOXO calculated as described [19]. LIP integrity after BBB crossing was evaluated by Nanoparticle Tracking Analysis (NanoSight NS300, Malvern Panalytical). Impact of free-DOXO or DOXO-LIPs on cell monolayers was checked by measuring TEER and EP of Lucifer

Yellow (50 μM) after hCMEC/D3 incubation. For cytotoxicity experiments, hCMEC/D3 were co-culture with U87-MG, A172 cells ($5.4x10^4$ cells/well) adherent to the bottom of the basolateral compartment. 25 μg/ml of DOXO, free or embedded in LIP, were added to apical compartment and incubated for 3h. Then, upper inserts were removed and GBM cells cultured for additional 48h in the lower chambers. Viability was evaluated by MTT assay.

Patient-derived GSCs

Patient-derived GSC cultures were obtained from GBM patients undergoing surgery for brain tumor removal. Surgical specimens were collected from consenting patients in the Department of Neurosurgery at Neurological Institute "C. Besta" (Italy) under "C. Besta" research ethics committee approval. Tumor samples were processed as by Gritti et al. [20].

mApoE-LIP biodistribution

All procedures involving animals were conducted according to Italian laws and the Animal Utilization Protocols approved by the Italian Ministry of Health. 6–8 weeks old male Balb/c mice (3 mice/group; Charles-River Laboratories) were injected via the tail vein with 100 μL of radiolabelled mApoE-DOXO-LIP (10mM total lipids, 5 mg/kg DOXO, 0.5 μCi/mouse [^{3}H]-Sm, 0.3 μCi/mouse [^{14}C]-DOXO) or free DOXO (5 mg/kg, 0.3 μCi/mouse [^{14}C]-DOXO) in PBS. After mice were sacrificed a total of 0.1 g of each tissue or 100 μl of blood, in triplicate, were solubilized at 55°C for 2h and cooled to room temperature. Radioactivity was measured by liquid scintillation

counting. Data were expressed as percentage of injected dose on total organ weight/volume ± SD. The possible radioactivity derived from the blood was subtracted from the radioactivity values measured in the brain (-5% of measured radioactivity).

GSC orthotopic xenografts and treatments

To study mApoE-DOXO-LIP antitumor activity, luciferase transfected GSC1luc cells (4×10^4) were stereotactically injected into the right striatum of 4-week-old male NOD/SCID mice (NOD.CB-17-Prkdcscid/J, Charles-River). Luciferase stable expression was obtained using the pRRL.sin.PPT.CMV.Luciferase.iresEMCVwt.eGFP.pre lentiviral vector engineered by Dr E.Vigna and kindly provided by Dr. C.Boccaccio (Candiolo Cancer Institute, Candiolo, Torino, Italy) [21]. From 6 weeks after intracranial inoculation, tumors were monitored by BLI imaging (IVIS® II Imaging, Caliper Life Sciences-PerkinElmer) once a week. Treatments started at 8 weeks after tumor injection (D60) when tumors were detectable by BLI. In order to obtain comparable results, animals were randomized according to BLI imagines into four groups homogeneous for tumor dimension (at least 3 animals/group). All treated mice received 37,5 mg/dose/mouse of DOXO delivered by DOXO-LIPs or mApoE-DOXO-LIPs administered intraperitoneal. Whole-brain radiation (2Gy) was performed using an X-ray irradiator operating at 12 mA/190kV (RADGIL, Gilardoni). mApoE-DOXO-LIPs were administered 18h after radiation.

Statistical Analysis

Data of *in vitro* assays were expressed as mean values ± standard deviation (SD) or standard error (SE) of at least three independent experiments performed in replicates. Statistical significance was evaluated with GraphPad Prism software. Data were analyzed by Student *t*-test. Differences were considered significant for P-value < 0.05.

3. RESULTS

mApoE-DOXO-LIP are able to cross the BBB *in vitro* and affect GBM cell viability

Liposome (**Figure1A**) preparation and characterization are detailed in the Supplementary Methods. The physiochemical characterization showed that, under physiological conditions (pH 7.4), the final preparations were formed by LIPs < 130 nm, monodispersed and negatively charged. Release kinetic from mApoE-DOXO-LIP showed a DOXO release rate of 0.11%/h at pH 5 and 0.05%/h at pH 6.5 and 7.4 (**Supplementary Figure 1**).

mApoE-DOXO-LIP ability to cross the BBB and target GBM cells was investigated *in vitro* using a transwell system combined with a human brain capillary endothelial cell monolayer (hCMEC/D3), as a model of BBB (**Figure 1B**), and, when required, with adherent GBM cells cultured in the basolateral chamber (**Figure 1F**). hCMEC/D3 cell monolayer were used when TEER values were >40 Ωcm^2 and the endothelial permeability to LY was < $2x10^{-3}$ cm/min, accordingly to previous data [22].

mApoE-DOXO-LIPs, DOXO-LIPs or free-DOXO were added to the apical compartment and BBB integrity was measured after treatment. A lower toxicity, in terms of Transendothelial Electrical Resistance (TEER) and Endothelial Permeability (EP) to Lucifer Yellow, was detected in hCMEC/D3 cells exposed to DOXO encapsulated into LIPs compared to free-DOXO, suggesting that the drug incorporation reduces its cytotoxicity (**Figure 1C**). EP of DOXO, free or incorporated into LIPs, was measured by means of DOXO fluorescence in the basolateral compartment over time. A significant improvement (approximately 5-fold) in DOXO permeation through the BBB was observed for mApoE-DOXO-LIPs compared to DOXO-LIPs (**Figure 1D**). Measurement of LIP size after BBB crossing revealed the lack of significant differences in LIP dimension confirming the preserved integrity of mApoE-DOXO-LIP (**Figure 1E; Supplementary Figure 1C**).

To assess if encapsulated DOXO is able to exert anti-tumor activity after BBB crossing, the BBB transwell model was integrated with U87MG and A172 GBM cells (**Figure 1F**) and GBM cell viability was evaluated by MTT assay. The results (**Figure 1D**) showed that mApoE-DOXO-LIPs added in the upper chamber was able to significantly reduce, after BBB crossing, the viability of both U87MG and A172 cells by approximately 53% and 60%, respectively.

To confirm that mApoE-DOXO-LIPs cytotoxicity was due to specific LIP intracellular uptake, DOXO fluorescence was measured by microscopy image analysis. Results indicated a 3- to 6-fold increase of nuclear DOXO triggered by mApoE surface LIP functionalization (**Figure 1H; Supplementary Figure 2**). Incubation with the clathrin-

mediated endocytosis inhibitor Chlorpromazine or the dynamin inhibitor Dynasore significantly reduced mApoE-DOXO-LIP intracellular uptake compatible with a receptor-mediated recognition of the mApoE peptide responsible for the cellular uptake (**Figure 1I**).

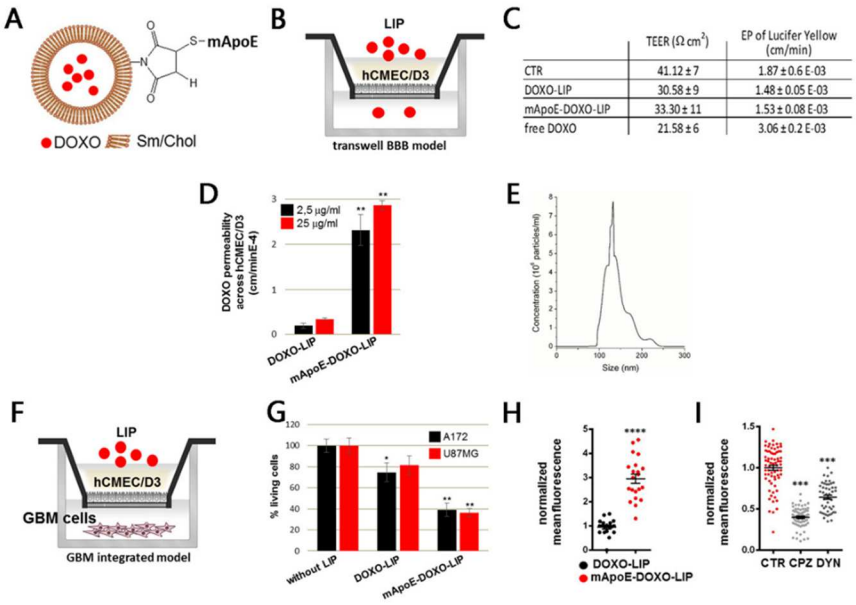

Figure 1. ***In vitro*** **DOXO-LIP BBB crossing and GBM cell viability.**
(**A**) Schematic representation of Sphingomyelin (Sm)/Cholesterol (Chol) LIPs functionalized with mApoE peptide and embedding DOXO. (**B**) Schematic representation of the *in vitro* BBB model prepared using hCMEC/D3 cells seeded on the transwell filter. (**C**) TEER and EP to LY of endothelial monolayers after 3h DOXO (25□g/ml), free or embedded, incubation. (**D**) EP to embedded DOXO determined by adding samples in the apical compartment and monitoring DOXO fluorescence in the basolateral one after 3h. (**E**) mApoE-DOXO-LIP size after BBB crossing determined by nanoparticle tracking analysis of LIPs present in the basolateral compartment. (**F**) Schematic representation of the integrated transwell system prepared seeding adherent GBM cells in the basolateral compartment. (**G**) hCMEC/D3 cells, in co-culture with U87MG or A172, were incubated with DOXO-LIPs or mApoE-DOXO-LIPs added in the apical compartment (DOXO 25 □g/ml). After 3h incubation, the transwell insert was removed and GBM cells viability was determined by MTT assay after additional 72h of culture. (**H**) Nuclear DOXO quantification in U87MG cells incubated with indicated LIPs and (**I**) with mApoE-DOXO-LIPs alone (CTRL) or in

the presence of chlorpromazine (CPZ) and dynasore (DYN). All data are reported as the mean of at least three independent experiments ± SD. *P< 0.05, **P< 0.01, **** P<0.0001

mApoE-DOXO-LIP intracellular uptake and cytotoxicity in patient-derived GSCs

To investigate whether mApoE-LIPs could be exploited to target GSCs, we established primary cell lines from surgical samples of patients at first diagnosis. Patients characteristics are provided in **Supplementary Table 1**. Three GSC lines (**Figure 2A** and **2B**) were selected based on their different degree of response to DOXO including cells with high (GSC1, proneural subtype) and moderate (GSC2, proneural subtype) sensitivity to DOXO and non-responder cells (GSC3, mesenchymal subtype) (**Supplementary Figure 3**). Using the extreme limiting dilution assay [23], the selected cell lines displayed self-renewal capacity at the following frequencies: 1/3,74 for GSC1; 1/5,21 for GSC2 and 1/4,22 for GSC3 cell lines.

mApoE-DOXO-LIP intracellular uptake was evaluated through nuclear DOXO fluorescence quantification. DOXO-LIP conjugation with mApoE significantly augmented nuclear DOXO accumulation in all GSC cultures, particularly in GSC3 cells (**Figure 2C** and **2D**). To verify if DOXO carried by mApoE-LIPs was functional and effective, cell viability was assessed. Non-targeted DOXO-LIPs did not significantly affect GSC viability, even at the highest DOXO dosage, excluding cellular adverse responses to endotoxin contaminants possibly present in the LIP preparations. Conversely, a dose-dependent inhibition of cell viability was observed when GSCs were exposed to mApoE-targeted DOXO-LIPs (**Figure 2E**).

Interestingly, the higher level of nuclear DOXO displayed in GSC3 does not correlate with a decreased cell viability, but it is consistent with GSC3 intrinsic drug-resistance to DOXO. The lower IC_{50} values of free-DOXO (**Supplementary Figure 3**) compared to mApoE-DOXO-LIPs (**Figure 2 D and 2E**) confirms that mApoE-DOXO-LIPs are internalized through active, energy dependent endocytosis whereas free-DOXO promptly enters the cells by passive diffusion.

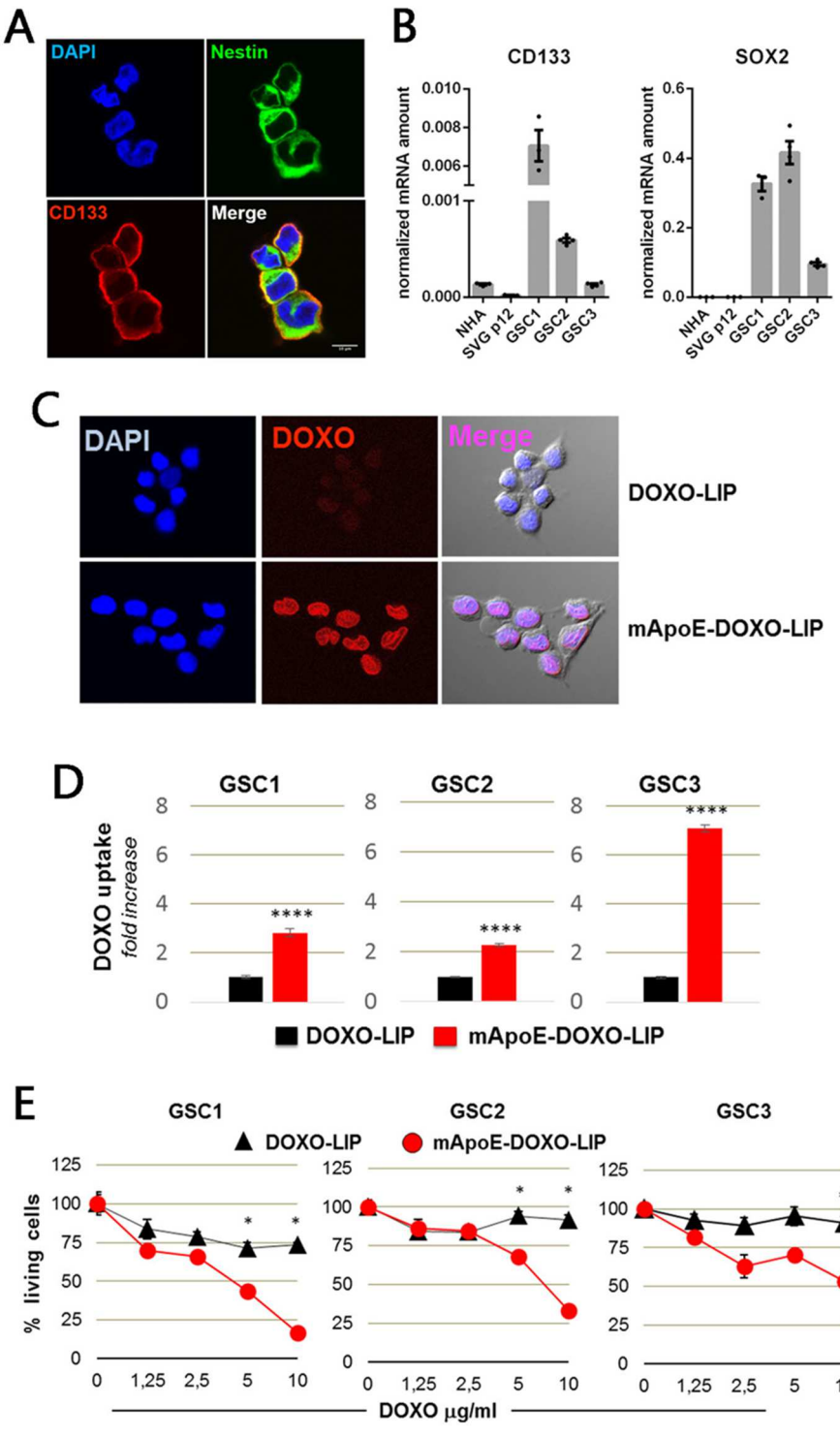
A
DAPI
Nestin
CD133
Merge
B
CD133
SOX2
normalized mRNA amount
0.010
0.008
0.006
0.001
0.000
0.6
0.4
0.2
0.0
NHA
SVG p12
GSC1
GSC2
GSC3
C
DAPI
DOXO
Merge
DOXO-LIP
mApoE-DOXO-LIP
D
GSC1
GSC2
GSC3
DOXO uptake
fold increase
8
6
4
2
0
****
DOXO-LIP
mApoE-DOXO-LIP
E
GSC1
GSC2
GSC3
DOXO-LIP
mApoE-DOXO-LIP
% living cells
125
100
75
50
25
0
*
0
1,25
2,5
5
10
DOXO µg/ml

Figure 2. LIP internalization and cytotoxicity in patient-derived GSC lines.
Established GSC lines were investigated for stemness. (**A**) Representative confocal images of staminal markers nestin (green) and CD133 (red). In blue is the DAPI signal for nucleus detection. (**B**) Real-time PCR detection of *PROM1* and *SOX2* genes in GSC lines and human astrocyte cell lines (NHA and SVGp12) included as controls. Expression data were normalized on *GAPDH*. Results are shown as mean values ± SEM of triplicates. (**C**) Representative images of DOXO, DAPI and bright-field differential interference contrast merged signals in GCS3 cells incubated with mApoE-DOXO-LIP or DOXO-LIP. (**D**) Nuclear DOXO quantification expressed as mean fluorescence intensity (MFI) ± SE normalized to MFI detected in cells incubated with DOXO-LIPs (4h, DOXO 4mg/ml). (**E**) Cell viability after 48h incubation with LIPs at the indicated increasing DOXO concentrations. Values are expressed as mean percentage survival (six replicates ± SE) normalized to corresponding untreated. *P<0.05, ****P<0.0001.

Effect of radiations on LDLR expression and mApoE-DOXO-LIP uptake

Although RT is a GBM standard of care, it is known to promote the expression of several mediators of tumor growth, invasion and metastasis [24]. In this context, we evaluated if radiation, by enhancing LDLR expression on GSCs, could increase mApoE-DOXO-LIP therapeutic potential. Results showed a variable response among GSCs. Upon irradiation, GSC1 and GSC2 exhibited an approximate 2-fold and 4-fold increase of LDLR expression respectively. No LDLR modulation was observed in GSC3 culture (**Figure 3A** and **Supplementary Figure 4**). Radiation-induced LDLR expression paralleled with higher levels of mApoE-DOXO-LIP uptake by GSC1 and GSC2 cells. Consistently, no difference in mApoE-DOXO-LIP uptake was observed in irradiated GSC3 cells (**Figure 3B**).

To verify the possibility to boost mApoE-DOXO-LIP cytotoxic effect, GSC viability was investigated upon mApoE-DOXO-

LIPs/radiations combined treatment. An increased cytotoxic effect was achieved only in GSC2 cells (**Figure 3C**), which are characterized by low/moderate responsiveness to DOXO. Notably, this additive effect was observed only when cells were exposed to mApoE-DOXO-LIPs but not to free-DOXO (**Figure 3D**). This is consistent with a radiation-dependent higher intracellular DOXO accumulation due to increased mApoE-DOXO-LIP uptake mediated by ligand (mApoE)-receptor (LDLR) interaction, which appears essential for the synergic effect. As expected, despite the higher amount of intracellular DOXO, the combined treatment did not affect GSC1 and GSC3 viability (**Figure 3C**). This could be explained by the already high sensitivity to DOXO of GSC1 (**Supplementary Figure 3**), and by GSC3 low DOXO sensitivity together with the lack of LDLR induction.

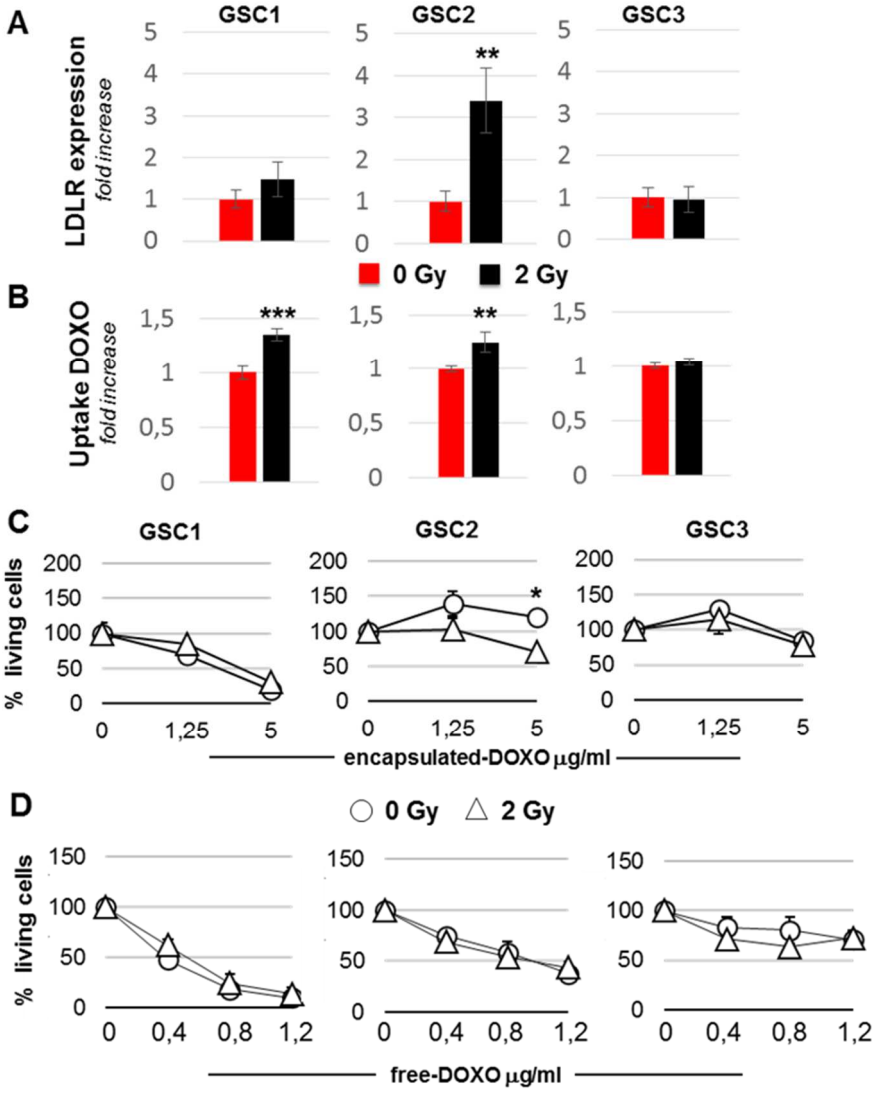

Figure 3. Effect of radiations on LDL-R expression and mApoE-DOXO-LIP intracellular uptake.

(**A**) LDLR level of expression in GSCs 24h after irradiation (2Gy). The results are expressed as mean LDLR fluorescent area (Supplementary Figure 4) respect to non-irradiated (0Gy) samples ± SE. (**B**) Intracellular DOXO quantification in irradiated and non-irradiated GSCs incubated with mApoE-DOXO-LIPs. Results are expressed as MFI normalized to MFI of non-irradiated cells ± SE. (**C**, **D**) Cell viability after 48h incubation with mApoE-DOXO-LIPs (**C**) or free-DOXO (**D**) of irradiated and non-irradiated cells. *P < 0.05, **P<0.01, ***P<0.001.

mApoE-DOXO-LIP biodistribution in healthy mice

Dually radiolabelled mApoE-DOXO-LIPs or radiolabelled free-DOXO were administered intravenously to BALB/c mice. Three and 24 hours after injection, radioactivity was measured. Results (**Figure 4A**) showed that DOXO incorporation into mApoE-LIPs increases its circulation half-life, as indicated by the higher radioactivity levels in the peripheral blood 3h after injection of mApoE-[^{14}C]-DOXO-[^{3}H]-SmLIPs compared to free-[^{14}C]-DOXO. Moreover, [^{14}C]-DOXO incapsulation significantly reduced its accumulation in liver, kidneys, lungs and heart compared to free-[^{14}C]-DOXO. Consistent with the observation that nanoparticles accumulate in the brain over time [25], a progressive increase of radioactivity was detected upon mApoE-DOXO-LIP delivery. Results indicated that 24h after injection the radioactivity of free-[^{14}C]-DOXO in the brain was reduced by 2.7 folds whereas it was 4.4-fold higher after the administration of mApoE-[^{14}C]-DOXO-[^{3}H]-LIP. Furthermore, the ratio between [^{14}C]-DOXO and [^{3}H]-Sm detected in the brain (1:1.2; ^{14}C:^{3}H) was comparable to that of injected mApoE-DOXO-LIPs, consistent with mApoE-DOXO-LIP intact BBB crossing.

The observed moderate/low amount of mApoE-DOXO-LIP crossing undamaged BBB advocates for dull therapeutic effects. Thus, we investigated whether the presence of tumor cells could affect BBB permeability and consequently mApoE-DOXO-LIP brain delivery. Our results (**Figure 4B and 4C**) indicated that the incubation of the transwell BBB model with GSC1 conditioned media could alter BBB properties. In particular, CM from irradiated GSCs increased BBB permeability and CM from non-irradiated and irradiated GSCs induced

an upregulation of LDLR expression on endothelial hCMEC/D3 cells (**Figure 4C**).

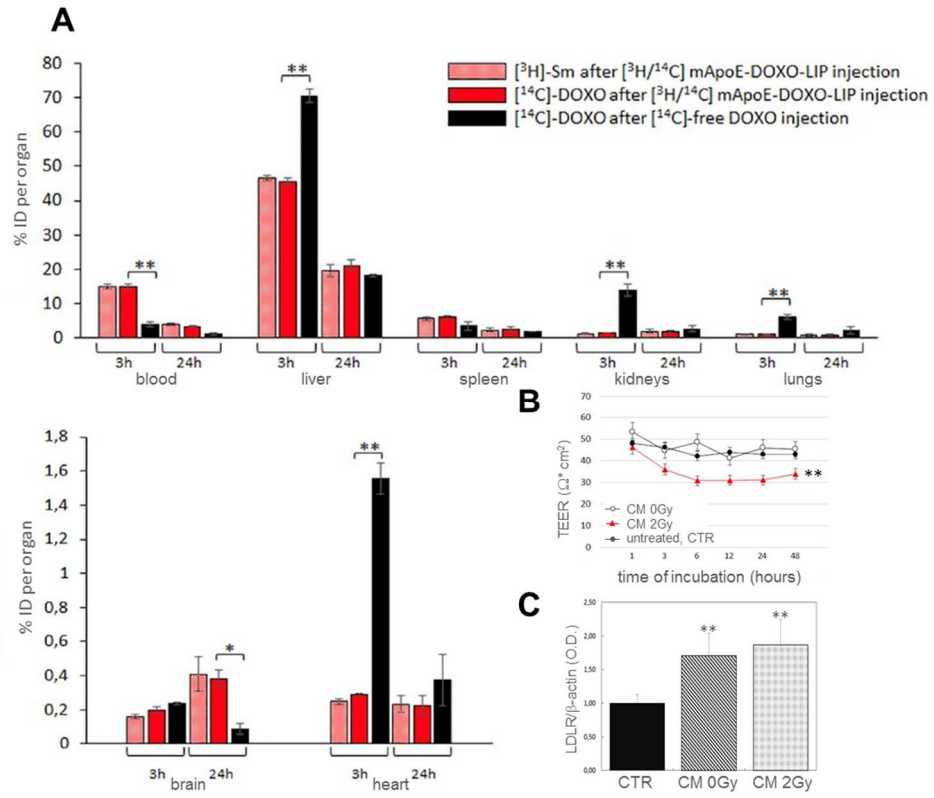

Figure 4. mApoE-DOXO-LIP biodistribution of in peripheral organs and across intact BBB.

(**A**) Dually radiolabelled mApoE-DOXO-LIP ([^{3}H]-Sm/[^{14}C]-DOXO) or free-[^{14}C]-DOXO were intravenously injected in healthy Balb/C mice. Mice were sacrificed 3h or 24h after the injection. Radioactivity in peripheral organs was measured by liquid scintillation counting. The amount of [^{3}H]-Sm or [^{14}C]-DOXO is expressed as percentage of injected dose (ID) ± SD. (**B**) TEER values of BBB transwell model untreated (CTR) or incubated with GSC1 conditioned media (CM) before (0Gy) and after radiation (2Gy). (**C**) LDLR protein level in hCMEC/D3 cells (CTR) and after 12h-incubation with CM from GSC1 untreated and after radiation. *P< 0.05, **P< 0.01.

mApoE-DOXO-LIP antitumor activity in orthotopic GSC-PDX

To prove possible therapeutic potential, mApoE-DOXO-LIPs were administrated as single or radiation-combined therapy to luciferase-transfected GSC1 (GSC1luc)-PDXs (**Figure 5A**). BLI analyses performed at 8 weeks after intracranial xenograft (D60) and at the end of treatment (D75) indicated a low tumor growth rate, consistent with GSC1 stemness features. Tumor growth inhibition was observed only in mice receiving mApoE-DOXO-LIPs both alone or together with radiation. Mice receiving combined treatment showed more manifest tumor reduction (~31%) compared to mice treated with mApoE-DOXO-LIPs only (~25%). No tumor growth inhibition was observed in mice treated with DOXO-LIPs (**Figure 5B** and **5C**).

Histological analyses of GSC1luc xenografts confirmed tumor shrinkage in mice receiving mApoE-DOXO-LIPs. Moreover, GSC1 cells detection by HU immunohistochemistry revealed a reduction of tumor cell spreading across the brain upon combined treatment as indicated by the considerably lower number of HU-positive cells migrating in the contralateral hemisphere along commissural fibers (**Figure 5D**, **Supplementary Figure 5** and **Figure 6**).

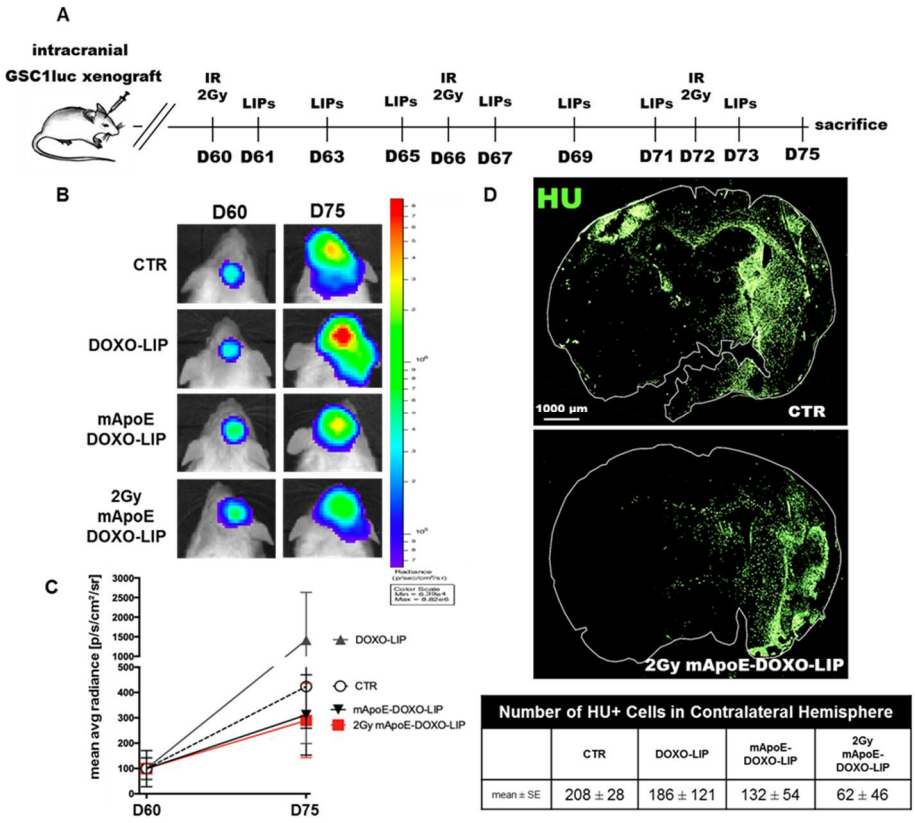

Number of HU+ Cells in Contralateral Hemisphere				
	CTR	DOXO-LIP	mApoE-DOXO-LIP	2Gy mApoE-DOXO-LIP
mean ± SE	208 ± 28	186 ± 121	132 ± 54	62 ± 46

Figure 5. Tumor growth in mApoE-DOXO-LIP/radiation treated GSC1luc xenografts

(**A**) Treatment schedule. (**B**) Representative BLI imagines: mice untreated (CTR); treated with DOXO-LIPs (DOXO-LIP), mApoE-DOXO-LIPs as single agent (mApoE-DOXO-LIP) or concomitant with radiation (2Gy/mApoE-DOXO-LIP). Treatments started 60 days (D60) after intracranial injection of GSC1luc cells. (**C**) Tumor growth quantification after 2-weeks treatment (D75) measured by BLI area detected with fixed ROI. Results are expressed as mean average values normalized to D60 ± SE. (**D**) Representative coronal cryosections from untreated (CTR) and 2Gy/mApoE-DOXO-LIP treated mice. GSC1 cells were detected by anti-human nuclei (HU) immunofluorescence. GSC1 quantification in contralateral, not-injected hemisphere was calculated as number of single HU+/DAPI+ nuclei and a fixed area range of 12-50 mm^2. The analysis was carried out using the FIJI software on 3 sections/brain (Supplementary Figure 5). Results are expressed as mean of HU+/DAPI+ nuclei/cells ± SE.

GAMM phagocytosis of apoptotic GSCs and immune cell death

Apoptosis analysis by *in situ* TUNEL assay indicated a co-localization between TUNEL and HU staining (**Supplementary Figure 7**). A significative increase of apoptotic GSC1 cells was detected in mice injected with mApoE-DOXO-LIPs, both as single agent (0Gy) or concomitant with radiation (2Gy), compared to untreated (CTR) or DOXO-LIP treated mice. Importantly, a low level of TUNEL staining was observed in HU-negative nuclei (murine cells) (**Figure 6A**).

Apoptotic cells are normally removed from tissues via efferocytosis by phagocytes to maintain tissue homeostasis. Macrophages are the most common professional efferocytes [26]. Glioma-associated microglia/macrophages (GAMMs) heavily infiltrate GBM [27]. Therefore, GAMM infiltration was evaluated by immunofluorescence using the myeloid marker Iba1. Results showed no relevant difference in GAMM infiltration extent (**Supplementary Figure 8A**). Conversely, a profound difference in the morphology of Iba1-positive cells was observed (**Supplementary Figure 8B**). Infiltrating Iba1-positive cells in untreated tumors displayed a ramified, highly branched shape disclosing a resting status. In contrast, Iba1-positive cells in mApoE-DOXO-LIP treated tumors had an amoeboid morphology revealing a phagocytic/activated phenotype. Consistently, HU-positive fragments were visible inside Iba1-positive cells of mApoE-DOXO-LIP-treated mice (**Figure 6B** and **Supplementary Figure 8B**). Of note, GAMM amoeboid morphology and HU-positive fragments co-localize with TUNEL staining (**Figure 6C** and **6E**), indicating GAMM-mediated phagocytosis of cellular/nuclear debris released by apoptotic

GSC1 cells. As a further support, Iba1-positive cells associated to vital TUNEL-negative GSC1 cells had a branched morphology and an intact nucleus (**Figure 6D** and **6E**).

In line with the knowledge that DOXO can trigger ICD and that CD11c-positive myeloid phagocytes are required for antigen presentation [28], we investigated CD11c in Iba1-phagocytic cells (**Figure 6F**). No CD11c induction was detected in resting microglia/macrophages from both untreated and irradiated mApoE-DOXO-LIP-treated mice, whereas CD11c was upregulated in activated GAMM upon mApoE-DOXO-LIP/radiation combined treatment (**Figure 6F** and **Supplementary Figure 9**).

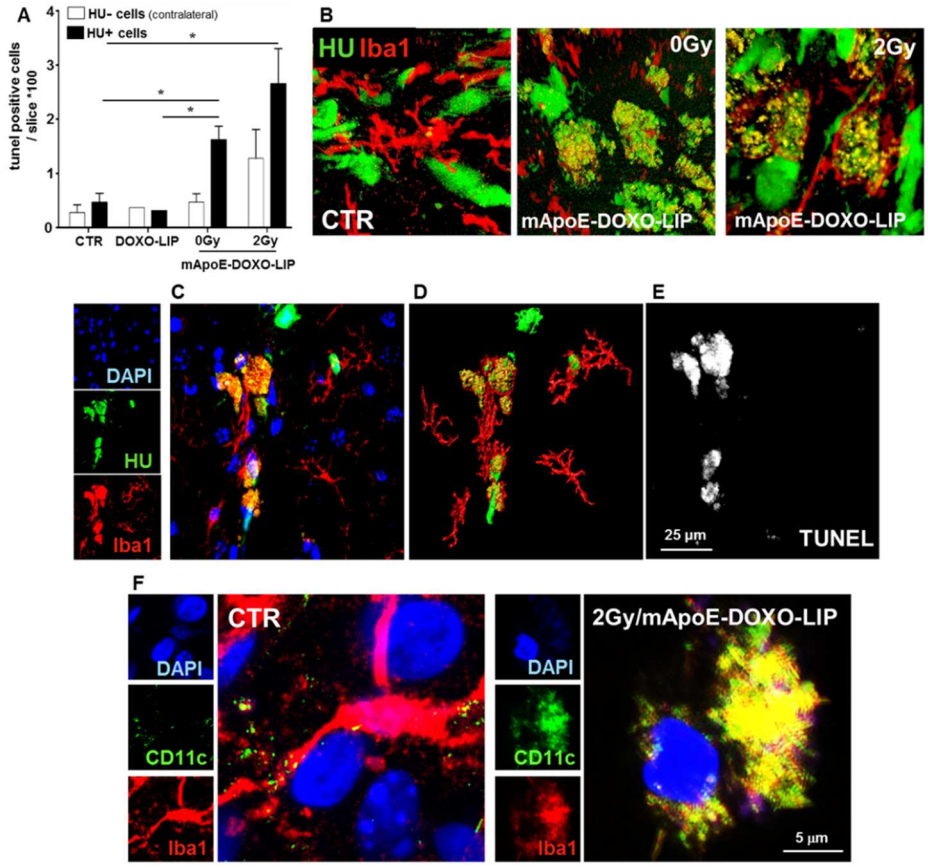

Figure 6. Apoptosis and immune activation in GSC1 xenografts.
(**A**) Quantification of apoptotic cells defined by nuclear HU, DAPI and TUNEL co-localization (Supplementary Fig. S7). Results are expressed as mean values ± SE of HU-positive (human) and HU-negative (murine) in the contralateral hemisphere. (**B**) Representative 3D images of Iba-positive, tumor infiltrating microglia/macrophage in untreated (CTR) and mApoE-DOXO-LIP, without (0Gy) and with (2Gy) radiation, treated mice. Yellow staining indicates HU and Iba1 co-localization. (**C** and **E**) *In situ* TUNEL detection within Iba1-positive cells at tumor border. (**D**) 3D rendering of panel C; (**F**) CD11c immunohistochemical detection in Iba1-positive cells in untreated and 2Gy/mApoE-DOXO-LIPs treated mice. Representative confocal images. Yellow staining indicates CD11c and Iba1 co-localization.

3. DISCUSSION

Current standard of care is not successful in delivering effective and persistent treatments to GBM. Several elements concur to therapy failure, including the high amount of chemo-, radio-resistant tumor-initiating GSCs and the presence of intact BBB in peripheral niches [29]. To approach these issues, we used liposomes surface-functionalized with the mApoE peptide, known to enhance LIP passage across the BBB [30], as nanovehicles to deliver DOXO to the brain and to target GSCs.

In vitro characterization of mApoE-DOXO-LIPs showed that liposome preparations were homogeneous and stable at pH 6.5 the typical value of tumor environment. DOXO encapsulation into LIPs strongly reduced its toxicity on endothelial cells and, as expected, mApoE surface functionalization significantly enhanced DOXO-LIPs passage across the BBB. LDLR expression on BBB endothelial cells would ensure for receptor-mediated transcytosis of mApoE-DOXO-LIPs. Indeed, we observed that after BBB crossing, mApoE-DOXO-LIPs stayed intact and able to impact on the viability of GBM cells by targeted delivery rather than passive intracellular diffusion of DOXO. mApoE-specific, receptor-mediated intracellular uptake was confirmed by (*i*) incubation with endocytosis inhibitors preventing DOXO nuclear accumulation in cells incubated with mApoE-DOXO-LIPs; (*ii*) mApoE functionalization significantly augments DOXO nuclear accumulation and GSC cell death; (*iii*) radiation-induced LDLR upregulation in GSCs correlating with increased DOXO cellular internalization. Overall, these data point out the fundamental role of mApoE in conferring

efficacy to non-functionalized DOXO-LIPs and strongly support the indication of mApoE as a valuable targeting moiety for GSCs.

In vivo biodistribution indicated that healthy BBB allowed a modest accumulation of mApoE-DOXO-LIPs into the brain. However, parallel experiments *in vitro* provided evidence that GSCs, particularly irradiated GSCs, have the capacity to modify neighboring BBB in term of induction of LDLR expression on endothelial cells and compromised permeability that could ease mApoE-DOXO-LIP delivery. Indeed, we observed apoptosis of HU-negative (murine) cells only in mice receiving whole brain irradiation together with mApoE-DOXO-LIPs, which suggests an increased LIP accumulation in non-tumoral brain areas due to impaired permeability of irradiated BBB. A low crossing rate through intact BBB combined to a greater capacity to cross tumor adjacent and irradiated BBB, would confer selectivity to mApoE-DOXO-LIPs delivery within the tumor area protecting healthy brain parenchyma from off-target effects. This is relevant considering that GBM patients receive a localized RT limited to the surgical margins where most of the recurrences originate [31].

mApoE-DOXO-LIP anti-tumor activity was evaluated in GBM-PDXs obtained by intracranial injection of GSCs in NOD/SCID mice, the *in vivo* experimental model that ensure stemness maintenance [32]. This model generated slow-growing, diffused tumors with elevated invasion capacity, proved by the migration of the injected GSC1luc cells into the non-transplanted hemisphere through commissural fibers. This emphasizes the high experimental value of the GSC-NOD/SCID

model that allowed mApoE-DOXO-LIP *in vivo* assessment in a faithful pre-clinical setting [33]. In this context, mApoE-DOXO-LIPs severely affected GSC viability causing specific tumor growth inhibition, besides, noteworthy, reducing cell migration. Untargeted DOXO-LIPs did not affect tumor growth and invasion, thus once again pointing out the pivotal role exerted by mApoE functionalization. Most importantly, mApoE-DOXO-LIPs, but not DOXO-LIPs, triggered a significant level of apoptosis in GSC xenografts.

It could be questioned the mechanism by which mApoE-DOXO-LIPs limit the invasion of the contralateral hemisphere. Although a direct effect on mobility cannot be excluded, it is more reasonable to believe that it would be consequential to cellular death caused by intracellular DOXO accumulation. Nevertheless, the result is highly remarkable given that cell migration and invasion is one of the major GBM pathognomonic features that contributes to the poor prognosis in patients (34).

We recently described that radiations improve the intracellular uptake and tumor accumulation of chlorotoxin-targeted-nanovectors in GBM [2]. Here, we confirmed that a combined strategy augments mApoE-DOXO-LIP anti-tumor effects. One explanation could be the LDLR overexpression in irradiated GSC1 cells that enhances DOXO cellular internalization. However, as GSC1 displayed a strong cytotoxic response to DOXO, the synergistic effect due to increased DOXO accumulation could most likely be neutralized by the high drug sensitivity. Thus, additional mechanisms, other than LDLR

overexpression, should be advocated. It is conceivable that extracellular matrix degradation by matrix metalloproteinases, highly activated in irradiated tumors [24], would facilitate LIP diffusion in the tumor microenvironment after extravasation. In addition, it is known that radiation can increase BBB permeability [35,36] underlining the importance of the combined use of RT and mApoE-DOXO-LIPs to reach effective anti-tumor effects and target selectivity.

A boost of drug internalization would be particularly relevant for those cells, such as GSC2, characterized by a low/moderate response to cytotoxic drugs. In irradiated GSC2 cells, the increased mApoE-DOXO-LIP internalization was associated with a significative dose-response reduction of cell viability. This did not occur when GSC2 cells were exposed to free-DOXO in combination with radiations.

Interestingly, mApoE-DOXO-LIPs did not affect GAMM viability and phagocytic activity, demonstrating mApoE specific uptake by GSCs. This was observed also at the tumor burden suggesting the absence of brain off-target effects. Clearance of apoptotic cells and debris by phagocytic cells is of fundamental importance for restoring tissue homeostasis and for *in situ* shaping and restoring anti-tumor immuneresponse [37]. As consequence of the phagocytosis, we observed the induction of CD11c, marker of antigen-presenting cells, in activated GAMMs. Despite further investigation are needed, CD11c induction is reminiscent of DOXO-driven immunogenic GSC cell death known to induce and/or enhance cancer cells immunogenicity and to trigger T cell priming [38]. This further supports the use of mApoE-

DOXO-LIP for GSC targeting and re-activation of anti-tumor immune response.

DOXO is one of the most commonly used chemotherapeutic agent for the treatment of a broad range of cancers. Yet, in GBM it is known to display excellent antineoplastic activity *in vitro* but poor efficacy *in vivo* due to extrusion by multidrug resistance-related proteins present on both BBB and GBM cells [39]. To constrain DOXO severe adverse effects such as cardiotoxicity and myelosuppression different FDA-approved liposomal DOXO formulations are currently in use in clinic. However, they are untargeted with no surface functionalization [40]. This preclude their use for GBM due to their absent/inefficient BBB crossing. As we demonstrated that mApoE-LIPs could efficiently deliver DOXO to the brain, we propose the adjuvant use of mApoE-functionalized nanovector combined to RT as a promising approach to overcome the impediments handed by the BBB including drug resistance by molecular extrusion and to deliver drug-loaded nanovectors to GBM particularly those known to elicit ICD.

Finally yet importantly, differently from other approaches involving temporary BBB perturbation to facilitate nanovector delivery [41], patients undergoing RT and adjuvant nanomedicine would not need additional procedures to deliver drug-loaded nanovectors.

4. CONCLUSIONS

In this report, we provide proof of concept for RT and adjuvant mApoE-functionalized, drug-loaded LIPs combined treatment as an effective precision strategy to deliver anti-tumor molecules limited to the irradiated area surrounding the GBM invasive edges. This is of relevance considering that healthy brain parenchyma would be preserved from off-target effects and that therapy-resistant GSCs reside at burden, are responsible for tumor invasion and recurrence. mApoE functionalization would guarantee selective crossing of irradiated BBB and targeting of GSCs that ultimately lead to apoptosis and anti-tumor immune response activation. Therefore, in addition to inhibit tumor viability, DOXO-loaded mApoE-nanovectors can be instrumental for immunotherapeutic approaches.

Abbreviations

ApoE: Apolipoprotein E; BBB: Blood Brain Barrier; BLI: bioluminescence; Chol: Cholesterol; CM: conditioned media; CPZ: chlorpromazine; DOXO: doxorubicin; DYN: dynasore; EP: endothelial permeability; GAMM: Glioma-associated microglia/macrophages; GBM: glioblastoma; GSC: Glioblastoma Stem-like Cell; HU: Human Nuclei; ICD: immunogenic cell death; LDLR: Low-Density Lipoprotein Receptor; LIPs: liposomes; LY: Lucifer Yellow; PDX: patient-derived xenograft; RT: radiotherapy; Sm: Sphingomyelin; TEER: transendothelial electrical resistance; TUNEL: terminal deoxynucleotidyl transferase dUTP nick end labeling.

Supplementary materials

A

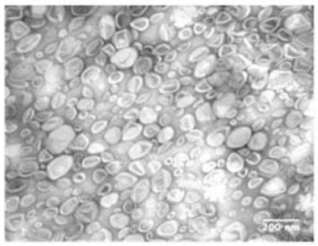

B

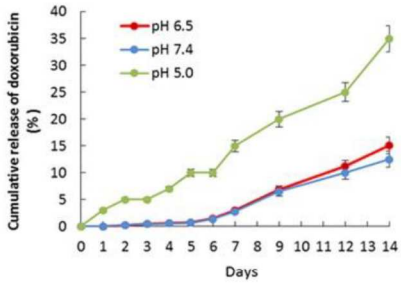

C

Sample	Size ± SD (nm)	Polydispersion Index (PDI)	ζ-pot ± SD (mV)
LIP	102 ± 5	0.077	-25.51 ± 0.82
DOXO-LIP	117 ± 12	0.106	-18.74 ± 1.25
mApoE-DOXO-LIP	128 ± 15	0.081	-12.48 ± 2.02

Supplementary Figure 1. Characterization of mApoE-DOXO-LIPs.

(A)Representative TEM image of mApoE-DOXO-LIP. Scale bar: 200nm. Transmission electron microscopy analyses demonstrated that mApoE-DOXO-LIPs are predominantly unilamellar structures with a mean diameter of 113.33 ± 22.88 nm. (B) Cumulative DOXO release (percentage) over time from mApoE-DOXO-LIPs at pH 5.0, 6.5 or pH 7.4, at 37 °C. The reported data are the mean of at least five different measurements ± SD. (D)Physicochemical parameters of synthetized LIPs: mean diameter (size), polydispersion index(PDI) by dynamic light scattering(DLS); Zeta-potential (ζ-pot) by Zeta-potential analyzer. All liposome preparations maintained a constant size and ζ-potential for up to 10 days within the experimental error (<2.6% of variation). The yield of DOXO encapsulation into LIP was 95±3% and the final preparation contained 220-±12 μg of DOXO/μmol of lipids. The yield of LIP surface functionalization with mApoE peptide ranged between 55% and 65% corresponding to 1.25% of total lipids.

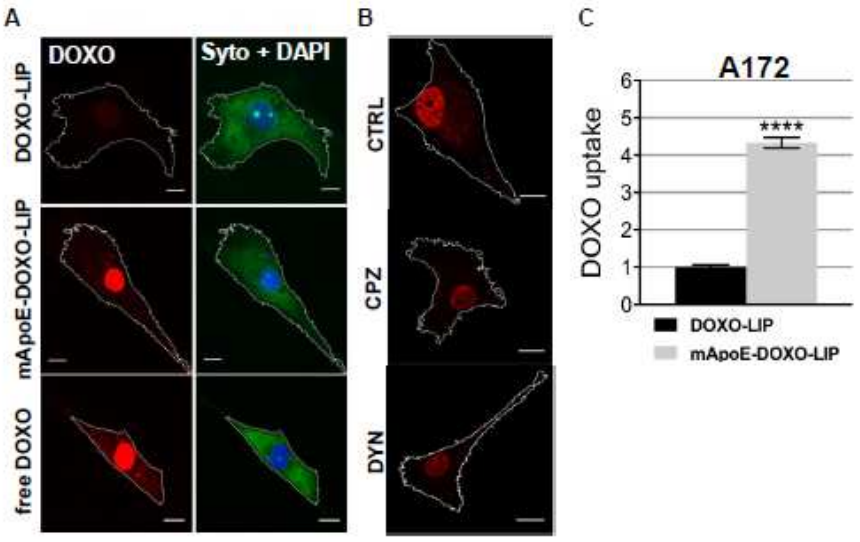

Supplementary Figure 2. LIP internalization in GBM cells.
(A)Maximum projections of DOXO and Syto/DAPI merged signals acquired by means of confocal microscopy in U87MG cells incubated with liposomes (DOXO-LIP or mApoE-DOXO-LIP) or free-DOXO. (B)Maximum projections of DOXO signals in U87MG cells incubated with mApoE-DOXO-LIP alone (CTRL) or in the presence of the endocytosis inhibitors chlorpromazine (CPZ) and dynasore (DYN). (D)Nuclear DOXO quantification in the sample incubated with mApoE-DOXO-LIP in the presence/absence of endocytosis inhibitors. Scale bar 10 µm. (C)Nuclear fluorescence quantification (DOXO uptake) in A172 cells incubated with the indicated liposomes. Refers to the mean fluorescence values were normalize d by the sample incubated with DOXO-LIPs. ****P<0.0001. GBMcells(U87-MG, A172) were seeded on glass coverslips at a concentration of 3500 cell/cm^2. The day after the cells were incubated with liposomes (DOXO-LIP or mApoE-DOXO-LIP) or free-DOXO (DOXO, 4µg/ml in every condition) for 4h in complete medium with 5% FBS. In the experiments with the endocytosis inhibitors, CPZ (10µM) or DYN (80µM) were added to the cell medium one hour before the incubation with liposomes. The inhibitors were kept into the cell medium during the whole experiment (5-hour incubation). During the last 45 min of liposomes incubation (with or without endocytosis inhibitors) the cells were loaded with Syto45 (Molecular Probe) then washed with PBS, fixed in PFA4% in PBS for 15min, DAPI (Sigma-Aldrich) stained (10µg/ml in PBS, 30min) and mounted in 90% glycerol in PBS. The Z-stack series of the cells in different experimental conditions were acquired by means of a confocal microscope (TCSSP5, Leica Microsystems GmbH) with the HCXPLAPO 63x/1.4OIL objective. The DAPI (ex/em:405/415-450nm), Syto45 (ex/em:458/470-500nm) and DOXO autofluorescence (488/570-700) signals were acquired sequentially at high scan rate. Images were processed using Image J (Wayne Rasband, National Institute

of Mental Health, Bethesda, Maryland, USA) using the DAPI signal to segment the nucleus and the Syto45 signal to identify the cell contour. The DOXO fluorescence was quantified in the nuclei as mean grey values in the optical section were the nucleus area were maximized.

Supplementary Table 1. Patient Characteristics

	IDH	MGMT met	EGFRvIII	p53	PTEN
GCS1	wt	focally +	-	+	+
GCS2	wt	-	-	-	-
GCS3	wt	na	na	+	na

wt: wild type; met: methylation; na: not available; + mutated; - wild type.

Supplementary Table 1.

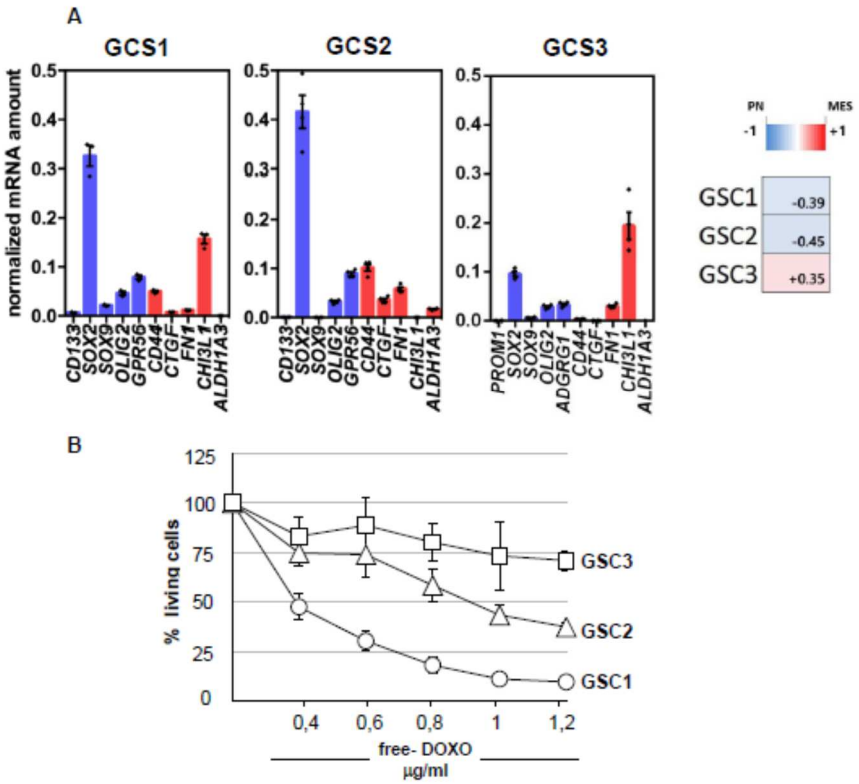

Supplementary Figure 3. GSC line characterization.

(A) Proneural (PN) *vs* Mesenchymal (MES) molecular subtyping. The PN/MES metagene calculation was performed as previously described (Bhat KPL et al., 2013). Briefly, metagene score was calculated for each sample and compared to others after Z-score correction, being +1.00 value indicating a complete MES culture and a -1.00a pure PN subtype. Given the score obtained, analysed cultures displayed a PN (GSC1 and GSC2) or MES (GSC3) signature.

(B) Effect of free-DOXO on GSC culture viability, measured by MTT assay. Cells were exposed to increased concentrations of DOXO for 48h. The obtained relative values were normalized to the values from the corresponding untreated cells and are shown as percentage of survival. Results are expressed as mean percentage of 4 indipendent experiments performed in triplicate ± SE

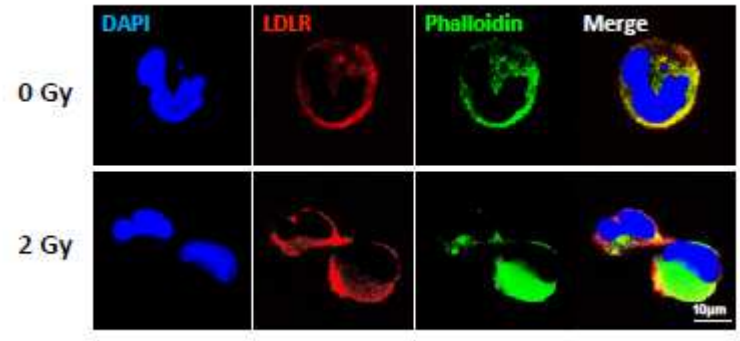

Supplementary Figure 4. LDLR expression on GSCs before and after radiation. Representative confocal images of irradiated (2Gy) and non-irradiated (0Gy) GSC2 cells immunostained for human LDL-R (red).In blue is the nuclear staining (DAPI). The cell border s were defined by Phalloidin staining (green).

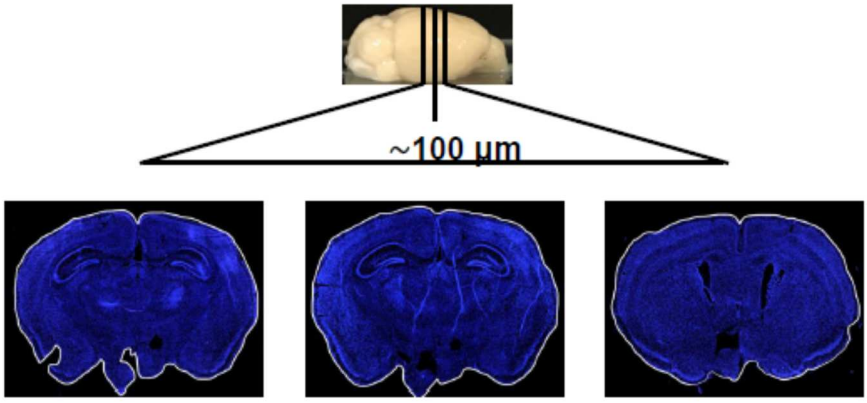

Supplementary Figure 5. GSC1 luc xenograft histological analysis
GSC1 luc cells were injected into the right striatum of NOD/SCID mice. Treatments started approximately 8 weeks after tumor injection (D60). After 2 weeks (D75), animals were euthanized with intracardiac perfusion of saline solution, followed by 4% paraformaldehyde. Three coronal brain cryosections (10mm) were analysed for each single treated and untreated mouse. Cryosections at the intersection of the tumor injections ite and serial anterior/posterior sections (50mm distance) were considered. Coronal images were acquired using a DM i8 fluorescent microscope and a Leica

Application SuiteX (LASX) Imaging system (LeicaMicrosystems). DAPI signal (blue) for nuclei detection was used to delimitate brain section contour (white lane).

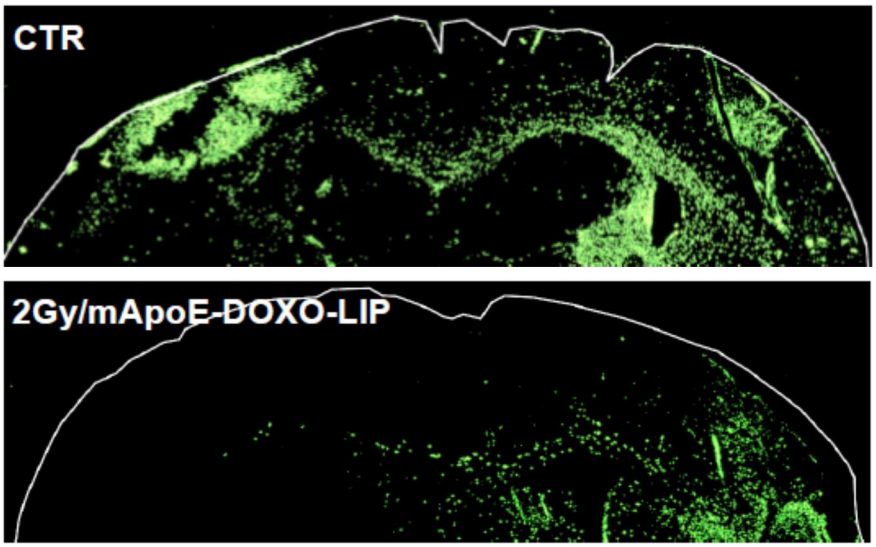

Supplementary Figure 6. GSC1 luc cell migration.
Enlargement of Fig. 7D showing in more details GSC1 luc cell migration into contralateral hemisphere through commissural fibers in untreated (CTR) and treated (mApoE-DOXO-LIPs and 2G y radiation) mice.

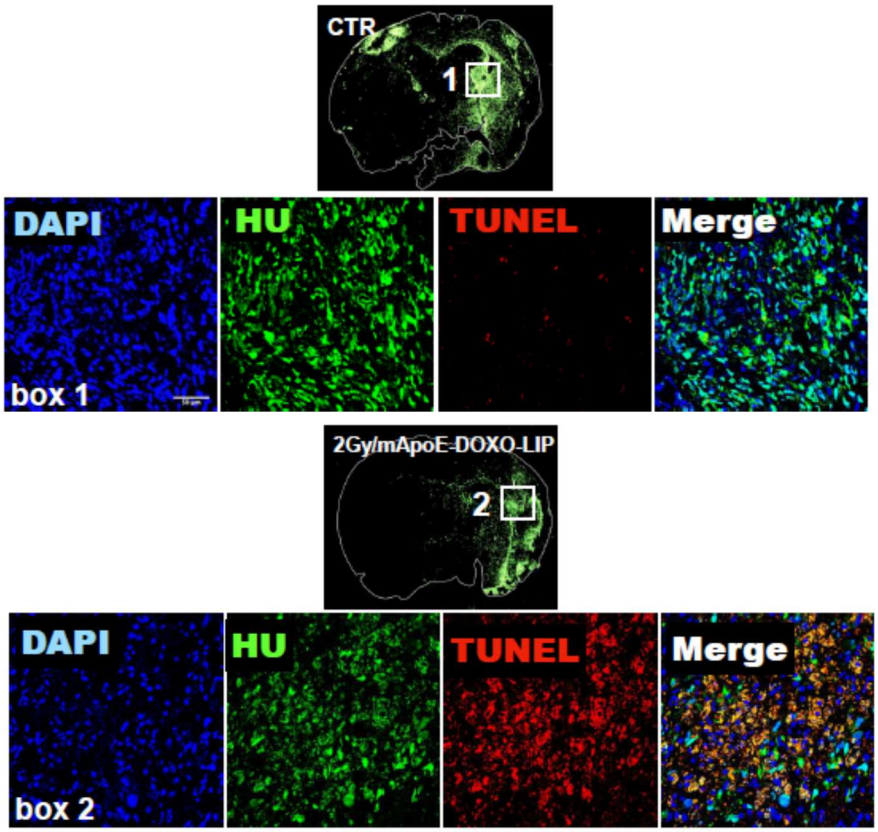

Supplementary Figure 7. In situ apoptposis detection in GSC1 xenografts. Brain cryosections were co-stained with anti-HU, TUNEL and DAPI. Higher magnification (63X) of selected regions (box1 and 2) within coronal sections described in Fig.7 and reported here for clarity.

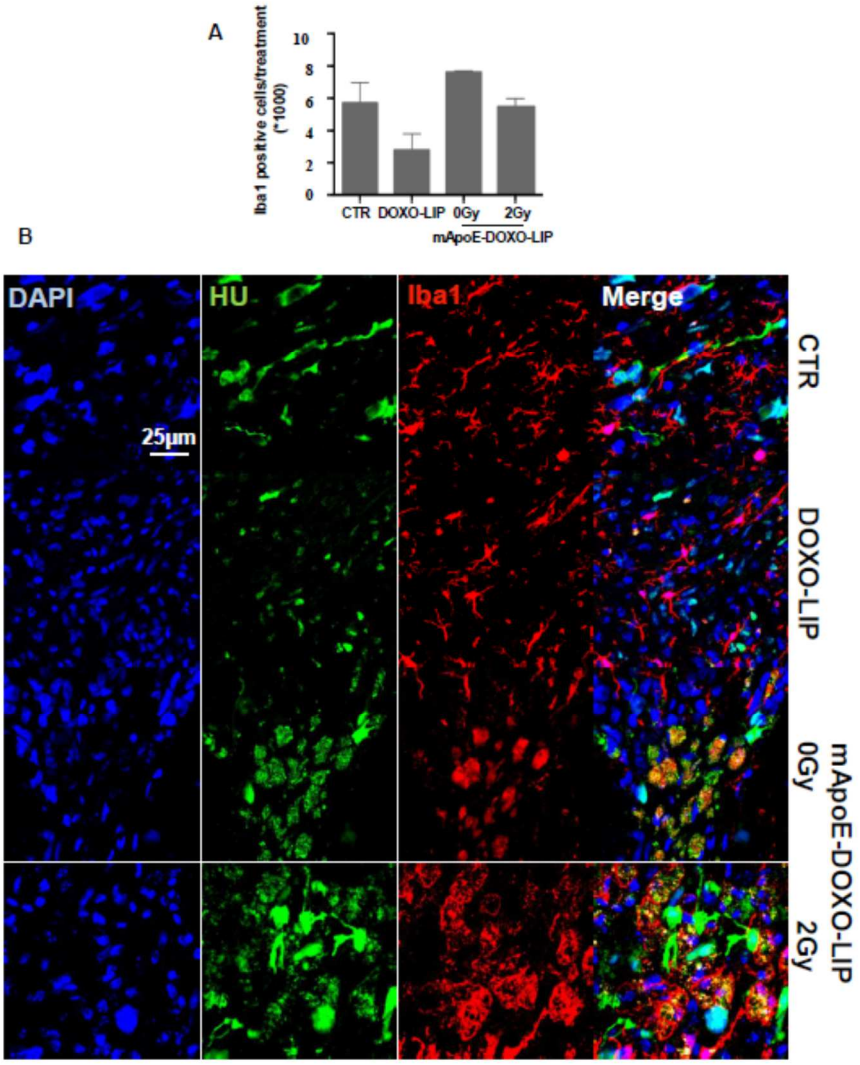

Supplementary Figure 8. Microglia/macrophage infiltration in GSC1 xenografts. Brain cryosections were co-stained with anti-HU, anti-Iba1 and DAPI. (A)Quantification of microglia/macrophages in brain cryosections by Iba1 and DAPI staining detected using a DM i8 fluorescent microscope (Leica Microsystems). Iba1/DAPI-positive cells present in the tumor-injected hemisphere were counted in three serial section for each brain (see Supplementary Figure 5). Quantification was carried out by imaging analysis (FIJI software). Results are expressed as mean values±SE of at least nine sections of the indicated treatment group. (B)Representative images of cryosectons in the tumoral area from untreated mice (CTR) and animals treated with DOXO-LIPs or mApoE-DOXO-LIPs alone (0Gy) or in combination with radiation (2Gy).

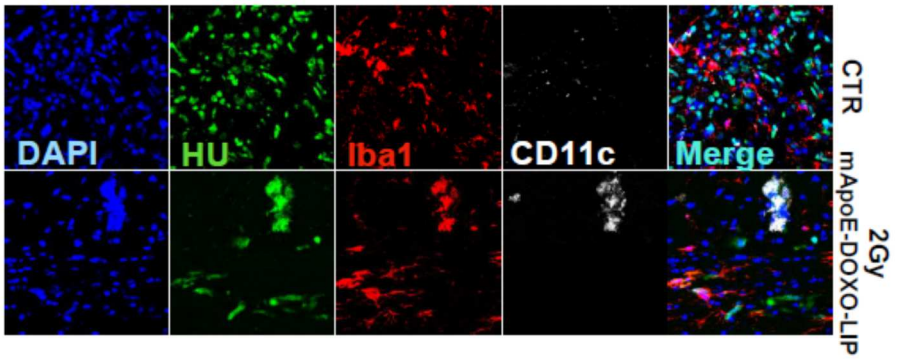

Supplementary Figure 9. Microglia/macrophage immune activation in GSC1 xenografts. Brain cryosections were co-stained with anti-HU, anti-Iba1, anti-CD11c and DAPI. Representative images of cryosectons from untreated mice (CTR) and animals treated with mApoE-DOXO-LIPs in combination with radiation (2Gy).

Supplementary Methods

Preparation and characterization of mApoE-DOXO-LIPs

LIP composed of Sm/Chol/PE-PEG-mal (48.75:48.75:2.5 molar ratio) in ammonium sulphate (500 mM, pH 5.5) were prepared by extrusion procedure. LIPs (5 μmolstotal lipids) were incubated with 1 mg/ml DOXO for 1 h at 65°C to obtain DOXO-LIP. DOXO-LIPs were then functionalized with mApoE as described previously to obtain mApoE-DOXO-LIPs. mApoE (CWGLRKLRKRLLR-NH2) was purchased from DBA Italia (Segrate, Italy).

LIPs were purified by gel filtration (Sephadex G-25 fine resin). DOXO loading was quantified by measuring the DOXO fluorescence (λex = 495 nm; λem =592 nm) after liposomes disruption with 0.1% Triton X-100. Phospholipids content was quantified by Stewart Assay. The amount of mApoE attached on LIP surface was determined by measuring the shift of tryptophan fluorescence intensity (λex = 280

nm). Non-functionalized LIP and DOXO-LIP were used as controls. Stability was measured in PBS by following size and polydispersity index (PDI) by DLS for 10 days. The reported data are the mean of at least five different measurements. For transmission electron microscopic (TEM) evaluation, mApoE-DOXO-LIP were deposited on formvar and carbon coated 300 mesh copper grids (EMS, Hatfield—PA) and negatively stained with a solution of 2% Uranyl Acetate. After drying, the grids were examined under a Philips CM10 TEM (FEI, Eindhoven, NL) with an accelerating voltage of 80 kV and images were acquired with a Morada camera and iTEM software (Olympus, Tokyo, JP).

In vitro DOXO release

Release of DOXO from loaded LIP was monitored at 37°C in phosphate buffered saline (PBS) at pH 7.4, 6.5 or 5.0. At various time points up to 14 days, an aliquot was withdrawn from LIP suspension and filtered using a 10 kDaMWCO spin filter, at 4000 rpm. The filtrate, which contained DOXO released from the LIP, was analyzed for DOXO content as described above by spectrofluorimetry. DOX release was calculated using Eq. (1):

DOXO release (%) = ([DOXO]filtrate / [DOXO]initial sample) * 100

Evaluation of LIP internalization in GSCs

GSCs were seeded on glass coverslips (5x104 cells on 18mm coverslips) and incubated with DOXO-LIP or mApoE-DOXO-LIP for 4 h (DOXO, 4 μg/ml in every condition). Irradiated GSCs were incubated with LIPs 20h after radiation treatment. Cells were irradiated

with a single dose of 2Gy using an X-ray biological irradiator operating at 12 mA/190kV (RADGIL, Gilardoni, Lecco, Italy) at a dose rate of 0.65 Gy/min. The Z-stack series of the cells in different experimental conditions were acquired by means of a confocal microscope (fv1000 TIRF, Olympus) with 63X1.35 OIL objective. The DAPI signal (ex/em: 405/450 nm) and DOXO autofluorescence were acquired sequentially at high scan rate. Images were processed using ImageJ software using the DAPI signal to segment the nucleus and bright field (Nomanski) to identify the cell contour. At least 30 cells/experimental group from 10 microscopy fields were analyzed.

Immunofluorescence

LDLR level of expression in GSC cultures was detected by immunostaining incubating the cells (5x104 cells on 18mm coverslips) with primary antibody against human LDLR (1:100, Sigma-Aldrich) over night at 4°C. After primary antibody, samples were incubated with anti-mouse secondary antibody conjugated with Alexa Fluor® 488 (1:200, Thermo Fisher) and anti-Phalloidin conjugated with Alexa Fluor® 647 (1:100, Thermo Fisher) for 1h at room temperature. Glasses were mounted with a PBS/glycerol mixture (1:1) with DAPI (1:40.000) (Sigma-Aldrich, St. Louis, MO). LDLR level of expression was quantified by confocal images processed using ImageJ software. The central, upper, and lower sections of 1μm z-stack were analyzed for each image and the LDLR threshold, determined on the negative control, was kept constant in each experimental conditions. LDLR level was calculated as LDLR-positive fluorescent area normalized to the cellular cytoplasmatic area demarcated by the phalloidin staining.

In vitro viability assay

GSCs (104 cells/well) and endothelial hCMEC/D3 cells (5000 cells/well) were plated in 96-well plates in a final volume of 200 µl of medium in the absence/presence of increasing doses of different LIPs at the indicated doses of DOXO. Only in the experiments using the GBM integrated BBB model, LIPs were removed 3 h after treatment. 48-72 h after treatment, GSCs and/or GBM cell lines respectively, the mitochondrial enzymatic activity, index an indicator of cell viability, was assessed by MTT assay.

Histopathology analysis and TUNEL assay

Animals were euthanized with intracardiac perfusion of saline solution, followed by 4% paraformaldehyde fixation. Harvested brains were frozen, and serial cryosections (10m thick) were prepared and stored at -80C°. Three coronal sections (one at the intersection of the tumor injection site plus one anterior and one posterior sections at 50 m distance, (Supplementary Fig. S5) were analyzed for each single treated and untreated mouse.

Frozen brain sections were immunostained with mouse anti-Human Nuclei (clone 235-1, Sigma), rabbit anti-Iba1 (Wako) primary antibodies followed by anti-mouse Alexa Fluor 488 and anti-rabbit Alexa Fluor 555 secondary antibodies (Thermo Fisher). The Click-iT Plus Alexa Fluor 647 TUNEL Assay (Thermo Fisher) was used to detect in situ apoptosis and DAPI for nuclei staining. Coronal images were acquired using a DMi8 fluorescent microscope and Leica Application Suite X (LAS X) imaging system (Leica Microsystems). Confocal microscopy was performed using a Leica TCS SP8 confocal

microscope. Maximum projections were obtained from 29-35 Z-stacks. Image analysis was carried out by FIJI (SchindelinJ; Arganda-Carreras I; FriseE; et al. Fiji: an open-source platform for biological-image analysis. Nature methods 2012;9(7):676-682) or Imaris (Bitplane, Zurich, Switzerland) for 3D rendering.

References

1. Stupp R; Lukas RV.; Hegi ME. Improving survival in molecularly selected glioblastoma. Lancet. 2019; 393(10172): 615-617.
2. Campos,B; Olsen LR; Urup T; Poulsen HS. A comprehensive profile of recurrent glioblastoma. Oncogene. 2016.
3. Tamborini M; Locatelli E; Rasile M, et al. A Combined Approach Employing Chlorotoxin-Nanovectors and Low Dose Radiation To Reach Infiltrating Tumor Niches in Glioblastoma. Acs Nano. 2016; 10(2); 2509-2520.
4. Joo KM; Kim J; Jin J; et al. Patient-specific orthotopic glioblastoma xenograft models recapitulate the histopathology and biology of human glioblastomas in situ. Cell Rep. 2013; 3(1): 260-273.
5. Geng F; Cheng X; Wu XN; et al. Inhibition of SOAT1 Suppresses Glioblastoma Growth via Blocking SREBP-1-Mediated Lipogenesis. Clin Cancer Res. 2016; 22(21): 5337-5348.
6. Villa GR; Hulce JJ; Zanca C; et al. An LXR-Cholesterol Axis Creates a Metabolic Co-Dependency for Brain Cancers. Cancer Cell. 2016: 30(5): 683-693.
7. Guo D; Reinitz F; Youssef M; et al. An LXR agonist promotes glioblastoma cell death through inhibition of an EGFR/AKT/SREBP-1/LDLR-dependent pathway. Cancer Discovery. 2011; 1(5); 442-456.
8. Maletinska L; Blakely EA; Bjornstad KA; et al. Human glioblastoma cell lines: levels of low-density lipoprotein receptor and low-density lipoprotein receptor-related protein. Cancer Res. 2000; 60(8): 2300-2303.

9. Pulgar VM. Transcytosis to Cross the Blood Brain Barrier, New Advancements and Challenges. Front Neurosci 2018;12:1019
10. Malcor JD, Payrot N, David M, Faucon A, Abouzid K, Jacquot G, et al. Chemical optimization of new ligands of the low-density lipoprotein receptor as potential vectors for central nervous system targeting. Journal of medicinal chemistry 2012;55:2227-41
11. Bregoli L, Movia D, Gavigan-Imedio JD, Lysaght J, Reynolds J, Prina-Mello A. Nanomedicine applied to translational oncology: A future perspective on cancer treatment. Nanomedicine : nanotechnology, biology, and medicine 2016;12:81-103
12. Marchal S, El Hor A, Millard M, Gillon V, Bezdetnaya L. Anticancer Drug Delivery: An Update on Clinically Applied Nanotherapeutics. Drugs 2015;75:1601-11
13. Wicki A, Witzigmann D, Balasubramanian V, Huwyler J. Nanomedicine in cancer therapy: challenges, opportunities, and clinical applications. J Control Release 2015;200:138-57
14. Bana L, Minniti S, Salvati E, Sesana S, Zambelli V, Cagnotto A, et al. Liposomes bi-functionalized with phosphatidic acid and an ApoE-derived peptide affect Abeta aggregation features and cross the blood-brain-barrier: implications for therapy of Alzheimer disease. Nanomedicine : nanotechnology, biology, and medicine 2014;10:1583-90
15. Re F, Cambianica I, Zona C, Sesana S, Gregori M, Rigolio R, et al. Functionalization of liposomes with ApoE-derived peptides at different density affects cellular uptake and drug transport across a blood-brain barrier model. Nanomedicine : nanotechnology, biology, and medicine 2011;7:551-9
16. Kroemer G, Galluzzi L, Kepp O, Zitvogel L. Immunogenic cell death in cancer therapy. Annu Rev Immunol 2013;31:51-72
17. Galluzzi L, Buque A, Kepp O, Zitvogel L, Kroemer G. Immunogenic cell death in cancer and infectious disease. Nat Rev Immunol 2017;17:97-111
18. Rapoport BL, Anderson R. Realizing the Clinical Potential of Immunogenic Cell Death in Cancer Chemotherapy and Radiotherapy. International journal of molecular sciences 2019;20

19. Cecchelli R, Dehouck B, Descamps L, Fenart L, Buee-Scherrer V, Duhem C, et al. In vitro model for evaluating drug transport across the blood-brain barrier. Adv Drug Deliver Rev 1999;36:165-78
20. Gritti A, Parati EA, Cova L, Frolichsthal P, Galli R, Wanke E, et al. Multipotential stem cells from the adult mouse brain proliferate and self-renew in response to basic fibroblast growth factor. The Journal of neuroscience : the official journal of the Society for Neuroscience 1996;16:1091-100
21. De Bacco F, D'Ambrosio A, Casanova E, Orzan F, Neggia R, Albano R, et al. MET inhibition overcomes radiation resistance of glioblastoma stem-like cells. EMBO molecular medicine 2016;8:550-68
22. Cox A, Andreozzi P, Dal Magro R, Fiordaliso F, Corbelli A, Talamini L, et al. Evolution of Nanoparticle Protein Corona across the Blood-Brain Barrier. Acs Nano 2018;12:7292-300
23. Hu Y, Smyth GK. ELDA: extreme limiting dilution analysis for comparing depleted and enriched populations in stem cell and other assays. J Immunol Methods 2009;347:70-8
24. Pei J, Park IH, Ryu HH, Li SY, Li CH, Lim SH, et al. Sublethal dose of irradiation enhances invasion of malignant glioma cells through p53-MMP 2 pathway in U87MG mouse brain tumor model. Radiat Oncol 2015;10:164
25. Lee JH, Kim YS, Song KS, Ryu HR, Sung JH, Park JD, et al. Biopersistence of silver nanoparticles in tissues from Sprague-Dawley rats. Particle and fibre toxicology 2013;10:36
26. Werfel TA, Cook RS. Efferocytosis in the tumor microenvironment. Seminars in immunopathology 2018;40:545-54
27. Gieryng A, Pszczolkowska D, Walentynowicz KA, Rajan WD, Kaminska B. Immune microenvironment of gliomas. Laboratory investigation; a journal of technical methods and pathology 2017;97:498-518
28. Hume DA. Macrophages as APC and the dendritic cell myth. J Immunol 2008;181:5829-35

29. Geraldo LHM, Garcia C, da Fonseca ACC, Dubois LGF, de Sampaio ESTCL, Matias D, et al. Glioblastoma Therapy in the Age of Molecular Medicine. Trends in cancer 2019;5:46-65
30. Mancini S, Minniti S, Gregori M, Sancini G, Cagnotto A, Couraud PO, et al. The hunt for brain Abeta oligomers by peripherally circulating multi-functional nanoparticles: Potential therapeutic approach for Alzheimer disease. Nanomedicine : nanotechnology, biology, and medicine 2016;12:43-52
31. Petrecca K, Guiot MC, Panet-Raymond V, Souhami L. Failure pattern following complete resection plus radiotherapy and temozolomide is at the resection margin in patients with glioblastoma. Journal of neuro-oncology 2013;111:19-23
32. Lan X, Jorg DJ, Cavalli FMG, Richards LM, Nguyen LV, Vanner RJ, et al. Fate mapping of human glioblastoma reveals an invariant stem cell hierarchy. Nature 2017;549:227-32
33. Mughal AA, Zhang L, Fayzullin A, Server A, Li Y, Wu Y, et al. Patterns of Invasive Growth in Malignant Gliomas-The Hippocampus Emerges as an Invasion-Spared Brain Region. Neoplasia 2018;20:643-56
34. Reardon DA, Wen PY. Glioma in 2014: unravelling tumour heterogeneity-implications for therapy. Nature reviews Clinical oncology 2015;12:69-70
35. d'Avella D, Cicciarello R, Albiero F, Mesiti M, Gagliardi ME, Russi E, et al. Quantitative study of blood-brain barrier permeability changes after experimental whole-brain radiation. Neurosurgery 1992;30:30-4
36. Yuan H, Gaber MW, Boyd K, Wilson CM, Kiani MF, Merchant TE. Effects of fractionated radiation on the brain vasculature in a murine model: blood-brain barrier permeability, astrocyte proliferation, and ultrastructural changes. International journal of radiation oncology, biology, physics 2006;66:860-6
37. Larson SR, Atif SM, Gibbings SL, Thomas SM, Prabagar MG, Danhorn T, et al. Ly6C(+) monocyte efferocytosis and cross-presentation of cell-associated antigens. Cell death and differentiation 2016;23:997-1003

38. Mishchenko T, Mitroshina E, Balalaeva I, Krysko O, Vedunova M, Krysko DV. An emerging role for nanomaterials in increasing immunogenicity of cancer cell death. Biochimica et biophysica acta Reviews on cancer 2019;1871:99-108
39. Haar CP, Hebbar P, Wallace GC, Das A, Vandergrift WA, Smith JA, et al. Drug Resistance in Glioblastoma: A Mini Review. Neurochemical research 2012;37:1192-200
40. Cagel M, Grotz E, Bernabeu E, Moretton MA, Chiappetta DA. Doxorubicin: nanotechnological overviews from bench to bedside. Drug discovery today 2017;22:270-81
41. Zhang P, Hu C, Ran W, Meng J, Yin Q, Li Y. Recent Progress in Light-Triggered Nanotheranostics for Cancer Treatment. Theranostics 2016;6:948-68

CHAPTER 3

The synergistic effect of chlorotoxin-mApoE in boosting drug-loaded liposomes across the BBB.

Beatrice Formicola, Roberta Dal Magro, Carlos V Montefusco-Pereira, Claus-Michael Lehr, Marcus Koch, Laura Russo, Gianvito Grasso, Marco A. Deriu, Andrea Danani, Sandrine Bourdoulous, and Francesca Re

Journal of Nanobiotechnology, in press.

Abstract

We designed liposomes dually functionalized with ApoE-derived peptide (mApoE) and chlorotoxin (ClTx) to improve their blood-brain barrier (BBB) crossing. Our results demonstrated the synergistic activity of ClTx-mApoE in boosting doxorubicin-loaded liposomes across the BBB, keeping the anti-tumour activity of the drug loaded: mApoE acts promoting cellular uptake, while ClTx promotes exocytosis of liposomes.

Main text

The blood–brain barrier (BBB) penetration of drugs is one of the biggest challenges in the development of therapeutics for central nervous system (CNS) disorders [1].

The complexity of the BBB hampers the CNS drug delivery: it is formed by specialized brain capillary endothelial cells in direct communication with other cells of the CNS, with the circulating immune cells, and with the peripheral tissues *via* macromolecules exchange with the blood [2].

However, the BBB targeting and crossing, exploiting different mechanisms, remains the most promising strategy to deliver drugs to the brain without distrupting the barrier [3].

In this context, the incorporation of drugs in nanoparticles allowed the enhancement of drug permeation across the BBB, achieving a more favourable drug pharmacokinetics. Moreover, through the multiple functionalization of nanoparticles surface, a more targeted delivery can be attained [4].

We have reported that liposomes functionalized with a modified Apolipoprotein E-derived peptide (CWG-LRKLRKRLLR; mApoE) are able to cross intact the BBB and to deliver the drug cargo into the brain, using both *in vitro* and *in vivo* models [5-8]. However, in animal models, the amount of mApoE-LIP reaching the brain after peripheral administration is 0.2-0.3 % of injected dose [7,8]. This order of magnitude should be not enough to achieve

a therapeutic effect of carried drugs for the treatment of CNS diseases. Moreover, it should be pointed out that also the BBB alterations, in aging or disease, could limits the drug delivery [9]. To this purpose, we have reported on the reduction of brain penetration of mApoE-LIP in animal models of Alzheimer's disease, respect to healthy control mice [10].

In the present work, we aim to improve the performance of mApoE-LIP in BBB crossing by adding the neurotoxin, chlorotoxin (ClTx), as second surface functionalization of LIP. ClTx is a 36-amino acid peptide isolated from the venom of Giant Yellow Israeli scorpion. Since the first isolation, about 25 years ago to date, ClTx has awakened strong interest in oncology due to its high binding affinity to cancer cells, brain tumours included [11-13]. It has been shown that ClTx is able to overcome the BBB in *in vivo* models without damaging it, but the mechanism by which ClTx crosses the BBB is not fully understood [14,15].

We designed, synthesized and characterized LIP dually functionalized with mApoE peptide and with a lipid-modified ClTx. Furthermore, we studied the ability of these nanovectors to cross the BBB *in vitro*, carrying doxorubicin (DOX) payload as a drug model.

The ClTx was chemically modified by attaching 1,2-Distearoyl-sn-Glycero-3-Phosphoethanolamine-polyethylene glycol 2000 with active succinimidyl ester (DSPE-PEG-NHS) *via* the amide bond formation reaction on Lys15, Lys23 and Lys27 of the peptide (Fig. 1A), following the procedure previously described [16].

Liposomes, composed of cholesterol/sphingomyelin/DSPE-PEG-maleimide (48.75/48.75/2.5 molar ratio), [5] were prepared by extrusion procedure through 100-nm filter pores at 60±4°C (Tc sphingomyelin=54°C; Tc DSPE=74°C) in 500 mM ammonium sulphate pH 5.5. These non-functionalized liposomes were defined as LIP. LIP were then dialyzed against 10 mM Hepes, 150 mM NaCl pH 7.4 in order to obtain a pH gradient between inner and outer lipid bilayer. DOX was incorporated in LIP core by remote-

loading (DOX-LIP) [16]. Subsequently, mApoE peptide with a C-terminal cysteine (Cys) was conjugated to the LIP surface through the maleimide-thiol coupling reaction using an excess of the peptide [5,6]. These mApoE-LIP embedding DOX have been named as ADOX-LIP. These particles, or DOX-LIP, were functionalized with lipid-ClTx by post-insertion procedure, generating CDOX-LIP (ClTx-DOX-LIP) and CADOX-LIP-LIP (ClTx-mApoE-DOX-LIP) (Fig. 1B). LIP were purified by size-exclusion chromatography and physico-chemically characterized. The yield of DOX encapsulation into LIP was 72±10 % and the final preparations contained 210±15 µg of DOX/µmol of lipids. The yield of LIP surface functionalization with mApoE peptide was 63±3 %, according to previously published data [5,6]. The post-insertion yield of lipid-ClTx was 70±6 %. Since the post-insertion of a new lipid is expected to alter the membrane of the LIP, [17] which may cause leakage of the entrapped drug, the DOX release after functionalization with ClTx was measured. No significant leakage of DOX was observed after lipid-ClTx post-insertion. Cryo-TEM results (Fig. 1C) showed particles with a mean diameter in the order of 200 nm, predominantly unilamellar structure (>80%). The morphological changes of CADOX-LIP-LIP, compared to empty LIP, are due to the encapsulation of the drug, generating the previously reported "coffee-bean" shape [18], with DOX/sulfate co-crystals inside LIP core. All samples displayed a size < 200 nm, were monodispersed (polydispersity index, PDI < 0.2) and negatively charged (Fig. 1D). These parameters remained constant for up to 15 days within the experimental error (<3.1% of variation). Considering that, ~ 100.000 lipids are in the outer layer of a 200-nm diameter LIP, which contain 2.5 mol % of DSPE-PEG-maleimide, the mApoE density after incubation is of ~ 1200 peptide molecules per single LIP. The ClTx density ranging from 200 to 300 peptide molecules per single LIP.

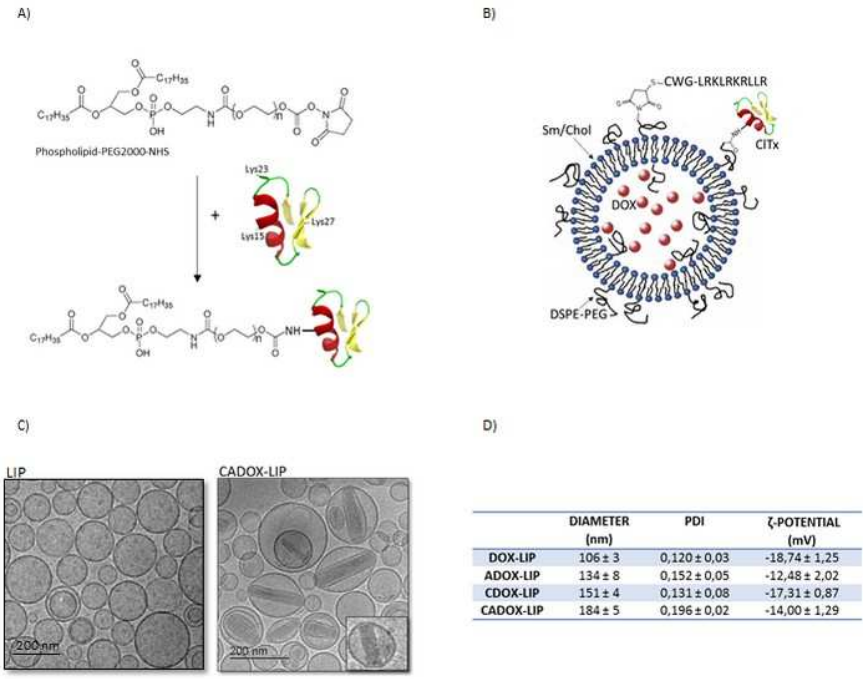

	DIAMETER (nm)	PDI	ζ-POTENTIAL (mV)
DOX-LIP	106 ± 3	0,120 ± 0,03	-18,74 ± 1,25
ADOX-LIP	134 ± 8	0,152 ± 0,05	-12,48 ± 2,02
CDOX-LIP	151 ± 4	0,131 ± 0,08	-17,31 ± 0,87
CADOX-LIP	184 ± 5	0,196 ± 0,02	-14,00 ± 1,29

Fig. 1 (A) Conjugation reaction of ClTx to DSPE-PEG-NHS. (B) Graphical representation of CADOX-LIP-LIP. (C) Cryo-TEM images of non-functionalized LIP and CADOX-LIP-LIP. Image inset is a magnification of a single liposome carrying DOX. (D) Characterization of LIP by Dynamic Light scattering and □-potential analyser. Data are expressed as a mean ± SD of at least three independent LIP preparation, each of them in triplicates.

The capacity of CADOX-LIP to translocate across brain endothelial cells, carrying drug payload, was assessed in an *in vitro* human BBB model. Immortalized human brain capillary endothelial cells (hCMEC/D3) were cultured on semipermeable membrane filters of a transwell system (Fig. 2A). First, the effect of liposomes treatment on hCMEC/D3 features was assessed by measuring: i) transendothelial electrical resistance (TEER), ii) endothelial permeability (EP) to the paracellular probe Lucifer Yellow (LY); iii) cell viability by MTT assay; iv) morphological cell features by optical microscopy [7,19]. Free DOX showed an important toxic effect on BBB model, as reflected by alterations of bioelectrical (TEER=16±3 $\Omega \cdot cm^2$, compared to

29±3 Ω·cm^2 of untreated cells), functional (EP to LY=3.06±0.2·10^{-3} cm/min, respect to 1.87±0.6·10^{-3} cm/min of untreated cells) and structural properties (<20% of viable cells) of hCMEC/D3 monolayer. These effects were prevented by incorporation of DOX in the LIP core, indicating that the BBB integrity can be preserved. Moreover, the surface functionalization of LIP with mApoE and ClTx did not shown significant toxic effect on the BBB model features (Fig. 2, B-D).

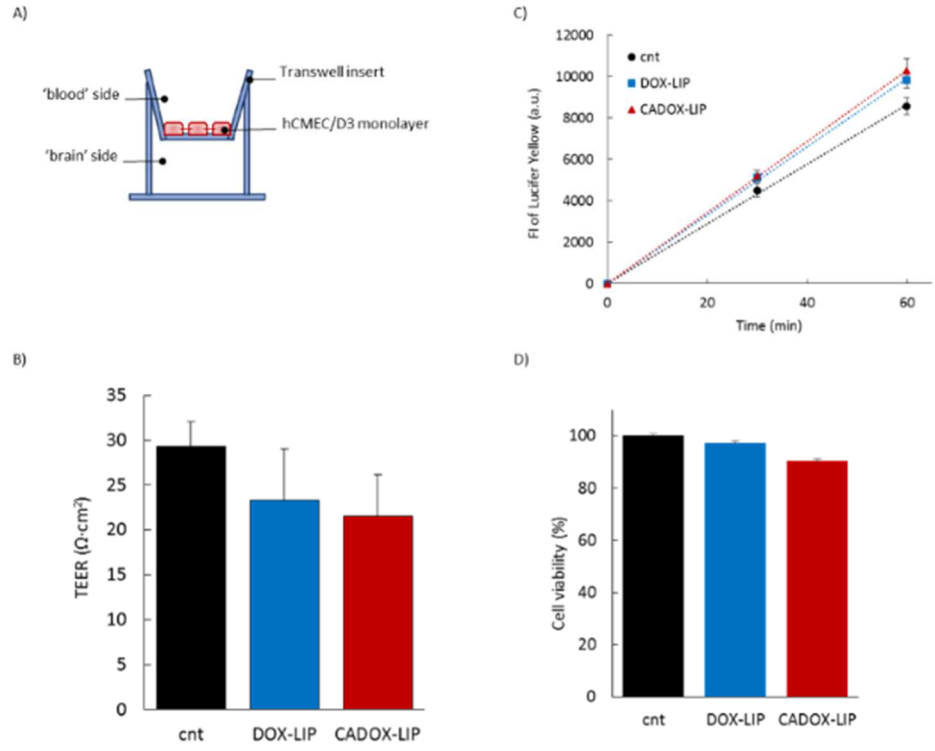

Fig. 2 (A) Graphical representation of the transwell system used to mimic the BBB. (B) TEER values; (C) fluorescence intensity of LY in the 'brain' side of the transwell system before and after 1 h of incubation with DOX-LIP or CADOX-LIP-LIP. (D) hCMEC/D3 cell viability assessed by MTT assay after 24 h of incubation with DOX-LIP or CADOX-LIP-LIP. Data are expressed as a mean ± SD of at least three independent LIP preparation, each of them in triplicates.

Afterwards, the EP to the different LIP formulations was calculated by measuring over time the amount of DOX in the apical ('blood' side) and in

the basolateral ('brain' side) compartment of the transwell system, as reported [20]. Non–functionalized LIP were not able to transport DOX across the BBB model in a significant amount, while ADOX-LIP allowed a 10-fold increase of EP to DOX, as expected and already reported using a different drug [6]. Unexpectedly, CDOX-LIP did not shown a substantial enhancement of DOX passage across the cells monolayer, suggesting that the capability of ClTx to permeate the BBB is too weak. This is in agreement with previously published data, showing that ClTx is able to cross human endothelial cells by active transcytosis, but this passage is probably not enough to deliver drugs across the BBB [21]. Interestingly, CADOX-LIP were able to boost (~30-fold increase) DOX passage across the BBB, respect to DOX-LIP. Moreover, the increase of DOX passage was 3-times and 10-times higher when incorporated in CADOX-LIP, compared to ADOX-LIP and CDOX-LIP, respectively (Fig. 3A). This suggests the existence of a synergistic effect between the two ligands: ClTx and mApoE. Nanosight analysis of LIP passed through the cells monolayers (i.e. in the basolateral compartment of the transwell system) suggested that LIP remain intact after BBB crossing (Fig. 3B), thus excluding the possibility to have follow only the passage of DOX released from LIP. The EP to free DOX was $1.27\pm0.2x10^{-3}$ cm/min, a lot greater than when it was incorporated in LIP. This is almost certainly due to its toxic effect on hCMEC/D3 monolayer, as described above. It is important to point out that these results were obtained using endothelial cells grown in a monoculture that does not properly represent the in vivo BBB tightness. Unfortunately, we could not performed these experiments in advanced multicellular BBB models because of the liposomes uptake by astrocytes, which in turn affects the calculation of EP.

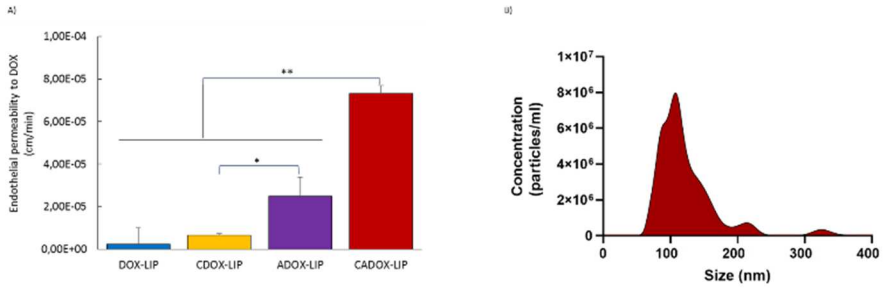

Fig. 3 Permeability of LIP across human in vitro BBB cellular model. (A) Endothelial permeability to DOX in different LIP formulations. (B) Analysis of CADOX-LIP-LIP size and quantity in the basolateral compartment of the transwell system, after BBB crossing, measured by nanosight. Data are expressed as a mean ± SD of at least five independent LIP preparation, each of them in triplicates

In order to investigate the ClTx-mApoE synergy in enhancing the LIP passage across the BBB, we evaluated the mApoE-ClTx binding by spectrofluorimetry, the type of interaction by computational docking and molecular modelling analysis and the cellular uptake of DOX. Following the tryptophan (Trp) fluorescence shift of mApoE after binding with increasing amounts of ClTx, we observed that mApoE-ClTx are able to interact between them, with a calculated affinity constant of K_a=1.65±0.3x10^{-3} nM (Fig. 4A, B). Molecular dynamics simulations (MDS) confirmed that the two proteins are able to interact (Fig. 4C) and the residues mainly involved in the interaction are M1, F6, P31 of ClTx and L9, R11 of mApoE (Fig. 4D), which are not engaged in reactions for LIP functionalization. However, the interaction is fleeting and not very stable. In fact, it is possible to observe many protein-protein breakdown events in the movie (movie S1, Additional File). This is probably due to the strong electrostatic repulsion between the two ligands, since they are both positively charged sequences.

Finally, comparing the cellular internalization of DOX, its uptake was ~30% higher when incorporated in ADOX or CADOX-LIP (i.e. 7.80±1.29% and 10.64±0.74% of administered DOX was measured inside the cells,

respectively), respect to DOX-LIP and CDOX-LIP (Fig. 4E). The increased DOX uptake in ADOX-LIP and CADOX-LIP-LIP supports the higher BBB permeability of these two formulations. Most interestingly, considering that the extent of DOX uptake between ADOX-LIP and CADOX-LIP-LIP is similar, and the functionalization of LIP only with ClTx (CDOX-LIP) did not improve the DOX uptake, we can speculate that ClTx is not involved in the cellular internalization. Rather it is possible to assert that ClTx is involved in the LIP egress from the basolateral side of endothelial cells.

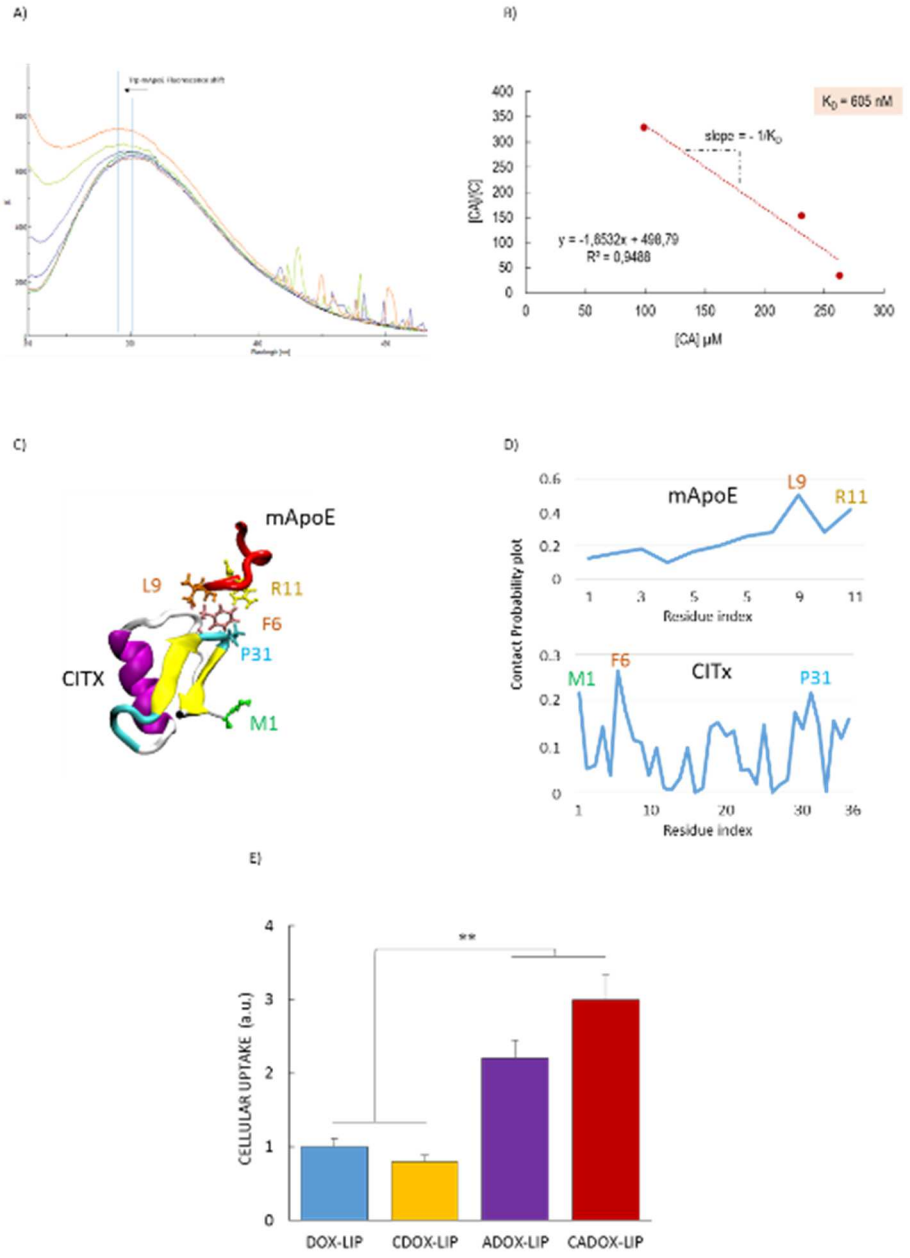

Fig. 4 (A) Trp fluorescence of 30 µM mApoE after incubation with different doses of ClTx ranging from 0-30 µM. (B) Scatchard plot to determine the binding constant between mApoE e ClTx in solution, where [CA] is the concentration of ClTx-mApoE complex and [C] is concentration of ClTx. (C) Visual Inspection of mApoE-CITX interaction by MDS. Residues mainly responsible for the protein-protein interaction are also highlighted. (D) Contact probability plot reporting the probability of each

protein residue to be part of the protein-protein contact surface. (E) Cellular uptake of DOX in different LIP formulations. Data are expressed as a mean ± SD of triplicates.

Taken together these results suggest that there is not a cooperative action of ClTx and mApoE in entering the endothelial cells, but there is a synergistic activity in BBB crossing. In particular, mApoE acts promoting the interaction of CADOX-LIP with the apical side of human endothelial cells, probably *via* LDL-receptor mediated endocytosis as already demonstrated [5-7], whereas ClTx acts by boosting CADOX-LIP-LIP outside of the endothelial cells, promoting their exocytosis though the basolateral side of cell monolayers.

If we consider that the amount of DOX internalized in hCMEC/D3 is similar between ADOX and CADOX-LIP, we can propose differences in the exocytosis process. In this case, a more effective exocytosis would explain the enhanced transcytosis properties of CADOX-LIP-LIP, when compared to CDOX-LIP and ADOX-LIP.

The mechanism by which ClTx is able to promote exocytosis of CADOX-LIP-LIP will deserves further investigation. However, data from literature suggest an interaction of ClTx with Annexin A2, which is expressed in vascular endothelial cells, BBB included [22,23]. Recently, it has been shown that Annexin A2 is involved in the BBB transcytosis processes of CNS pathogens, but not in their cellular adhesion and uptake, suggesting a role of Annexin A2 in the exocytosis pathway across the BBB [24,25]. Then, ClTx may promote the LIP exocytosis interacting with Annexin A2. This mechanism of action is speculative and the demonstration needs further research to deep this issue, for example by testing alternatives to CITx known for their interaction with Annexin A2.

Finally, we tested if the drug embedded in CADOX-LIP-LIP was able to retain its ability to target and to suppress the growth of a cellular model of brain tumour. To this purpose, a co-culture transwell system with hCMEC/D3 cells

seeded on filter and human U87 glioblastoma cells seeded in the basolateral compartment (Fig. 5A) was prepared. The results (Fig. 5B) showed that after BBB crossing, CADOX-LIP-LIP were able to reduce (-76.6%) the viability of U87 cells seeded in the basolateral compartment, as well as free DOX, but without damaging the endothelial monolayer.

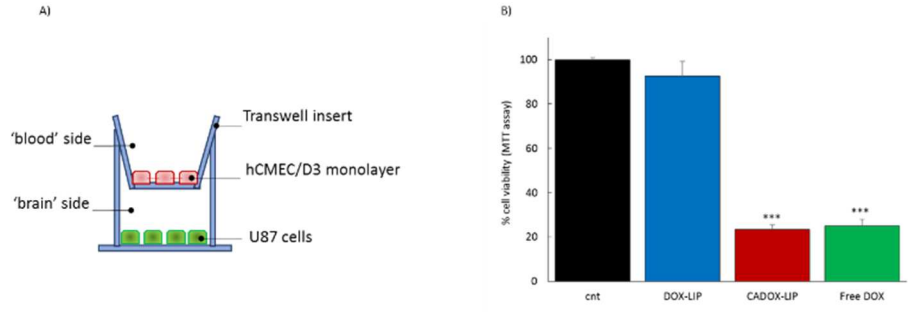

Fig. 5 (A) Graphical representation of co-culture transwell model utilized to test the efficacy of LIP after BBB crossing on human glioblastoma U87 cells. (B) Cell viability assessed by MTT assay on U87 cells seeded in the basolateral compartment of the transwell system. Data are expressed as a mean ± SD of triplicates and analysed with unpaired one-tailed Student's t test. *** $p<0.001$.

This proofs the capability of CADOX-LIP-LIP to carry active DOX to cancer cells *in vitro*.

In conclusion, our results reveal the synergistic effect of ClTx-mApoE in improving the permeability of drug-loaded LIP across a human cell-based BBB model. These data suggest that the already reported ability of mApoE to cross the BBB can be improved by ClTx, which enhances the exocytosis from hCMEC/D3 cell monolayers. On the other side, mApoE can improve the already reported ability of ClTx to translocate across the BBB *in vitro*, enhancing its penetration in endothelial cells. All these data support the use of mApoE-ClTx as a dual-targeting ligands to functionalize particles to facilitate the brain delivery of different drug cargoes across the BBB.

List of abbreviations

BBB= Blood–Brain Barrier

CNS= Central Nervous System

mApoE= modified Apolipoprotein E-derived peptide

Cys= cysteine

ClTx= Chlorotoxin

LIP= Liposomes

DOX= Doxorubicin

Lys= Lysine

DSPE-PEG=1,2-distearoyl-sn-glycero-3-phosphoethanolamine-N-[(polyethylene glycol)-2000]

DOX-LIP= liposomes embedding doxorubicin

ADOX-LIP=liposomes functionalized with mApoE and containing doxorubicin

CDOX-LIP=liposomes functionalized with chlorotoxin and containing doxorubicin

CADOX-LIP= liposomes bi-functionalized with chlorotoxin and mApoe, and containing doxorubicin

TEM= Transmission Electron Microscope

hCMEC/D3= Human Cerebral Microvascular Endothelial Cells/ Human brain capillary endothelial cells

TEER= Transendothelial Electrical Resistance

EP= Endothelial Permeability

LY= Lucifer Yellow

PDI= Polydispersity Index

MTT= 3-(4,5-dimethylthiazol-2-yl)-2,5-diphenyltetrazolium bromide

MDS= Molecular Dynamics Simulations

Trp= Tryptophan

References

1. Banks WA. From blood-brain barrier to blood-brain interface: new opportunities for CNS drug delivery. Nat Rev Drug Disc. 2016; 15: 275-92.

2. Hawkins BT, Davis TP. The blood-brain barrier/neurovascular unit in health and disease. Pharmacol Rev. 2005; 57: 173–85.

3. Villaseñor R, Lampe J, Schwaninger M, Collin L. Intracellular transport and regulation of transcytosis across the blood-brain barrier. Cell Mol Life Sci. 2019; 76: 1081-92.

4. Sharma G, Sharma AR, Lee SS, Bhattacharya M, Nam JS, Chakraborty C. Advances in nanocarriers enabled brain targeted drug delivery across blood brain barrier. Int J Pharm. 2019; 559: 360-72.

5. Re F, Cambianica I, Sesana S, Salvati E, Cagnotto A, Salmona M, Couraud PO, Moghimi SM, Masserini M, Sancini G. Functionalization with ApoE-derived peptides enhances the interaction with brain capillary endothelial cells of nanoliposomes binding amyloid-beta peptide. J Biotechnol. 2010; 156: 341–6.

6. Re F, Cambianica I, Zona C, Sesana S, Gregori M, Rigolio R, La Ferla B, Nicotra F, Forloni G, Cagnotto A, Salmona M, Masserini M, Sancini G. Functionalization of liposomes with ApoE-derived peptides at different density affects cellular uptake and drug transport across a blood-brain barrier model. Nanomedicine. 2011; 7: 551-9.

7. Bana L, Minniti S, Salvati E, Sesana S, Zambelli V, Cagnotto A, Orlando A, Cazzaniga E, Zwart R, Scheper W, Masserini M, Re F. Liposomes bi-functionalized with phosphatidic acid and an ApoE-derived peptide affect Aβ aggregation features and cross the blood-brain-barrier: implications for therapy of Alzheimer disease. Nanomedicine. 2014; 7: 1583-90.

8. Balducci C, Mancini S, Minniti S, La Vitola P, Zotti M, Sancini G, Mauri M, Cagnotto A, Colombo L, Fiordaliso F, Grigoli E, Salmona M, Snellman A, Haaparanta-Solin M, Forloni G, Masserini M, Re F. Multifunctional liposomes reduce brain β-amyloid burden and ameliorate memory impairment in Alzheimer's disease mouse models. J Neurosci. 2014; 34: 14022-31.

9. Zlokovic BV. Neurovascular pathways to neurodegeneration in Alzheimer's disease and other disorders. Nat Rev Neurosci. 2011; 12: 723–38.

10. Dal Magro R, Cox A, Zambelli V, Mancini S, Masserini M, Re F. The ability of liposomes, tailored for blood-brain barrier targeting, to reach the brain is dramatically affected by the disease state. Nanomedicine. 2018; 13: 585-94.

11. DeBin JA, Maggio JE, Strichartz GR. Purification and characterization of chlorotoxin, a chloride channel ligand from the venom of the scorpion. Am J Physiol. 1993; 264: 361-9.

12. Ojeda PG, Wang CK, Craik DJ. Chlorotoxin: Structure, activity, and potential uses in cancer therapy. Biopolymers. 2016; 106: 25-36.

13. Lyons SA, O'Neal J, Sontheimer H. Chlorotoxin, a scorpion-derived peptide, specifically binds to gliomas and tumors of neuroectodermal origin. Glia. 2002; 39: 162-73.

14. Cohen-Inbar O, Zaaroor M. Glioblastoma multiforme targeted therapy: The Chlorotoxin story. J Clin Neurosci. 2016; 33: 52-58.

15. Tamborini M, Locatelli E, Rasile M, Monaco I, Rodighiero S, Corradini I, Franchini MC, Passoni L, Matteoli M. A Combined Approach Employing Chlorotoxin-Nanovectors and Low Dose Radiation To Reach Infiltrating Tumor Niches in Glioblastoma. ACS Nano. 2016; 10: 2509-20.

16. Xiang Y, Liang L, Wang X, Wang J, Zhang X, Zhang Q. Chloride channel-mediated brain glioma targeting of chlorotoxin-modified doxorubicine-loaded liposomes. J Control Release. 2011; 3: 402-10.

17. Uster PS, Allen TM, Daniel BE, Mendez CJ, Newman MS, Zhu GZ. Insertion of poly(ethylene glycol) derivatized phospholipid into pre-formed liposomes results in prolonged in vivo circulation time. FEBS Lett. 1996; 386: 243-6.

18. Gaillard PJ, Appeldoorn CCM, Dorland R, van Kregten J, Manca F, Vugts DJ, Windhorst B, van Dongen GAMS, de Vries HE, Maussang D, van Tellingen O. Pharmacokinetics, brain delivery, and efficacy in brain tumor-bearing mice of glutathione pegylated liposomal doxorubicin (2B3-101). PLoS ONE. 2014; 9: e82331.

19. Mancini S, Balducci C, Micotti E, Tolomeo D, Forloni G, Masserini M and Re F. Multifunctional liposomes delay phenotype progression and prevent memory impairment in a presymptomatic stage mouse model of Alzheimer disease. J Control Release, 2017; 258: 121-9.

20. Cecchelli R, Dehouck B, Descamps L, Fenart L, Buée-Scherrer VV, Duhem C. In vitro model for evaluating drug transport across the blood-brain barrier. Adv Drug Deliv Rev. 1999; 36: 165-78.

21. Díaz-Perlas C, Varese M, Guardiola S, García J, Sánchez-Navarro M, Giralt E, Teixidó M. From venoms to BBB-shuttles. MiniCTX3: a molecular vector derived from scorpion venom. Chem Commun. 2018; 54: 12738-41.

22. Kesavan K, Ratliff J, Johnson EW, Dahlberg W, Asara JM, Misra P, Frangioni JV, Jacoby DB. Annexin A2 is a molecular target for TM601, a peptide with tumor-targeting and anti-angiogenic effects. J Biol Chem. 2010; 285: 4366-74.

23. Maule F, Bresolin S, Rampazzo E, Boso D, Della Puppa A, Esposito G, Porcù E, Mitola S, Lombardi G, Accordi B, Tumino M, Basso G, Persano L. Annexin 2A sustains glioblastoma cell dissemination and proliferation. Oncotarget. 2016; 7: 54632-49.

24. Na Pombejra S, Salemi M, Phinney BS, Gelli A. The Metalloprotease, Mpr1, Engages AnnexinA2 to Promote the Transcytosis of Fungal Cells across the Blood-Brain Barrier.Front Cell Infect Microbiol. 2017; 7: 296.

25. Fang W, Fa ZZ, Xie Q, Wang GZ, Yi J, Zhang C, Meng GX, Gu JL, Liao WQ. Complex Roles of Annexin A2 in Host Blood-Brain Barrier Invasion by Cryptococcus neoformans. CNS Neurosci Ther. 2017; 4: 291-300.

CHAPTER 4

Differential exchange of multifunctional liposomes between glioblastoma cells and healthy astrocytes *via* tunnelling nanotubes (TnTs)

Beatrice Formicola, Alessia D'Aloia, Roberta Dal Magro, Simone Stucchi, Roberta Rigolio, Michela Ceriani, Francesca Re.

Submitted to Frontiers in Bioengineering and Biotechnology, section Nanobiotechnology

Abstract

Despite advances in cancer therapies, nanomedicine approaches included, the treatment of glioblastoma (GBM), the most common, aggressive brain tumour, remains inefficient. These failures are likely attributable to the complex, and not yet completely know, biology of this tumour, which is responsible for its strong invasiveness, high degree of metastasis, high proliferation potential and resistance to radiation and chemotherapy. The intimate connection through which the cells communicate between them plays an important role in these biological processes. In this scenario, tunneling nanotubes (TnTs) are recently gaining importance as a key features in tumor progression and in particular in the re-growth of GBM after surgery.

In this context, we firstly identified structural differences of TnTs formed by U87-MG cells, as model of GBM cells, in comparison to those formed by normal human astrocytes (NHA), used as a model of healthy cells. Successively, we have studied the possibility to exploit U87-MG TnTs as drug-delivery channels in cancer therapy, using liposomes composed of cholesterol/sphingomyelin and surface functionalized with mApoE and chlorotoxin peptides (Mf-LIP) as nanovehicle model. The results showed that U87-MG cells formed almost exclusively thick and long protrusions, while NHA formed more thin and short TnTs. Considering that thick TnTs are more efficient in transport of vesicles and organelles, we showed that fluorescent-labelled Mf-LIP can be transported via TnTs between U87-MG cells, and with less extent through the protrusions formed by NHA cells. Our results demonstrate that nanotubes are potentially useful as drug-

delivery channels for cancer therapy, facilitating the intercellular redistribution of this drug in close and far away cells, thus reaching isolated tumour niches that are hardly targeted by simple drug diffusion in the brain parenchyma. Moreover, the differences identified in TnTs formed by GBM and NHA cells can be exploited to increase treatments precision and specificity.

1 Introduction

The limits of conventional therapies against tumours, in terms of effectiveness/damage ratio, lead to the development and application in clinics of different nanotechnological drugs in the last 25 years (Stupp et al., 2009). Many advancements have been achieved in this field, but different issues, such as the complexities and heterogeneity of tumour biology still remain unsolved. Gliomas, intrinsic brain tumours, are a dissimilar group of oncological diseases for which there is currently no cure, and only very limited progress has been made in the control of the disease course over the past three decades (Westphal et al., 2011). Among gliomas, glioblastoma multiforme (GBM, also called grade IV astrocytoma) is one of the most deadly brain tumors, with a short median patient survival and a very limited response to therapies (Louis et al., 2016). In this context, many efforts are underway towards the development of new therapeutic approaches and nanomedicine seems to be one of the most promising. Nevertheless, many obstacles have not been overcome yet. GBM has a very complex pathogenesis that involves alterations of several key cellular pathways, diffuse invasiveness and capacity to escape therapies. An important component

of tumour growth is communication within cancer cells and with other cells in the microenvironments, which strengthen tumour progression and resistance to radio- and chemotherapy (Broekman et al., 2018).

Normal and tumour cells exploit different communication modalities and one of them is represented by the physical connection via tunnelling nanotubes (TnTs) and microtubes (TmTs), which form a cytoplasmic continuum between cells and allow the transport of non-secretable molecules and organelles. In particular, TnTs can mediate the transfer of cellular vesicles (Rustom et al., 2004; Onfelt et al., 2006), mitochondria (Ahmad et al., 2014), lysosomes (Abounit et al., 2016), miRNAs (Thayanithy et al., 2014), single proteins (Schiller et al., 2013) and viral particles (Sowinski et al., 2008) between cells, also very distant from each other (>100 µm of distance). TnTs are transient transcellular channels with a diameter of 50–200 nm, a length up to several cell diameters with variable lifetimes ranging from less than 60 min up to many hours. (Carone et al., 2015).

Lou et al. (2012a, 2012b) firstly described the presence of TnTs in human primary tumors and in many cancer cell lines, highlighting the key role of these membranous structures in cancer cell pathogenesis and invasion. The involvement of TnTs and TmTs has also been indicated in the re-growth of GBM after surgery and in conferring resistance to chemotherapy (Weil et al., 2017; Moschoi et al., 2016). Although TnTs are not apparent in some glioma cellular models (Van der Vos et al., 2016), they may represent a new tool for bidirectional intercellular transfer of drug-loaded nanoparticles.

In this context, there are some data supporting the direct cell-to-cell transfer of nanoparticles through TnTs and this strategy may be exploited to increase the range of drug delivery between cancer cells (Epperla et al., 2015; Sisakhtnezhad et al., 2015; Deng et al., 2018). One of the peculiarity of GBM is the presence of glioma stem cells both within the tumour bulk, which are able to reconstitute a whole tumour after surgical resection (Fan et al, 2010; Lin et al., 2010), and in other brain regions, where minor stem-cell niches represent a pool from which new tumour cells originate (Gould et al., 2007). Then, targeting primary GBM with nanotherapeutics may allow the possibility to reach via TnTs isolated, infiltrating tumor cells (stem cells included) that are hardly reached by drug diffusion in the brain parenchyma.

This study aims to evaluate in vitro the possible intercellular transport of multifunctional liposomes via TnTs between human primary glioblastoma cell line. We have recently designed liposomes carrying doxorubicin, as an anti-cancer drug model, and dually-functionalized with apoE-derived peptide and with chlorotoxin (ClTx), as GBM targeting ligands (DeBin et al., 1993; Maletínská et al., 2000; Lyons et al., 2002; Ojeda et al., 2016; Xiang et al. 2011). The ability of liposomes functionalized with apoE-derived peptide (namely mApoE) to cross the blood-brain barrier both in vitro and in vivo, was already reported (Re et al., 2011; Bana et al., 2014; Balducci et al., 2014; Dal Magro et al., 2018).

Liposomes trafficking via TnTs in GBM cells has not been reported yet. Moreover, we compared the heterogeneity of TnTs, in terms of structure, morphology, size and abundance between GBM cells and

human healthy astrocytes, with the aim to increase the precision and specificity of treatments.

2 Materials and Methods

2.1 Materials

Cholesterol (Chol), Doxorubicin (DOX), Thiazolyl Blue Tetrazolium Bromide, 4-(2-Hydroxyethyl)piperazine-1-ethanesulfonic acid (HEPES), Triton X-100, Ultra-low Range Molecular Weight Marker (M.W. 1.060-26.600), EZBlue Gel Staining Reagent, 1,1′-Dioctadecyl-3,3,3′,3′-tetramethylindocarbocyanine perchlorate (DiI probe), TRITC-phalloidin, mouse monoclonal anti-β-tubulin antibody were purchased from Sigma-Aldrich (Milano, Italy). 1,2-Distearoyl-sn-glycero-3-phospho-ethanolamine-N[maleimide(polyethyleneglycol)-2000](mal-PEG-DSPE) and sphingomyelin from bovine brain (Sm) were purchased from Avanti Polar Lipids, Inc (Alabaster, AL, USA). BODIPY™ FL C 12 -Sphingomyelin (BODIPY-Sm) was purchased from ThermoFisher Scientific. 1,2-Distearoyl-sn-glycero-3-phospho-ethanolamine-N[(polyethyleneglycol)-2000] n-hydroxysuccinimide ester (NHS-PEG-DSPE) was purchased from Nanocs (Boston, USA). Ultrapure and deionized water were obtained from Direct-Q5 system (Millipore, Italy). mApoE peptide (CWG-LRKLRKRLLR, MW 1698.18 g/mol) and chlorotoxin (ClTx, MW 4004 g/mol) were synthetized by Karebay Biochem (Monmouth Junction, NJ, USA). Dialysis membranes (cut-off 12000-14000 Da) were purchased from Medicell International Ltd, (London, UK). Penicillin-streptomycin (P/S) solution 100X was purchased from Euroclone (Milan, Italy); PBS

1X, collagen, trypsin/EDTA solution and NuPAGE Bis-Tris (4-12%) were from Invitrogen. All other chemicals were of analytical grade and were obtained from either Sigma–Aldrich or Merck. Alexa Fluor 488 goat anti-mouse IgG and CellTrace Far Red Dye (CT) were from Life Technologies. 3,3'-Dioctadecyloxacarbocyanine Perchlorate (DiO) was from Sigma Aldrich (Milan, Italy).

2.2 Preparation of ClTx-PEG-DSPE

ClTx-lipid was prepared as described in (Xiang et al., 2011) with small modifications. Briefly, 0.1 µmol NHS-PEG-DSPE in $CHCl_3$/MeOH (2:1, vol/vol) was dried under N_2 to remove organic solvents. Then 5 eq (0.5 µmol) of ClTx dissolved in 10 mM Hepes, 150 mM NaCl pH 7.4, was added to the dried lipid. The reaction was conducted under gentle stirring for 90 min at room temperature. The resulting solution was dialyzed against MilliQ water for two days in a dialysis tube (MWCO=3500 Da) to remove unreacted ClTx and then lyophilized overnight.

2.3 Preparation multifunctional liposomes (Mf-LIP)

Liposomes (LIP) were composed of sphingomyelin, cholesterol (1:1, mol/mol) added with 2.5 mol % of mal-PEG-PE, for the covalent binding of mApoE peptide, and with 0.5 mol % of BODIPY-Sm as fluorescent probe (Re et al., 2010; Re et al., 2011). LIP were prepared in 10 mM Hepes, 150 mM NaCl pH 7.4 by extrusion procedure through polycarbonate membranes of 100 nm diameter pores, under N_2. mApoE peptide was covalently attached on LIP surface by thiol-maleimide coupling, as previously described (Re et al., 2010; Re et al., 2011). ClTx-lipid was added to mApoE-LIP by post-insertion

technique, following the procedure previously described (Mare et al., 2018). This sample will be referred as Mf-LIP. As controls, LIP composed of sphingomyelin, cholesterol (1:1, mol/mol) were prepared in ammonium sulphate (500 mM, pH 5.5) by extrusion procedure as described above. LIP were dialyzed against 10 mM Hepes, 150 mM NaCl pH 7.4, overnight, and then incubated with DOX (1.5 µmol DOX/ 10 µmol total lipids) for 1 h at 65°C to allow the incorporation of DOX in the LIP core. This sample will be referred as DOX-LIP. Mf-LIP and DOX-LIP were purified with a Sepharose G-25 fine column (25x1cm) to remove unbounded and unincorporated materials.

2.4 Characterization of Mf-LIP

After purification, the amount recovered for each compound was determined by different techniques. Briefly, phospholipids content was quantified by Stewart Assay (Stewart, 1980); the amount of ClTx and mApoE on LIP surface was assessed by SDS-PAGE. DOX loading was quantified spectrofluorometrically (λex = 495 nm; λem =592 nm) after vesicle disruption with 0.1% Triton X-100. The DOX encapsulation yield in liposomes was calculated by comparing fluorescence intensities with a previously established calibration curve of free DOX in 10mM Hepes, 150 mM NaCl pH 7.4. Size and polydispersity index (PDI) were analyzed by dynamic light scattering (DLS) technique (Brookhaven Instruments Corporation, Holtsville, NY, USA). ζ-potential was determined by using an interferometric doppler velocimetry with the same instrument equipped with ZetaPALS device. LIP stability was measured in 10 mM Hepes, 150 mM NaCl pH 7.4 by following size and PDI by DLS for 1 week.

2.5 Cell cultures

U87-MG glioblastoma cells were purchased from American Type Culture Collection (ATCC, VA, USA) and were grown in DMEM High Glucose, 10% FBS, 1% P/S, 1% glutamine (Tamborini et al., 2016). Normal Human Astrocytes (NHA), purchased from Lonza (Walkersville, Maryland, USA), were maintained in Astrocytes Basal Medium supplemented with AGM BulletKitTM. All cell lines were cultured at 37 °C under a humidified atmosphere containing 5% CO2.

2.6 TnTs analysis by confocal microscopy

NHA and U87-MG cells were seeded at a density of 5x103 cells/cm2 or 1.5x104 cells/cm2 respectively on porcine gelatin pretreated coverslips. One day after seeding, cells were treated for 1 h or 24 h with free DOX (15 or 25 µg/ml) or with DOX-LIP (15 µg/ml of DOX, 200 nmols of total lipids) or with fluorescent-labelled Mf-LIP (200 nmols of total lipids) at 37°C in 5% CO2. Untreated cells were used as a control. After treatment, cells were then left for 2 h in each culture complete medium and then stained for 20 min with 1.9 µl/ml of DiI in PBS (membrane/endocytic vesicles), or with 5 µl/ml of DiO in PBS, to label cell membranes, TnTs included, according to the manufacturer's instructions. Cells were then fixed for 8 min with 3.7% paraformaldehyde in phosphate-buffered saline (PBS). Fluorescence images were examined with a 40x magnification on A1R Nikon (Nikon, Tokyo, Japan) laser scanning confocal microscope. Cells were carefully scored for the presence of TnTs. About #200 cells for each experiment were analyzed. TnTs were counted. Experiments were performed in triplicate. Images were analyzed by Image J software.

2.7 Cellular uptake of DOX-LIP and Mf-LIP

U87-MG cells were seeded on a 6-well plate (5x103 cells/cm2) and after two days of culture, cells were treated with free DOX (15 μg/ml) or LIP formulations (DOX 15ug/ml) for 1 h and 3 h. At the two different time points free DOX and LIP formulations were removed, the cells were washed with PBS, detached and treated with lysis buffer (50 mM Tris-HCl pH 7.4, 150 mM NaCl, 2 mM EDTA, 1% Triton X-100, 0.1% SDS, 1 mM DTT). Samples were centrifuged at 12000 rpm for 15 min at 4°C and the DOX fluorescence (λex=495 nm; λem=592 nm) in the pellets was measured by Jasco FP-8500 spectrofluorometer. Results were expressed as DOX fluorescence in pellets / DOX fluorescence in initial sample x100 and indicated as cell uptake (%).

High-throughput images of living U87-MG cells on a 96-well plate (3x104 cells/cm2) were acquired automatically with an Operetta® High Content Imaging System (PerkinElmer, UK). After two days of culture, cells were treated with free DOX (15 μg/ml) or LIP formulations (DOX 15ug/ml) and the uptake was evaluated by acquiring images at three different time points (0, 1 h, 3h). Before imaging, cells were washed three times with PBS. Images were acquired in the DOX channel and in the brightfield channel, using a 40x air objective lens and standard instrument filters. Ten different fields were imaged in each well. The image were then analysed by the Harmony® analysis software (PerkinElmer, UK).

2.8 Actin, tubulin and DAPI staining

NHA and U87-MG cells were plated at a density of 5x103 cells/cm2 or 1.5x104 cells/cm2, respectively, on porcine gelatin pretreated coverslips. One day after seeding cells were fixed for 10 min with 3.7% paraformaldehyde in phosphate buffered saline (PBS), permeabilized for 4 min with 0.1% Triton X-100/ PBS and finally stained with different antibodies. In particular, cells were treated with TRITC-phalloidin (1:40 in 1% BSA/PBS) for actin staining, as described previously (Ceriani et al., 2007). For tubulin staining, cells were incubated with mouse monoclonal anti-β-tubulin primary antibody (1:150 in 1% BSA/PBS) for 1h at 37°C. Then cells were washed and incubated with the secondary antibody Alexa Fluor 488 goat anti-mouse IgG (1:200 in 1% BSA/ PBS) for 45 min at 37°C.

For nuclei staining U87-MG and NHA cells were plated on gelatine pre-treated coverslips. Cells were leaved in culture complete medium for 48 h and then incubated with 15 µg/ml of free DOX for 1 h. Cells were then stained for 20 min with DiO (5 µl/ml), fixed, permeabilized and colored with DAPI (Sigma) (1µg/ml) for 10 minutes at room temperature.

2.9 Fluorescence-activated cell sorting analysis (FACS) of cell-to-cell LIP transfer

U87-MG cells and NHA cells were seeded on 12-well plates at a cell density of 6.5x 103 and 15x104 cells/cm2, respectively. Three days after seeding “donor” cells were incubated with BODIPY-Sm Mf-LIP

(200 nmol total lipids) for 1h at 37°C while “acceptor” cells were treated with CellTrace Far Red Dye (CT) at 1μM for NHA and 10μM for U87-MG cells for 30 min. Cells were detached and the following co-culture between “donor” and “acceptor” cells were set-up: U87-MG (donor) → NHA (acceptor); U87-MG (donor) → U87-MG (acceptor); NHA (donor) → NHA (acceptor); NHA (do□or) → U87-MG (acceptor). Co-culture were maintained for 24h at 37°C. Cell-to-cell transfer of Mf-LIP was assessed by FACS (FACSCantoI BD Biosciences) analysis. At least 50.000 events were acquired in an operator-defined gate designed on a physical parameter (FSC vs SSC) dot plot. The fluorescence intensity analysis on FITC (to detect BODIPY) and APC (to detect CT) histogram was performed on a single cell gate defined on a FSC-H vs FSC-A dot plot. The reported data refer only to the double FITC/APC positive events among this population, representing the Mf-LIP transfer to “acceptor” cells.

2.10 Statistical analysis

For TnTs quantification data were analyzed by Student t test. Data were expressed as a mean ± standard error (S.E.). For percentage distribution of thin and thick TnTs, data were analyzed by two-way or one-way ANOVA followed rispectively by Sidak’s multiple comparisons test or Dunnett’s post-hoc test.

All experiments were conducted at least in triplicate. All the analyses were performed with GraphPad Prism 8 software (license number: GP8-1519368-RFQS-B8CB4). Differences were considered significant at $p < 0.05$ (*); $p < 0.01$ (**); $p < 0.001$ (***).

3 Results

3.1 Characterization of LIP

The results showed that DOX-LIP displayed a diameter of 121 ± 6 nm with a PDI value of 0.098 ± 0.01; the ζ-potential was -19.32 ± 0.58 mV. Mf-LIP showed a diameter of 187 ± 5 nm with a PDI value of 0.087 ± 0.05; the ζ-potential was -14.5 ± 0.43 mV. These parameters remained constant for 1 week within the experimental error (<2.7 % of variation). For both preparations, the total lipid recovery after purification was 79.5 ± 8 %. For Mf-LIP the yield of functionalization with mApoE and ClTx was 88.5 ± 10 % (corresponding to 2.2 mol % of mApoE/total lipids) and 71.2 ± 3 % (corresponding to 1.42 mol% of ClTx/total lipids), respectively. For DOX-LIP, the incorporation yield of DOX was 70 ± 6 %, corresponding to 80 ± 5 µg of DOX/µmol of lipids. These results derived from at least five different batches.

3.2 U87-MG cells forms TnTs with different thickness, compared to NHA

To investigate if U87-MG cells (model of GBM tumor cells) are able to form in vitro intercellular connections with characteristics of TnTs, and if they are different from those formed by NHA cells (model of normal healthy astrocytes), we use confocal microscopy technique and 3D reconstruction. Both cell types form protrusions connecting distant cells with characteristics of TnTs (Fig. 1), which were not in contact with the substratum (Supplementary Fig. S1 and S2). To allow for a quantitative determination, the observed membrane protrusions of

about 200 cells were scored for each cell line. The results showed that the number of cells forming TnTs is comparable between U87-MG and NHA (44 ± 6.6 % and 57 ± 3.5 % respectively) (Supplementary Fig.S3). Confocal images show the presence of TnTs of different thickness, very thin (≤ 0.7 µm, measuring a minimum of 100–200 nm) and thick (≥ 0.7 µm, up to 1 µm) (Gerdes et al., 2007).

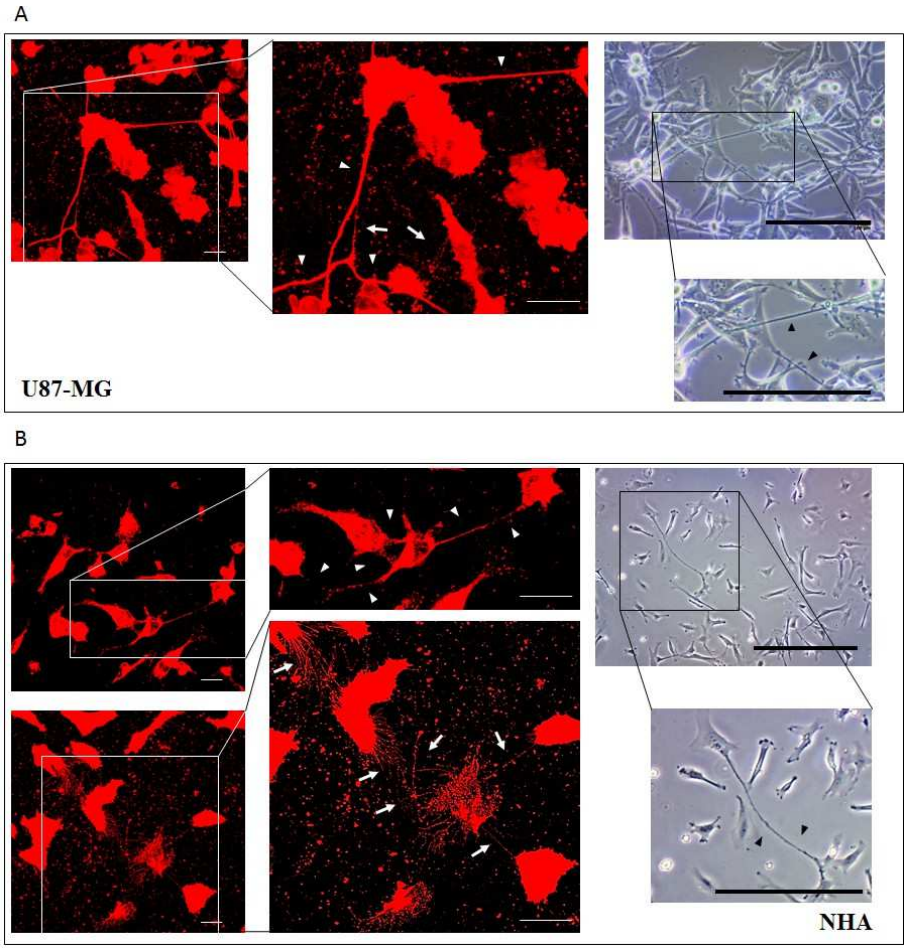

Figure 1. U87-MG and NHA cells forms thin and thick TnTs. U87-MG cells (A) or NHA cells (B) were plated on gelatin pre-treated coverslips, fixed and stained with DiI (1.9 µl/ml) to detect TnTs. Fluorescence images were acquired by a 40x magnification on A1R Nikon laser scanning confocal microscope. The images show the maximum projection obtained from the z-projections shown in figure S1 and S2.

White arrows indicate thin TnTs, while white triangles indicate thick TnTs. Scale bar: 10 µm. Optical images captured with an inverted Olympus CKX41 microscope were also shown. Black triangles indicate thick TnTs. Scale bar: 100 µm. Magnified views of protrusions are shown.

More interestingly, we detected significant differences in both, thin and thick of TnTs: U87-MG cells formed almost exclusively thick protrusions, while NHA formed either thin and thick TnTs (Fig. 2). The measuring of TnTs diameter by light microscopy was not accurate due to the resolution limit. Confocal microscopy showed that some TnTs reach thicknesses of over 700 nm, which could be due to incorporation of additional components inside the TnTs, such as microtubules, as previously suggested (Onfelt et al., 2006).

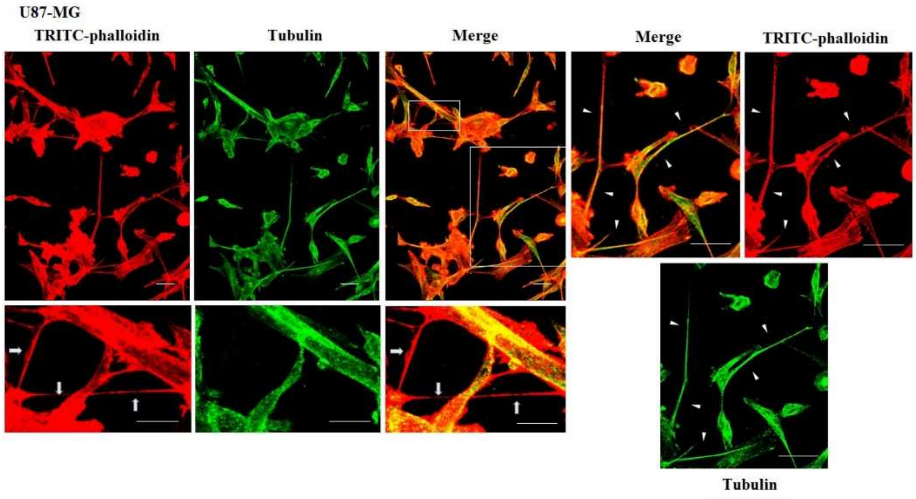

Figure 2. Characterization of TnTs in U87-MG cells. U87-MG cells were plated on gelatine pre-treated coverslips. Cells were fixed, permeabilized and immunostained either with the anti-β-tubulin antibody (1:150) and TRITC-phalloidin (1:40) to detect microtubules and actin filaments. Fluorescence images were captured by confocal microscopy. White triangles indicate thick TnTs and white arrows indicate thin TnTs. Magnified views of protrusions are shown for each channel. Scale bar: 10µm.

To evaluate the presence of tubulin, typical marker for thick TnTs, and of actin, typical marker for thin TnTs (D'Aloia et al., 2018), U87-GM and NHA cells were stained with anti-tubulin fluorescent antibody and fluorescent phalloidin.

The results showed that U87-MG were able to form thick TnTs, which contained both actin and tubulin (Fig. 3). NHA cells were able to form thick TnTs made of actin and tubulin, but they also established thin TnTs, which were positive only to actin staining (Fig. 4).

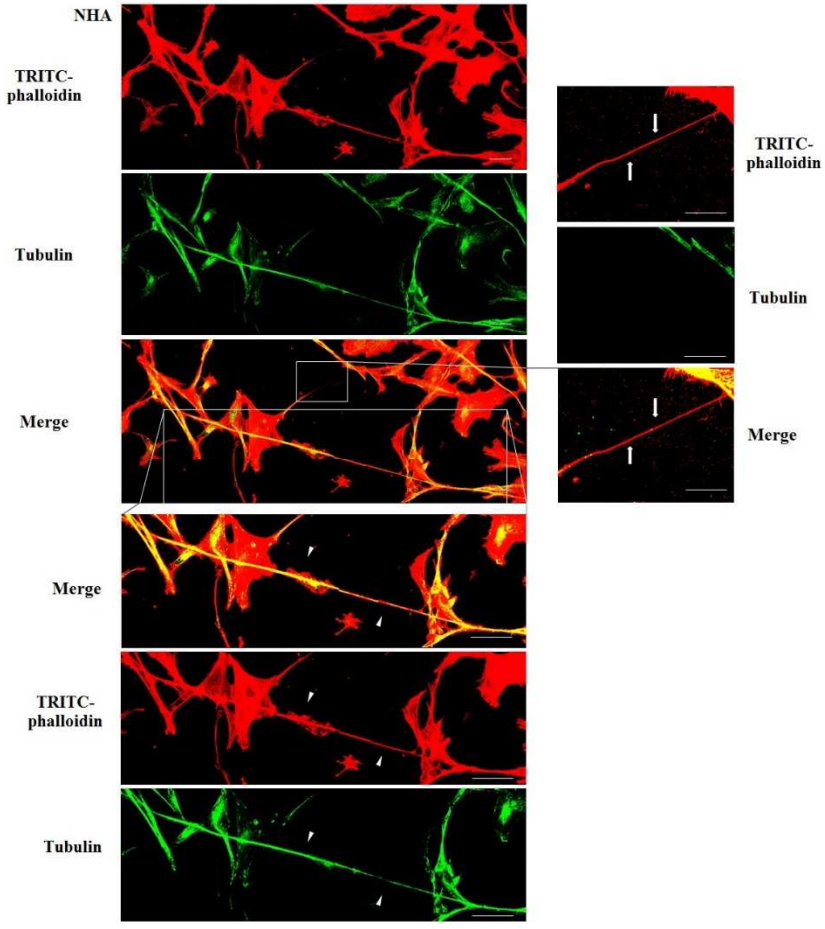

Figure 3. Characterization of TnTs in NHA cells. NHA cells were plated on gelatine pre-treated coverslips. Cells were fixed, permeabilized and immunostained either with the anti-β-tubulin antibody (1:150) and TRITC-phalloidin (1:40) to detect microtubules and actin filaments. Fluorescence images were captured by confocal microscopy. White triangles indicate thick TnTs and white arrows indicate thin TnTs. Magnified views of protrusions are shown for each channel. Scale bar: 10µm.

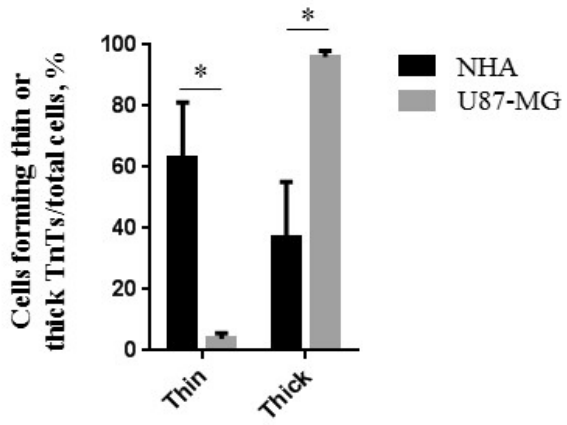

Figure 4. Percentage distribution of thin and thick TnTs in U87-MG and NHA cells. Percentage of U87-MG cells and NHA cells forming thin or thick TnTs on total cells is shown. At least 200 cells were analyzed per group in three independent experiments. Data are expressed as mean ± S.E from three independent experiments. Data were analyzed by two-way ANOVA followed by Sidak's multiple comparisons test; *$p < 0.05$

3.3 Doxorubicin treatment induced changes in the TnTs thickness of U87-MG cells

To evaluate the ability of U87-MG and NHA to exchange DOX via TnTs, cells were treated with two different doses of free DOX. Treatments with 25 µg/ml of DOX for 24 h induced a strong toxic effect

on both cell types, hindering the images analysis (data not shown). Then, all the subsequent experiments were carried out by incubating cells with 15 µg/ml of DOX for 1 h. Analysis performed at confocal microscope showed that DOX (λex = 495 nm; λem =592 nm) localizes principally at the nucleus in both cell lines (Fig. 5; Supplementary Fig. S4), as expected (de Lange et al., 1992), but it was not detectable along TnTs structures.

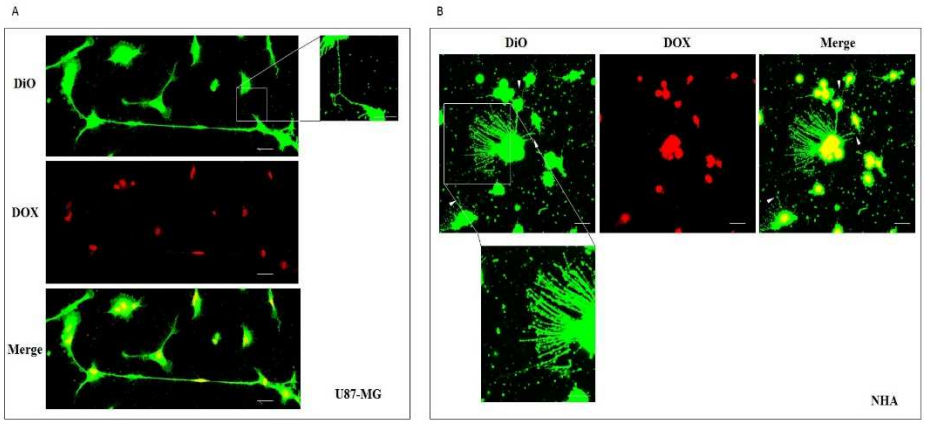

Figure 5. Doxorubicin localize into the nucleus of U87-MG and NHA cells. U87-MG cells (A) and NHA cells (B) were plated on gelatine pre-treated coverslips, incubated with 15 µg/ml of DOX for 1 h and then stained with DiO (5 µl/ml) to detect TnTs. Cells were fixed and fluorescence images were captured with a 40x magnification on A1R Nikon laser scanning confocal microscope. White triangles indicate thin TnTs. Magnified views of Thin TnTs protrusions are shown. Scale bar: 10µm. DOX = doxorubicin.

The quantitative determination of TnTs revealed that the % of cells forming TnTs was not affected by the treatment with free DOX (Fig. 6A,B), for both the cell types used.

Comparing the thickness of TnTs, the DOX treatment on U87-MG cells induced the formation of about 80% of thin TnTs, with a strong

reduction of thick TnTs (Fig. 6C). Prolonging the incubation time up to 24 h, TnTs disappeared and U87-GM cells died (Supplementary Fig. S5).

No significant changes in TnTs thickness were detected for NHA, which remained comparable to untreated NHA (Fig. 6D).

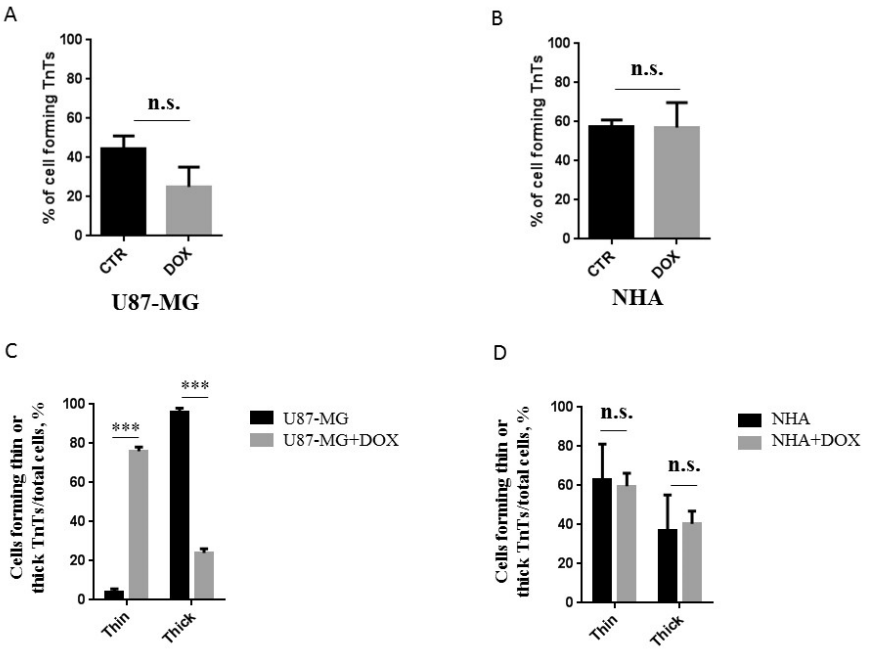

Figure 6. Percentage of cells forming TnTs after DOX treatment. Percentage of U87-MG cells (A) and NHA cells (B) forming TnTs on total cells is shown. At least 200 cells were analyzed per group in three independent experiments. Data are expressed as mean ± S.E from three independent experiments. Data were analyzed by Student t test; n.s.= not significant. DOX = doxorubicin; CTR = control untreated cells .n.s.= not significant. (C, D) Percentage distribution of thin and thick TnTs in U87-MG (C) and NHA (D) cells on total cells, after treatment with DOX. At least 200 cells were analyzed per group in three independent experiments. Data are expressed as mean ± S.E from three independent experiments. Data were analyzed by two-way ANOVA followed by Sidak's multiple comparisons test; n.s.= not significant; ***p< 0.001

3.4 Mf-LIP were differentially exchanged via TnTs in U87-MG compared to NHA.

The cellular uptake of Mf-LIP (LIP bi-functionalized with mApoE and ClTX) by U87-MG was evaluated by confocal microscopy and fluorescence measurements. The results showed that Mf-LIP displayed a 3-fold increase of cellular uptake, compared to DOX-LIP used as a control (Supplementary Fig. S6). Both DOX-LIP and Mf-LIP were localized only in thickest TnTs (Fig. 7, 8).

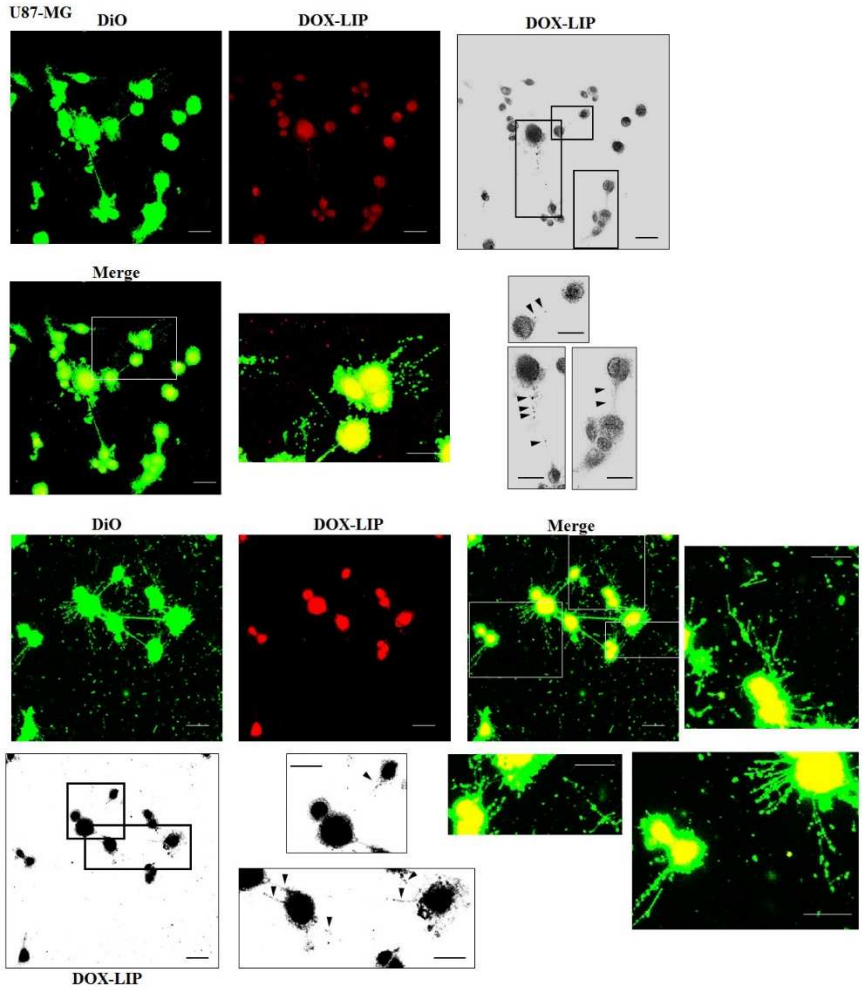

Figure 7. Localization of DOX-LIP in U87-MG TnTs. U87-MG cells were plated on gelatine pre-treated coverslips. Cells were left in culture complete medium for 48 h and then incubated with DOX-LIP (15 µg/ml of DOX, 200 nmols of total lipids) for 1 h. Cells were later stained for 20 min with DiO (5 µl/ml), fixed and fluorescence images were captured with a 40x magnification on A1R Nikon laser scanning confocal microscope. Black triangles indicate the DOX-LIP in thick TnTs. Magnified views of protrusions and black-and-white images are shown. Scale bar: 10µm. DOX-LIP = liposomes embedding doxorubicin.

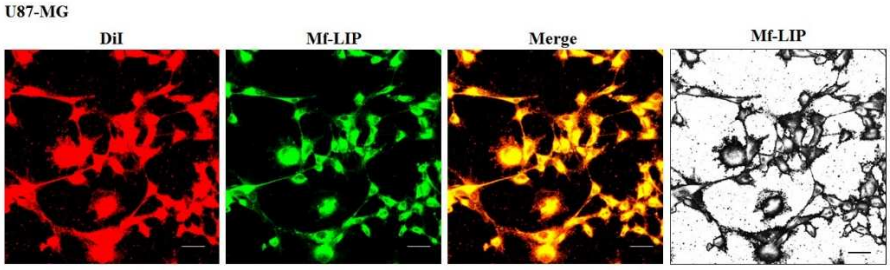

Figure 8. Localization of Mf-LIP in U87-MG TnTs. U87-MG cells were plated on gelatine pre-treated coverslips. Cells were left in culture complete medium for 48 h and then cells were incubated with Mf-LIP (200 nmols of total lipids) for 1 h. Cells were later stained for 20 min with DiI (1.9 µl/ml). Cells were fixed and fluorescence images were captured with a 40x magnification on A1R Nikon laser scanning confocal microscope. Black-and-white image is also shown. Scale bar: 10µm. Mf-LIP = multi-functionalized liposomes.

Contrarily, NHA cells were able to uptake only a small amount of DOX-LIP and Mf-LIP. Also in these cells LIP were localized only in thick TnTs (Fig. 9, 10).

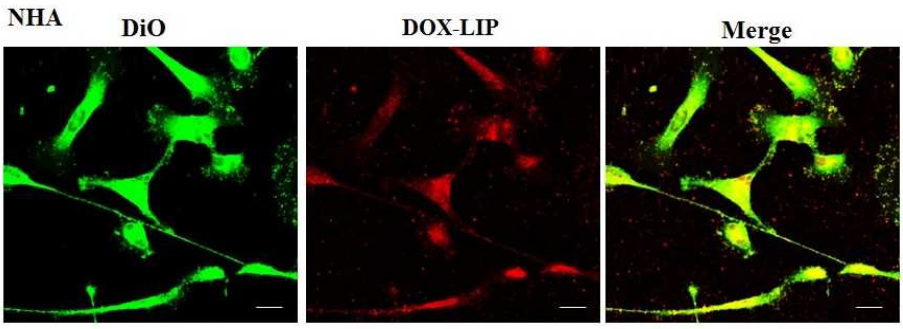

Figure 9. Localization of DOX-LIP in NHA TnTs. NHA cells were seeded on gelatine pre-treated coverslips. Cells were left in culture complete medium for 48 h and then incubated with DOX-LIP (15 µg/ml of DOX, 200 nmols of total lipids) for 1 h. Cells were later stained for 20 min with DiO (5 µl/ml), fixed and fluorescence images were captured with a 40x magnification on A1R Nikon laser scanning confocal microscope. Scale bar: 10µm. DOX-LIP = liposomes embedding doxorubicin.

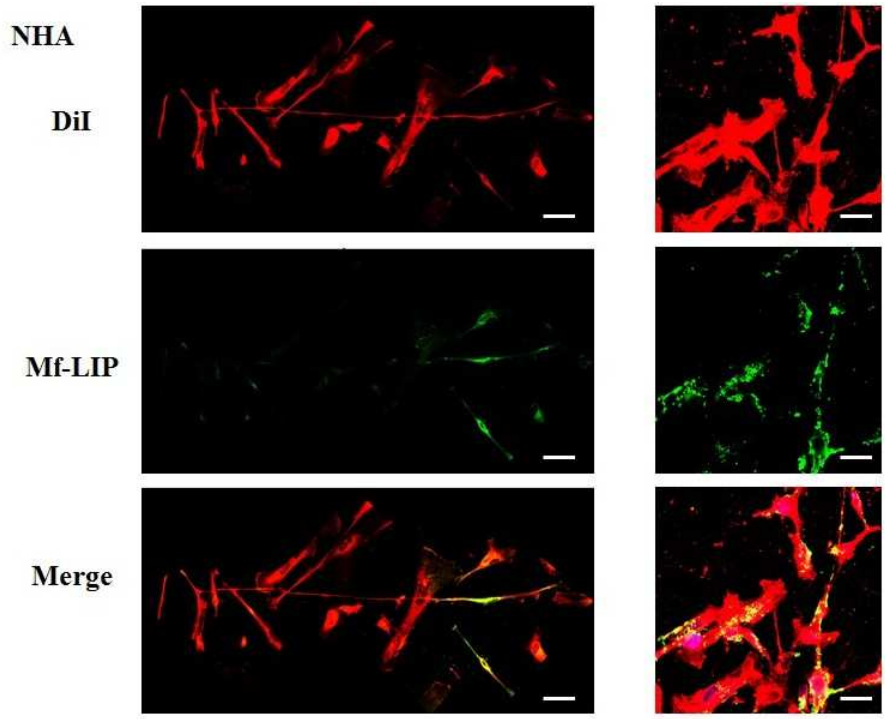

Figure 10. Localization of Mf-LIP in NHA TnTs. NHA cells were plated on gelatine pre-treated coverslips. Cells were left in culture complete medium for 48 h and then

incubating cells with Mf-LIP (200 nmols of total lipids) for 1 h. Cells were later stained for 20 min with DiI (1.9 µl/ml). Cells were fixed and fluorescence images were captured with a 40x magnification on A1R Nikon laser scanning confocal microscope. Black triangles indicate the presence of Mf-LIP in thick TnTs. Magnified views of protrusions and black-and-white images are shown. Scale bar: 10µm. Mf-LIP = multi-functionalized liposomes.

The treatment of U87-MG cells with DOX-LIP did not affects the % of cells forming TnTs (Supplementary Fig. S7A), but strongly increased thin TnTs, with a significant reduction of thick TnTs (Fig.11A, B), similarly to the effect exerted by free DOX.

The treatment of U87-MG and NHA cells with Mf-LIP didn't change the percentage of thin and thick TnTs compared to untreated cells (Fig. 11C, D). Also the treatment with Mf-LIP did not affects the % of cells forming TnTs (Supplementary Fig. S7A); neither the ratio between thin and thick TnTs (Fig. 11C, D). No differences were detected in TnTs formed by NHA cells after incubation with DOX-LIP or Mf-LIP (Supplementary Fig. S7B; Fig. 6; Fig. 11C, D).

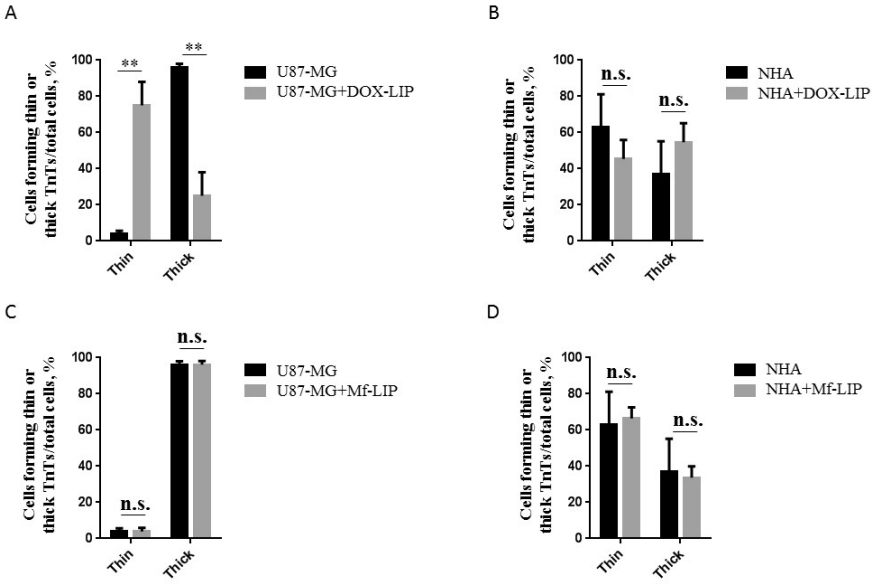

Figura 11. Percentage distribution of thin and thick TnTs in U87-MG and NHA cells after treatment with DOX-LIP or Mf-LIP. Percentage distribution of thin and thick TnTs in U87-MG (A) and NHA (B) cells after treatment with DOX-LIP. Percentage distribution of thin and thick TnTs in U87-MG (C) and NHA (D) cells after treatment with Mf-LIP. At least 200 cells were analyzed per group in three independent experiments. Data are expressed as mean ± S.E from three independent experiments. Data were analyzed by two-way ANOVA followed by Sidak's multiple comparisons test; n.s.= not significant; **p< 0.01.

Finally, to evaluate the integrity of LIP inside to TnTs, double labelled Mf-LIP (containing BODIPY-Sm and DOX) were used. As it is shown in Fig. 12, the co-localization of both fluorescent signals was detected in TnTs from both U87-MG and NHA cells.

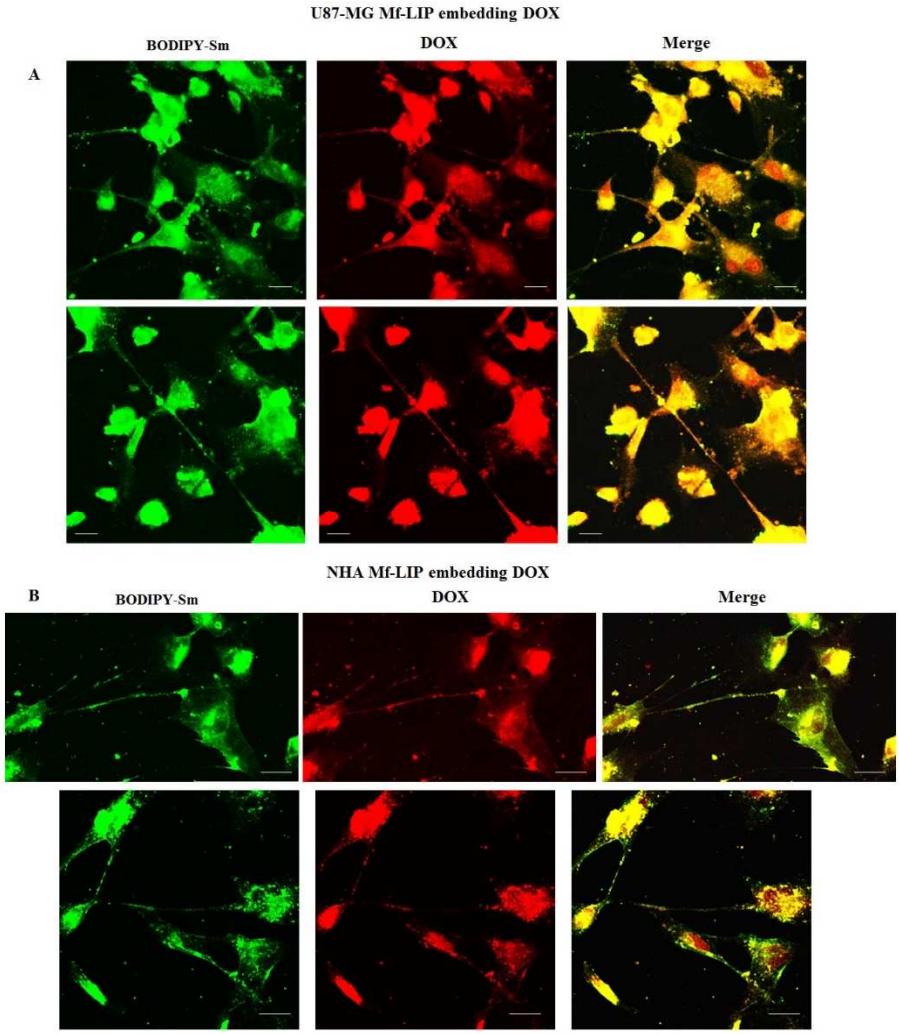

Figure 12. Mf-LIP embedding DOX localized in TnTs formed by U87-MG and NHA cells. U87-MG (A) and NHA (B) cells were plated on gelatine pre-treated coverslips. Cells were left in culture complete medium for 48 h and then incubated with Mf-LIP embedding DOX (15µg/ml of DOX, 200 nmols of total lipids) for 1h. Cells were fixed and fluorescence images were captured with a 40x magnification on A1R Nikon laser scanning confocal microscope. Scale bar: 10µm. BODIPY-Sm=Sphingomyelin present in Mf-LIP conjugate with fluorophore BODIPY.

3.5 Mf-LIP were preferentially exchanged via TnTs between U87-MG cells.

Cell-to-cell transfer of Mf-LIP between different co-culture mixtures was assessed by FACS analysis. The results showed that Mf-LIP were transferred via TnTs between NHA cells with a low rate, as demonstrated by the detection of 5±0.6% Mf-LIP positive “acceptor” cells. Interestingly, the rate of Mf-LIP exchange from U87-MG to NHA was 2-fold lower (3.8±0.2% of Mf-LIP positive “acceptor” NHA) than U87-MG to U87-MG transfer (8.2±1.5 % of Mf-LIP positive “acceptor” U87-MG).

4 Discussion

In the context of searching more effective therapies against GBM, which remains an incurable brain tumour, we focus our attention on the cells communication. Intercellular communication plays an important role in tumour progression, invasiveness and resistance to conventional treatments (Broekman et al., 2018). Among the different ways that cells used to exchange non-secretable messages, tunnelling nanotubes (TnTs) and microtubes (TmTs) are involved in the re-growth of GBM after surgery and in conferring resistance to radio- and chemotherapy (Weil et al., 2017; Moschoi et al., 2016). Starting from our expertise in the design of nanoparticles, we synthesized and characterized LIP carry doxorubicin, as an anti-cancer drug model, and dually-functionalized with mApoE and with ClTx, as GBM targeting ligands (Maletínská et al., 2000; DeBin et al., 1993; Ojeda et al., 2016; Lyons et al., 2002; Formicola et al. 2019). The ability of human primary glioblastoma cell

line (U87-MG), in comparison to normal human astrocytes (NHA), to exchange Mf-LIP via TnTs has been investigated. Mf-LIP characterization shown that the different batches herein prepared were highly reproducible and stable over time, with the yield of the reactions comparable to previously reported ones (Re et al., 2010; Re et al., 2011; Formicola et al. 2019).

Since it is reported in literature that TnTs are not observed in some glioma cellular models (Van der Vos et al., 2016), we checked if U87-MG cells and NHA cells herein used were able to form TnTs in vitro. The results showed that both types of cells were able to communicate between them by TnTs, as already reported (Reindl et al., 2019; Zhang et al., 2015; Rostami et al., 2017) and the percentage of cells forming TnTs was similar between U87-MG and NHA cells.

Since TnTs have been grouped into two main classes, very thin (≤ 0.7 µm, measuring a minimum of 100–200 nm) and thick (≥ 0.7 µm, up to 1 µm) (Gerdes et al., 2007), we analyzed the heterogeneity of TnTs formed by U87-MG and NHA.

Structural analysis and the comparison of the thickness of TnTs formed by these cells, shown that U87-MG cells formed almost exclusively thick protrusions, while NHA formed either thin and thick TnTs.

Considering that thick TnTs are more efficient in transport of molecules and organelles (Veranic et al., 2008; Mittal R.et al. 2019), this difference could may be exploited to increase the range of drug delivery between cancer cells. Moreover, TnTs are also classified according to their different morphology/function in TnTs type I, short dynamic structures, containing actin filament and engaged in exploring the

surrounding microenvironment, and TnTs type II, that are longer and more stable processes, containing actin and tubulin filaments and apparently involved in organelles shuttle (Veranic et al., 2008). Here reported immunofluorescence experiments staining actin and tubulin, showed that U87-MG mainly formed TnTs type II, compared to NHA, which formed mostly TnTs type I. Accordingly, U87-MG were able to better exchange Mf-LIP, as shown by the detection of liposomes-associated fluorescence in thick TnTs. Moreover, we showed that the LIP surface functionalization with mApoE and ClTx strongly increased the cell uptake by U87-MG, while no differences were detected with NHA in terms of LIP uptake. This suggest that the presence of these two ligands may promote a more specific targeting of cancer cells, probably due to the overexpression of LDL-receptor by U87-MG cells (Maletínská et al., 2000; DeBin et al., 1993), which is the target ligand of mApoE peptide, and ClTx, which has been shown to selectively bind a specific chloride channel on glioma cell surface (Ojeda et al., 2016; Lyons et al., 2002; Xiang et al. 2011).

Moreover, the encapsulation of DOX in LIP facilitates its passage through TnTs, respect to free DOX, that remains almost exclusively localized in the nuclear region. Considering that cells physiologically produced TnTs under stress conditions (e.g. hypoxia conditions, drugs, oxidative stress), we assessed the effect of DOX treatment on TnTs formed by U87-MG cells. The results showed that free DOX and DOX-LIP induced the formation of thin TnTs, with a strong reduction of thick TnTs and prolonging the incubation time, TnTs disappeared and U87-MG cells died as also showed for other cells types (Rustom, 2016). Comparing these results to those obtained in NHA cells, Mf-LIP were

localized in TnTs with a little extent and the few LIP inside in NHA's TnTs were again localized in the thick ones. This corroborate the fact that thick TnTs are mainly involved in the intercellular trafficking of drug-loaded liposomes.

More appealing, the structural difference between TnTs formed by GBM cells and NHA could be useful to design precise and specific nanotherapeutics.

As a proof-of-concept, the ability of cells to mutually exchange Mf-LIP was evaluated in different co-culture mixtures. Interestingly, the results showed that U87-MG were more inclined to transfer Mf-LIP to other cancer cells, than to healthy astrocytes.

The opportunity to exploit TnTs as drug-delivery channels can improve the cancer therapy, by reaching isolated, infiltrating tumor cells that are hardly targeted by drug diffusion in the brain parenchyma. Nowadays, few papers are available showing the involvement of TnTs-mediated intercellular transport of nanoparticles (Kristl et al., 2013; Epperla et al., 2015; Deng et al., 2018) and none of them is dedicated to the comparison between healthy and tumour cells in nanoparticles trafficking. It is important to highlight that all the results herein reported were obtained using one GBM-derived cell line, which are not fully representative of human GBM. For this reason, the validation of these results will be further performed on patient-derived glioblastoma cells, stem cells included.

In conclusion, the understanding of the possible intercellular delivery of nanotherapeutics cargo via TnTs can significantly influence the approaches to treat specific diseases.

Supplementary materials and figures

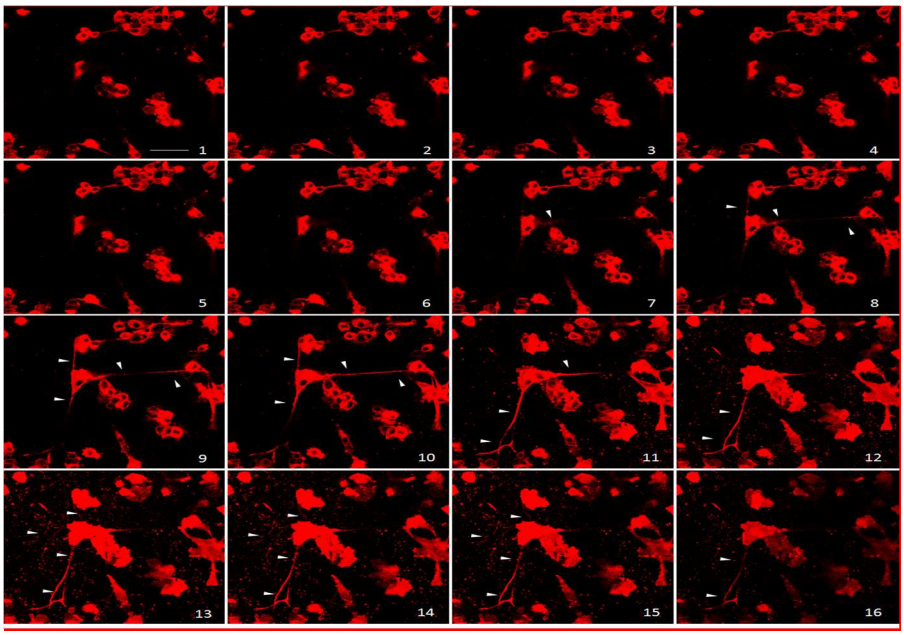

Figure S1. Series of confocal z-slides. U87-MG cells were plated on gelatine pre-treated coverslips. Cells were stained with the membrane dye DiI, fixed, and imaged via confocal microscopy. Series of DiI-stained confocal z-slides and maximum intensity projection of z-slides from U87-MG cells. White triangles indicate TnTs. Scale bar: 10 µm. The step size is 0.625 µm and the number of optical section is 16.

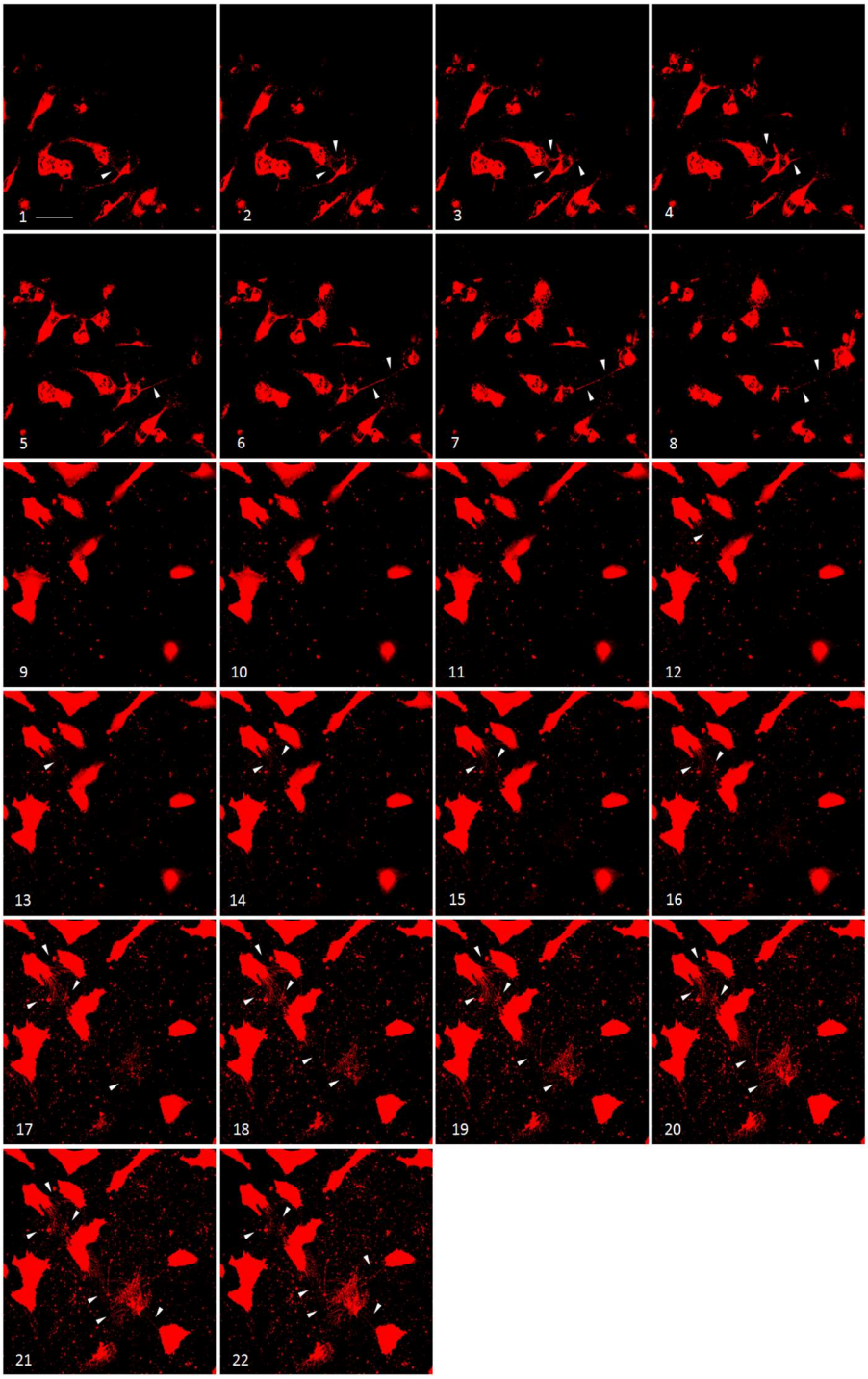

Figure S2. Series of confocal z-slides. NHA cells were plated on gelatine pre-treated coverslips. Cells were stained with the membrane dye DiI, fixed, and imaged via

confocal microscopy. Series of DiI-stained confocal z-slides and maximum intensity projection of z-slides from NHA cells. White triangles indicate TnTs. Scale bar: 10 μm. The step size is 0.454 μm and the number of optical section is 22.

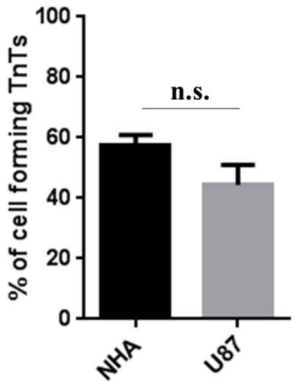

Figure S3. Percentage of cells forming TnTs. Percentage of U87-MG cells and NHA cells forming TnTs on total cells is shown. At least 200 cells were analyzed per group in three independent experiments. Data are expressed as mean ± S.E from three independent experiments. Data were analyzed by Student *t* test; n.s.= not significant.

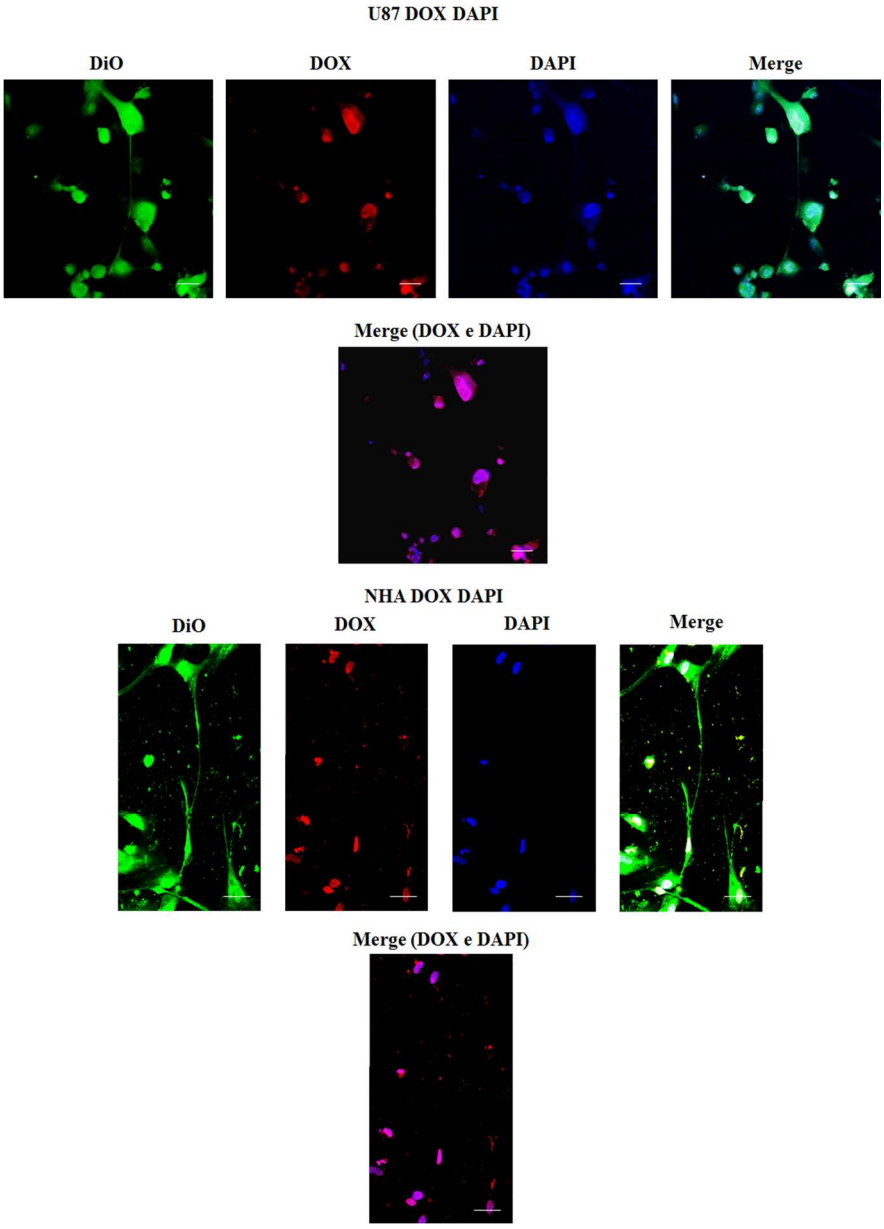

Figure S4. Doxorubicin (DOX) localizes principally at the nucleus in U87-MG and NHA cell lines. U87-MG and NHA cells were plated on gelatine pre-treated coverslips. Cells were leaved in culture complete medium for 48 h and then incubated with 15 µg/ml of free DOX for 1 h. Cells were later stained for 20 min with DiO (5 µl/ml), fixed, permeabilized and colored with DAPI (1µg/ml) for 10 minutes. Fluorescence images were captured with a 40x magnification on A1R Nikon laser scanning confocal microscope. Scale bar: 10µm. DOX = doxorubicin.

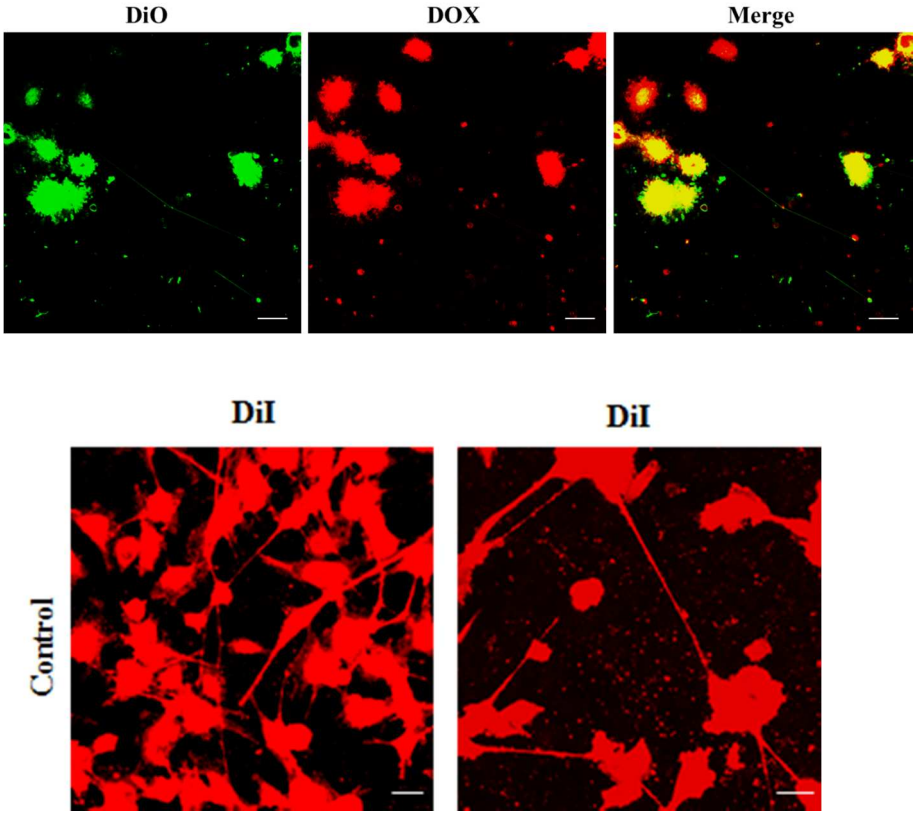

Figure S5. Free doxorubicin induces the TnTs disappearance and death of U87-GM cells.

U87-MG cells were plated on gelatine pre-treated coverslips. Cells were leaved in culture complete medium for 48 h and then incubated with 15 µg/ml of free DOX for 24 h. Cells were later stained for 20 min with DiO (5 µl/ml) or DiI (5µM), fixed and fluorescence images were captured with a 40x magnification on A1R Nikon laser scanning confocal microscope. Scale bar: 10µm. DOX = doxorubicin

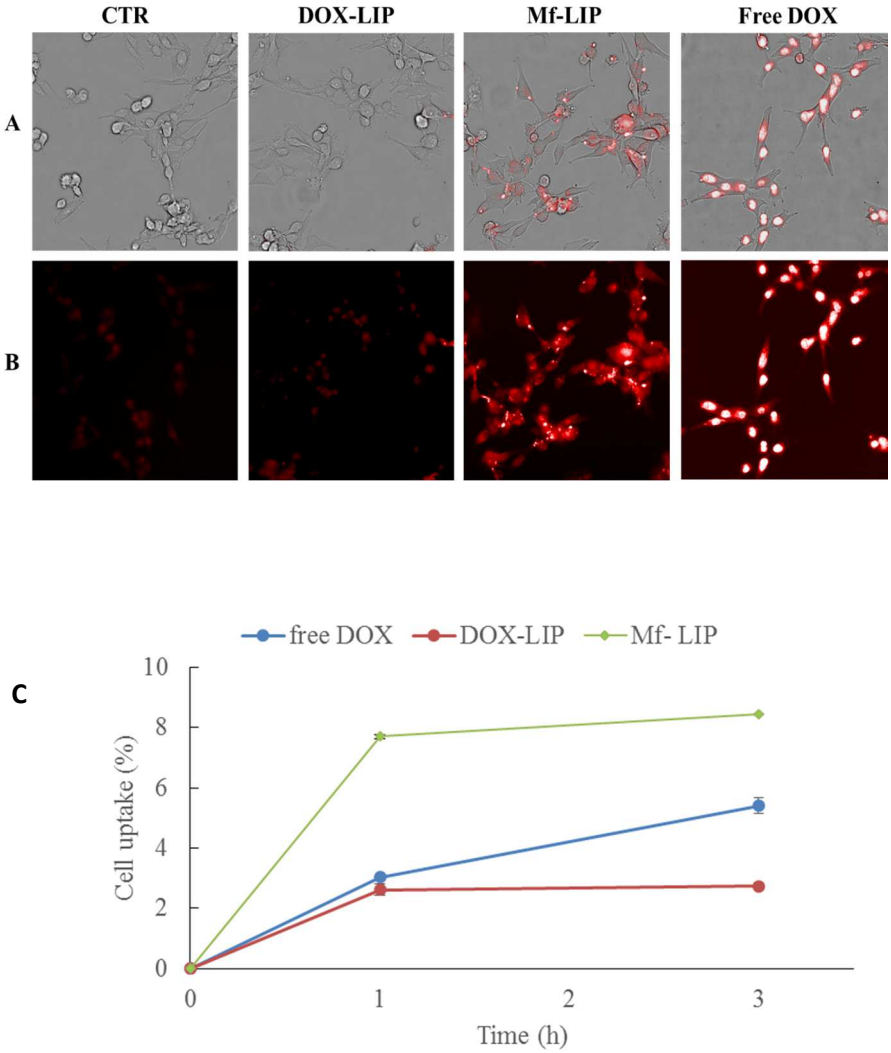

Figure S6. Cellular uptake of DOX by U87-MG cells. U87-MG cells were seeded on a 96-well plate (10^4 cells/well). After two days of culture, cells were treated with free DOX (15 µg/ml) or DOX-LIP or Mf-LIP (15 µg/ml of DOX, 200 nmols of total lipids) and the uptake was evaluated by acquiring images at three different time points (0, 1 h, 3 h). Representative images at 1h are shown. Images were acquired in the brightfield channel (**A**) and in the DOX channel (λex=495 nm; λem=592 nm) (**B**) using a 40x air objective lens and standard instrument filters. Time course DOX uptake by U87-MG was measured by Jasco FP-8500 spectrofluorometer (**C**).

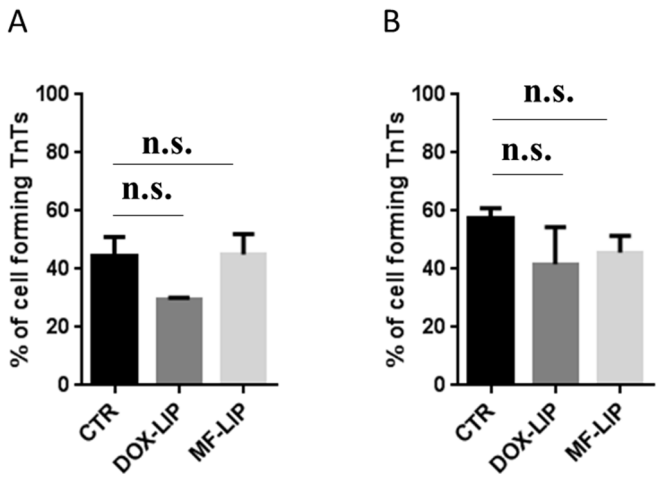

Figure S7. Percentage of cells forming TnTs after DOX-LIP or Mf-LIP treatment. Percentage of U87-MG cells (**A**) and NHA cells (**B**) forming TnTs on total cells is shown. At least 200 cells were analyzed per group in three independent experiments. Data are expressed as mean ± S.E from three independent experiments. Data were analysed by one-way ANOVA followed by Dunnett's post-hoc test; n.s.= not significant. DOX-LIP = liposomes carrying doxorubicin; Mf-LIP = multi-functionalized liposomes; CTR = control untreated cells.

References

1. Abounit, S., Bousset, L., Loria, F., Zhu, S., de Chaumont, F., Pieri, L., et al. (2016). Tunneling nanotubes spread fibrillar α-synuclein by intercellular trafficking of lysosomes. *EMBO J.* 35:19. doi:10.15252/embj.201593411

2. Ahmad, T., Mukherjee, S., Pattnaik, B., Kumar, M., Singh, S., Kumar, M., et al. (2014). Miro1 regulates intercellular mitochondrial transport & enhances mesenchymal stem cell rescue efficacy. *EMBO J.* 33:9. doi:10.1002/embj.201386030

3. Balducci, C., Mancini, S., Minniti, S., La Vitola, P., Zotti, M., Sancini, G., et al. (2014). Multifunctional liposomes reduce brain β-amyloid burden and ameliorate memory impairment in Alzheimer's disease mouse models. *J Neurosci*. 34:42. doi: 10.1523/JNEUROSCI.0284-14.2014

4. Bana, L., Minniti, S., Salvati, E., Sesana, S., Zambelli, V., Cagnotto, A., et al. (2014). Liposomes bi-functionalized with phosphatidic acid and an ApoE-derived peptide affect Aβ aggregation features and cross the blood-brain-barrier: implications for therapy of Alzheimer disease. *Nanomedicine*. 10:7. doi: 10.1016/j.nano.2013.12.001

5. Broekman, M.L., Maas, S.L.N., Abels, E.R., Mempel, T.R., Krichevsky, A.M., Breakefield, X.O. (2018). Multidimensional communication in the microenvironments of glioblastoma. *Nat Rev Neurol.* 14:8. doi: 10.1038/s41582-018-0025-8

6. Carone, C., Genedani, S., Leo, G., Filaferro, M., Fuxe, K., Agnati, L. F. In vitro effects of cocaine on tunneling nanotube formation and extracellular vesicle release in glioblastoma cell cultures. (2015). *J Mol Neurosci.* 55:1. doi: 10.1007/s12031-014-0365-9

7. Ceriani, M., Scandiuzzi, C., Amigoni, L., Tisi, R., Berruti, G., Martegani, E. (2007) Functional analysis of RalGPS2, a murine guanine nucleotide exchange factor for RalA GTPase. *Exp Cell Res.* 313:11. doi: 10.1016/j.yexcr.2007.03.016

8. D'Aloia, A., Berruti, G., Costa, B., Schiller, C., Ambrosini, R., Pastori, V., Martegani, E., Ceriani, M. (2018) RalGPS2 is involved in tunneling nanotubes formation in 5637 bladder cancer cells. *Exp Cell Res*. 362:2. doi: 10.1016/j.yexcr.2017.11.036

9. DeBin, J. A., Maggio, J. E., Strichartz, G. R. (1993). Purification and characterization of chlorotoxin, a chloride channel ligand from the venom of the scorpion. *Am. J. Physiol.* 264:2. doi:10.1152/ajpcell.1993.264.2.C361

10. de Lange. J,H,1, Schipper, N.W., Schuurhuis, G.J., ten Kate, T.K., van Heijningen, T.H., Pinedo, H.M., et al. (1992). Quantification by laser scan microscopy of intracellular doxorubicin distribution. *Cytometry*. 13:6. DOI: 10.1002/cyto.990130604

11. Deng, G., Wu, Z., Zhou, F., Dai, C., Zhao, J., Kang, Y., et al. (2018). Exchangeability of FITC-SiO_2 Nanoparticles Between

Cancer Cells Increases the Range of Drug Delivery. *J Biomed Nanotechnol*. 14:1. doi: 10.1166/jbn.2018.2509

12. Epperla, C. P., Mohan, N., Chang, C. W., Chen, C. C., Chang, H. C. (2015). Nanodiamond-Mediated Intercellular Transport of Proteins through Membrane Tunneling Nanotubes. *Small.* 11:45. doi: 10.1002/smll.201502089

13. Fan, X., Khaki, L., Zhu, T. S., Soules, M. E., Talsma, C. E., Gul, N., et al. (2010). NOTCH pathway blockade depletes CD133-positive glioblastoma cells and inhibits growth of tumor neurospheres and xenografts. *Stem Cells.* 28:1. doi: 10.1002/stem.254

14. Formicola, B., Dal Magro, R., Montefusco-Pereira, C.V., Lehr, C.M., Koch, M., Russo L., et al. (2019). The synergistic effect of chlorotoxin-mApoE in boosting drug-loaded liposomes across the BBB. *J Nanobiotech, in press*.

15. Gerdes, H.H., Bukoreshtliev, N.V., Barroso, J.F. (2007). Tunneling nanotubes: a new route for the exchange of components between animal cells. *FEBS Lett*. 581:11. doi: 10.1016/j.febslet.2007.03.071

16. Gould, E. (2017). How widespread is adult neurogenesis in mammals? *Nat Rev Neurosci.* 8:6. doi: 10.1038/nrn2147

17. Kristl, J., Plajnšek, K.T., Kreft, M.E., Janković, B., Kocbek, P. (2013). Intracellular trafficking of solid lipid nanoparticles and their distribution between cells through tunneling nanotubes. *Eur J Pharm Sci.* 50:1. doi: 10.1016/j.ejps.2013.04.013

18. Lin, J., Zhang, X. M., Yang, J. C., Ye, Y. B., Luo, S. Q. (2010). γ-secretase inhibitor-I enhances radiosensitivity of glioblastoma cell lines by depleting CD133+ tumor cells. *Arch Med Res.* 41:7. doi: 10.1016/j.arcmed.2010.10.006

19. Lou, E., Fujisawa, S., Barlas, A., Romin, Y., Manova-Todorova, K., Moore, M.A., et al. (2012,a). Tunneling Nanotubes: A new paradigm for studying intercellular communication and therapeutics in cancer. *Commun Integr Biol*. 1;5(4). doi: 10.4161/cib.20569

20. Lou, E., Fujisawa, S., Morozov, A., Barlas, A., Romin, Y., Dogan, Y., et al. Tunneling nanotubes provide a unique conduit for intercellular transfer of cellular contents in human malignant pleural mesothelioma. (2012,b). *PLoS One.* 7(3):e33093. doi: 10.1371/journal.pone.0033093

21. Louis, D.N., Perry, A., Reifenberger, G., von Deimling, A., Figarella-Branger, D., Cavenee, W.K., et al. (2016) The 2016 World Health Organization Classification of Tumors of the Central Nervous System: a summary. *Acta Neuropathol.* 131:6. doi: 10.1007/s00401-016-1545-1

22. Lyons, S. A., O'Neal, J., Sontheimer, H. (2002). Chlorotoxin, a scorpion-derived peptide, specifically binds to gliomas and tumors of neuroectodermal origin. *Glia.* 39:2. doi:10.1002/glia.10083 162-173

23. Maletínská, L., Blakely, E. A., Bjornstad, K.A., Deen, D. F., Knoff, L. J., Forte, T. M. (2000). Human glioblastoma cell lines:

levels of low-density lipoprotein receptor and low-density lipoprotein receptor-related protein. *Cancer Res.* 60:8

24. Magro, R.D., Cox, A., Zambelli, V., Mancini, S., Masserini, M., Re, F. (2018). The ability of liposomes, tailored for blood-brain barrier targeting, to reach the brain is dramatically affected by the disease state. *Nanomedicine (London).* 13:6. doi: 10.2217/nnm-2017-0317

25. Mare, R., Paolino, D., Celia, C., Molinaro, R., Fresta, M., Cosco, D. (2018). Post-insertion parameters of PEG-derivatives in phosphocholine-liposomes. *Int J Pharm.* 552:1-2. doi: 10.1016/j.ijpharm.2018.10.028

26. Mittal, R., Karhu, E., Wang, J. S., Delgado, S., Zukerman, R., Mittal, J., Jhaveri, V.M. (2019).Cell communication by tunneling nanotubes: Implications in disease and therapeutic applications. J. Cell Physiol. 234:2.doi: 10.1002/jcp.27072

27. Moschoi, R., Imbert, V., Nebout, M., Chiche, J., Mary, D., Prebet, T., et al. (2016). Protective mitochondrial transfer from bone marrow stromal cells to acute myeloid leukemic cells during chemotherapy. *Blood.* 128:2. doi: 10.1182/blood-2015-07-655860

28. Ojeda, P. G., Wang, C. K., Craik, D. J. (2016). Chlorotoxin: Structure, activity, and potential uses in cancer therapy. *Biopolymers.* 106:1. doi: 10.1002/bip.22748

29. Önfelt, B., Nedvetzki, S., Benninger, R. K. P., Purbhoo, M. A., Sowinski, S., Hume, A. N., et al. (2006). Structurally Distinct

Membrane Nanotubes between Human Macrophages Support Long-Distance Vesicular Traffic or Surfing of Bacteria. *J Immunol.* 177:12. doi:10.4049/jimmunol.177.12.8476

30. Re, F., Cambianica, I., Sesana, S., Salvati, E., Cagnotto, A., Salmona, M., Couraud, P. O., et al. (2010). Functionalization with ApoE-derived peptides enhances the interaction with brain capillary endothelial cells of nanoliposomes binding amyloid-beta peptide. *J. Biotechnol.* 156:4. doi: 10.1016/j.jbiotec.2011.06.037

31. Re, F., Cambianica, I., Zona, C., Sesana, S., Gregori, M., Rigolio, R., et al. (2011). Functionalization of liposomes with ApoE-derived peptides at different density affects cellular uptake and drug transport across a blood-brain barrier model. *Nanomedicine: NBM.* 7:5. doi: 10.1016/j.nano.2011.05.004

32. Reindl, J., Shevtsov, M., Dollinger, G., Stangl, S., Multhoff, G. (2019). Membrane Hsp70-supported cell-to-cell connections via tunneling nanotubes revealed by live-cell STED nanoscopy. *Cell Stress Chaperones*. 24:1. doi: 10.1007/s12192-018-00958-w

33. Rostami, J., Holmqvist, S., Lindström, V., Sigvardson, J., Westermark, G.T., Ingelsson, M. et al. (2017). Human Astrocytes Transfer Aggregated Alpha-Synuclein via Tunneling Nanotubes. *J Neurosci*. 37:49. doi: 10.1523/JNEUROSCI.0983-17.2017

34. Rustom, A. (2016). The missing link: does tunnelling nanotube-based supercellularity provide a new understanding of chronic and lifestyle diseases? *Open Biol.* 6:6. doi: 10.1098/rsob.160057

35. Rustom, A., Saffrich, R., Markovic, I., Walther, P., Gerdes, H. H. (2004). Nanotubular highways for intercellular organelle transport. *Science.* 303:5660. doi:10.1126/science.1093133

36. Schiller, C., Huber, J. E., Diakopoulos, K. N., Weiss, E.H. (2013). Tunneling nanotubes enable intercellular transfer of MHC class I molecules. *Hum. Immunol.* 74:4. doi:10.1016/j.humimm.2012.11.026

37. Sisakhtnezhad, S., Khosravi, L. (2015). Emerging physiological and pathological implications of tunneling nanotubes formation between cells. *Eur J Cell Biol.* 94:10. doi: 10.1016/j.ejcb.2015.06.010.

38. Sowinski, S., Jolly, C., Berninghausen, O., Purbhoo, M. A., Chauveau, A., Köhler, K., Oddos, S., et al. (2008). Membrane nanotubes physically connect T cells over long distances presenting a novel route for HIV-1 transmission. *Nat Cell Biol.* 10:2. doi:10.1038/ncb1682

39. Stewart, J. C. (1980). Colorimetric determination of phospholipids with ammonium ferrothiocyanate. *Anal Biochem.* 104:1. doi: 10.1016/0003-2697(80)90269-9

40. Stupp, R., Hegi, M.E., Mason, W.P., van den Bent, M.J., Taphoorn, M.J., Janzer, R.C., et al. (2009). Effects of

radiotherapy with concomitant and adjuvant temozolomide versus radiotherapy alone on survival in glioblastoma in a randomised phase III study: 5-year analysis of the EORTC-NCIC trial. *Lancet Oncol*. 10:5. doi: 10.1016/S1470-2045(09)70025-7

41. Tamborini, M., Locatelli, E., Rasile, M., Monaco, I., Rodighiero, S., Corradini, I., et al. (2016). A Combined Approach Employing Chlorotoxin-Nanovectors and Low Dose Radiation To Reach Infiltrating Tumor Niches in Glioblastoma. *ACS Nano.* 10:2. doi: 10.1021/acsnano.5b07375

42. Thayanithy, V., Dickson, E. L., Steer, C., Subramanian, S., Lou, E. (2014). Tumor-stromal cross talk: direct cell-to-cell transfer of oncogenic microRNAs via tunneling nanotubes. *Transl Res.* 164:5. doi:10.1016/j.trsl.2014.05.011

43. Van der Vos, K. E., Abels, E. R., Zhang, X., Lai, C.,, Carrizosa, E., Oakley, D., et al. (2016). Directly visualized glioblastoma-derived extracellular vesicles transfer RNA to microglia/macrophages in the brain. *Neuro Oncol.* 18:1. doi: 10.1093/neuonc/nov244

44. Veranic, P., Lokar, M., Schütz, G.J., Weghuber, J., Wieser, S., Hägerstrand, H., et al. (2008). Different types of cell-to-cell connections mediated by nanotubular structures. *Biophys J*. 95:9. doi: 10.1529/biophysj.108.131375

45. Weil, S., Osswald, M., Solecki, G., Grosch, J., Jung, E., Lemke, D., et al. (2017). Tumor microtubes convey resistance to

surgical lesions and chemotherapy in gliomas. *Neuro Oncol.* 19:10. doi: 10.1093/neuonc/nox070

46. Westphal, M., Lamszus, K. (2011). The neurobiology of gliomas: from cell biology to the development of therapeutic approaches. *Nature Rev*. 12:9. doi: 10.1038/nrn3060

47. Xiang, Y., Liang, L., Wang, X., Wang, J., Zhang, X., Zhang, Q. (2011). Chloride channel-mediated brain glioma targeting of chlorotoxin-modified doxorubicin-loaded liposomes. *J Control Release.* 152:3. doi: 10.1016/j.jconrel.2011.03.014

48. Zhang, L., Zhang, Y. (2015). Tunneling nanotubes between rat primary astrocytes and C6 glioma cells alter proliferation potential of glioma cells. *Neurosci Bull*. 31:3. doi: 10.1007/s12264-014-1522-4

CHAPTER 5

Summary, conclusions and future perspectives

Glioblastoma multiforme (GBM, WHO grade IV tumour) is the most frequently occurring malignant CNS tumour. It is carachterized by: high aggressiveness and invasiveness, a very limited response to therapies, and it is associated with poor prognosis, with a median patient survival of 12–15 months from diagnosis. Moreover, GBM presents a high rate of recurrence after surgical recection, with a new tumour occurring in 80% of patients [Pearson JRD and Regard T, 2017; D'Alessio A et al., 2019].

Currently, no cure is available for this disease, making the identification of new strategies an urgent need.

The failure of currently available approaches is mainly due: to the complex biology of the tumour, to the presence of the blood-brain barrier (BBB) that limit the drugs entrance into the brain, and to the existence of GBM Stem-like Cells (GSCs), a subpopulation of cells endowed of an intrinsic tumour-initiating potential and invasiveness and responsible for the increased tumour resistance to chemo- and radiotherapy (RT) [Ohgaki H et al., 2013; Brennan et al., 2013]. GSCs represent a crucial target for effective GBM therapies.

Moreover, the intimate connection through which the cells communicate between them plays an important role in all the biological processes involved in tumour formation and spreading [Broekman ML et al., 2018]. In this scenario, tunneling nanotubes (TnTs) are recently gaining importance as a key features in tumor progression and in particular in the re-growth of GBM after surgery [Weil et al., 2017; Moschoi et al., 2016].

Among all the possibilities, nanomedicine represents a promising approach for the treatment of GBM.

In this context, liposomes (LIP) are the most attractive NPs for biomedical applications thanks to their biocompatibility, non-immunogenicity, non-toxicity, biodegradability, high physical stability and versatility in surface functionalization. For this reason, doxorubicin-loaded multifunctionalized LIP have been proposed in this thesis work. LIP were dually functionalized with mApoE, a modified fragment of the human apolipoprotein E, which binds the LDL receptor, overexpressed both on BBB and on GBM cells, and chlorotoxin (ClTx) to improve the tumour targeting [Salvati E et al., 2013; Re F et al., 2011 Lyons SA et al., 2002; Cohen-Inbar O et al., 2016].

Our results demonstrated the synergistic activity of ClTx-mApoE in boosting doxorubicin-loaded LIP across the BBB *in vitro* model, keeping the anti-tumour activity of the drug loaded. In particular, mApoE acts promoting cellular uptake, while ClTx promotes exocytosis of liposomes. The encapsulation into mApoE-LIPs prevents DOX toxicity on BBB cells and enhances its accumulation within mouse brain *in vivo*. Moreover, when administered to patient-derived GSCs-derived NOD/SCID xenograft mouse, mApoE-DOXO-LIPs triggered GSCs apoptosis resulting in a remarkable reduction of tumour growth and invasion of the contralateral hemisphere.

Importantly, the concomitant administration of radiation enhanced the anti-tumour effects by altering BBB permeability and promoting the expression of LDLr on both BBB and GSCs. RT and adjuvant administration of drug-loaded targeted LIPs represent an effective strategy to treat GBM, circumventing the BBB hurdles and targeting GSCs.

On the other hand, our results demonstrate that TnTs are potentially useful as drug-delivery channels for cancer therapy, facilitating the intercellular redistribution of drugs in close and far away cells, thus reaching isolated tumour niches that are hardly targeted by simple drug diffusion in the brain parenchyma. The differences identified in TnTs formed by GBM cells and normal human astrocytes can be exploited to increase treatments precision and specificity.

Taken together, the data reported in the thesis work herein presented, strengthen the possibility to exploit anomedicine for the therapy of CNS tumours. However, further efforts are needed to validate the results obtained in other cellular and animal models, with the final aim to translate them into the clinics.

The future of nanomedicine is represented by the so-called "personalized" nanomedicine. In this context, the opportunity to exploit multiple NPs functionalization strategies plays a pivotal role. A recently founded project to our research group, aimed to use a multidisciplinary approach for the treatment of different CNS diseases, tumours included. This project require the use of NPs loaded with different drugs and modified on the surface with various ligands, accordingly to the pathology needs. Moreover, since a common feature of severe brain disorders is the impairment of the immune system and the presence of a chronic inflammatory condition, a bioactive lipid with anti-inflammatory properties, will be added to the nanoformulations.

References

- Pearson JRD, Regad T. *Targeting cellular pathways in glioblastoma multiforme*. Signal Transduct Target Ther. **2017** Sep 29;2:17040. doi: 10.1038/sigtrans.2017.40.eCollection 2017. Review. PubMed PMID: 29263927.
- Lyons SA, O'Neal J, Sontheimer H. *Chlorotoxin, a scorpion-derived peptide, specifically binds to gliomas and tumors of neuroectodermal origin.* Glia. **2002**; 39: 162-73.
- Cohen-Inbar O, Zaaroor M. *Glioblastoma multiforme targeted therapy: The Chlorotoxin story*. J Clin Neurosci. **2016**; 33: 52-58.
- D'Alessio A, Proietti G, Sica G, Scicchitano BM. *Pathological and Molecular Features of Glioblastoma and Its Peritumoral Tissue.* Cancers (Basel). **2019** Apr 3;11(4). pii: E469. doi: 10.3390/cancers11040469. Review. PubMed PMID: 30987226.
- Ohgaki H, Kleihues P. The definition of primary and secondary glioblastoma. Clin Cancer Res. 2013 Feb 15;19(4):764-72. doi: 10.1158/1078-0432.CCR-12-3002. Review. PubMed PMID: 23209033.
- Brennan CW, Verhaak RG, McKenna A, Campos B, Noushmehr H, Salama SR, Zheng S, Chakravarty D, Sanborn JZ, Berman SH, Beroukhim R, et al. TCGA Research Network. *The somatic genomic landscape of glioblastoma.* Cell. **2013** Oct 10;155(2):462-77. doi: 10.1016/j.cell.2013.09.034. PubMed PMID: 24120142.
- Moschoi, R., Imbert, V., Nebout, M., Chiche, J., Mary, D., Prebet, T., et al.. *Protective mitochondrial transfer from bone*

marrow stromal cells to acute myeloid leukemic cells during chemotherapy. Blood. **2016** 128:2. doi: 10.1182/blood-2015-07-655860

- Re, F., Cambianica, I., Zona, C., Sesana, S., Gregori, M., Rigolio, R., et al. *Functionalization of liposomes with ApoE-derived peptides at different density affects cellular uptake and drug transport across a blood-brain barrier model.* Nanomedicine: *NBM.* **2011** 7:5. doi: 10.1016/j.nano.2011.05.004

- Weil, S., Osswald, M., Solecki, G., Grosch, J., Jung, E., Lemke, D., et al. *Tumor microtubes convey resistance to surgical lesions and chemotherapy in gliomas*. Neuro Oncol. **2017**. 19:10. doi: 10.1093/neuonc/nox070

- Broekman, M.L., Maas, S.L.N., Abels, E.R., Mempel, T.R., Krichevsky, A.M., Breakefield, X.O. *Multidimensional communication in the microenvironments of glioblastoma*. Nat Rev Neurol.**2018** 14:8. doi: 10.1038/s41582-018-0025-8

- Salvati E, Re F, Sesana S, Cambianica I, Sancini G, Masserini M, Gregori M. *Liposomes functionalized to overcome the blood-brain barrier and to target amyloid-β peptide: the chemical design affects the permeability across an in vitro model.* Int J Nanomedicine. **2013**;8:1749-58. doi: 10.2147/IJN.S42783. PubMed PMID: 23674890.

Publications outside the thesis topic

1. Nanomedicine for the Treatment of Alzheimer's Disease

Beatrice Formicola, Alysia Cox, Roberta dal Magro∗, Massimo Masserini, and Francesca Re. *Journal of Biomedical Nanotechnology*, Vol. 15, **2019.**

Abstract

Alzheimer's disease affects millions of people worldwide and this figure is continuously increasing. Currently, there is no resolutive cure for this disorder, but a valid contribution could be provided by nanomedicine, utilizing multi-functionalized nanodevices as drug vehicles with additional features of specific brain targeting. Nanomedicine may represent also a practicable strategy for the pharmaceutical industry that moved from small MW pharmaceuticals to larger biologicals, such as antibodies and nucleotides, as the next generation of drugs, leading to the challenge of effective drug delivery. This review provides a survey on the nano-based strategies for Alzheimer's disease diagnosis and treatment, aiming at enhancing the passage of candidate pharmaceuticals across the BBB, and at supporting the evaluation of new therapeutic agents targeting this disease.

2. The Extent of Human Apolipoprotein A-I Lipidation Strongly Affects the β-Amyloid Efflux Across the Blood-Brain Barrier in vitro.
Roberta Dal Magro, Sara Simonelli, Alysia Cox, Beatrice Formicola, Roberta Corti, Valeria Cassina, Luca Nardo, Francesco Mantegazza, Domenico Salerno, Gianvito Grasso, Marco Agostino Deriu, Andrea Danani, Laura Calabresi and Francesca Re. *Frontiers in Neuroscience*, Vol. 13, **2019**.

Abstract

Much evidence suggests a protective role of high-density lipoprotein (HDL) and its major apolipoprotein apoA-I, in Alzheimer's disease (AD). The biogenesis of nascent HDL derived from a first lipidation of apoA-I, which is synthesized by the liver and intestine but not in the brain, in a process mediated by ABCA1. The maturation of nascent HDL in mature spherical HDL is due to a subsequent lipidation step, LCAT-mediated cholesterol esterification, and the change of apoA-I conformation. Therefore, different subclasses of apoA-I-HDL simultaneously exist in the blood circulation. Here, we investigated if and how the lipidation state affects the ability of apoA-I-HDL to target and modulate the cerebral β-amyloid (Aβ) content from the periphery, that is thus far unclear. In particular, different subclasses of HDL, each with different apoA-I lipidation state, were purified from human plasma and their ability to cross the blood-brain barrier (BBB), to interact with Ab aggregates, and to affect Ab efflux across the BBB was assessed in vitro using a transwell system. The results showed that discoidal HDL displayed a superior capability to promote Aβ efflux in vitro (9×10^{-5} cm/min), when compared to apoA-I in other lipidation states. In

particular, no effect on Aβ efflux was detected when apoA-I was in mature spherical HDL, suggesting that apoA-I conformation, and lipidation could play a role in Aβ clearance from the brain. Finally, when apoA-I folded its structure in discoidal HDL, rather than in spherical ones, it was able to cross the BBB in vitro and strongly destabilize the conformation of Aβ fibrils by decreasing the order of the fibril structure (-24%) and the β-sheet content (-14%). These data suggest that the extent of apoA-I lipidation, and consequently its conformation, may represent crucial features that could exert their protective role in AD pathogenesis.